Spatial organization of long-range inhibition in binaural hearing

Kathryn Maureen Tabor

A dissertation submitted in partial fulfillment

of the requirements for the degree of

Doctor of Philosophy

University of Washington

2012

Reading Committee:

Edwin Rubel, Chair

Rachel Wong, Co-Chair

Adrienne Fairhall

Program Authorized to Offer Degree: Neurobiology & Behavior

University of Washington

Abstract

Spatial organization of long-range inhibition in binaural hearing

by Kathryn Maureen Tabor

Chair of the Supervisory Committee:
Professor Edwin Rubel
Departments of Physiology & Biophysics, Otolaryngology H&NS

We are able to follow our friend's voice as she calls across a crowded plaza or whispers in a darkened theater. Amazingly our sense of hearing can identify and localize sounds ranging eight orders of magnitude in loudness. A highly specialized circuit in the auditory brainstem uses submillisecond differences in the arrival time of sound to the two ears, interaural time differences (ITDs), to localize a sound source. The avian nucleus laminaris (NL), analogous to the mammalian medial superior olive, processes ITDs. In NL, ITD sensitivity is maintained by sound-level-dependent inhibition arising from the superior olivary nucleus (SON). By studying the spatial organization of SON input to NL, this dissertation examines how inhibition may shape the precise activity patterns in NL and influence in binaural hearing. Chapter 1 provides an overview of topographic organization in the nervous system and introduces the chicken auditory brainstem system containing NL and SON. Chapter 2 describes quantitative analyses of the coarse tonotopic organization in SON. Chapter 3 demonstrates a broad topographic projection from SON to NL. Further, we present preliminary data from examining the widespread arborization patterns of single SON axons in NL in Chapter 4. This broad innervation pattern of inhibitory input is in stark contrast to the precise, narrow innervation pattern of excitatory inputs to NL. Finally Chapter 5 summarizes the main findings reported in this dissertation, proposes some functions of broadly arranged inhibition in auditory brainstem processing, and offers potential avenues for future study.

TABLE OF CONTENTS

LIST OF FIGURES

LIST OF TABLES

PREFACE

The work presented in Chapters 2 and 3 of this dissertation has been published as separate manuscripts:

Tabor KM, Coleman WL, Rubel EW, Burger RM. 2012. Tonotopic organization of the superior olivary nucleus in chickens. J Comp Neurol 520:1493-508.

Tabor KM, Wong RO, Rubel EW. 2011. Topography and morphology of inhibitory projection from superior olivary nucleus to nucleus laminaris in chickens (*Gallus gallus*). J Comp Neurol 519:358-75.

Chapter 4 has been prepared in publication format. Therefore, some redundancy is apparent in the Introduction and Methods sections.

ACKNOWLEDGEMENTS

I would first like to thank Drs. Edwin Rubel and Rachel Wong for welcoming me into their labs. Ed, my advisor, showed unending enthusiasm and support for my work. A great deal of thanks goes to him for encouraging me to pursue my research interests as they meander extensively from their original track. I am grateful to Rachel, my co-advisor, for her mentorship, enduring patience and fantastic food. Together, they have made graduate school a gratifying challenge.

I am thankful for the opportunity to work with Dr. Burger, whose enthusiasm and hard work enabled a collaboration described in Chapter 2. I would like to thank the members of my thesis committee, Drs. Adrienne Fairhall, Paul Phillips, Fred Rieke and Jenny Stone for their support and insightful suggests on my work.

All the members of the Rubel and Wong labs made many wise suggestions and provided a source of inspiration. I especially wish to thank Dr. Yuan Wang for the endless hours and effort she spent shaping me into a scientist.

A special thanks to my family and friends for their love, support and unwavering confidence in me.

Many thanks to Lucia Wisdom and Ann Wilkinson, administrators in the Neurobiology & Behavior program, without their help I would have never made it to my defense.

Chapter 1
BACKGROUND AND SIGNIFICANCE

1.1 The importance of topographic maps in the nervous system

Topographic organization – the ordered projection of a sensory surface, or effector system, to neuronal structures – is a robust and salient feature of sensory and motor areas in the brain. Anatomic and physiologic topography is thought to provide a neuronal substrate critical for processing sensory information. For example, the location of a visual stimulus is encoded at a specific area of the retina and then represented in retinotopically-organized structures throughout the visual pathways. Similarly, in the auditory system, sound frequency is encoded along the sensory epithelium in the inner ear giving rise to tonotopic maps throughout the central auditory pathways (for example, see Figure 1). Whether such topographic maps are necessary for brain function remains unknown; however, topographic mapping appears advantageous for development (Flanagan, 2006) and information processing (Knudsen et al., 1987).

Topographic mapping has been shown to increase the efficiency of information processing (Knudsen et al., 1987). Topographic maps, with parallel arrays of tuned neurons, are well-suited to process large amounts of information: they sort complex stimuli and represent the information in a systematic form. Information processed by mapped structures is represented as locations of peak activity within a population of neurons and is accessible for further processing by relatively straightforward patterns of connectivity. When a feature is represented topographically, a variety of neuronal mechanisms can operate to sharpen tuning, including; (1) local facilitation and lateral inhibition, (2) spike-independent synaptic interactions that operate over short distances (e.g. Watanabe and Bullock, 1960; Pearson, 1979), and (3) non-synaptic interactions that

result from changes in the electrical and chemical environment caused by synchronous activity of neighboring neurons (e.g. Haas and Jefferys, 1984).

Descriptions of maps provide information to understand how an external stimulus is represented and processed in the nervous system. Moreover, quantitative maps provide predictive tools to determine the optimal stimulus for a particular neuron based on its physical location in the tissue. Researchers can use this information to (1) relate anatomical, biophysical, and pharmacological characteristics of a neuron to its stimulus selectivity; (2) study principles of development and experience-dependent changes in the nervous system; and (3) compare the precision of processing across neuronal structures or across species.

The work described in Chapter 2 constructed a quantitative 3D map of the inhibitory superior olivary nucleus (SON) in a binaural processing circuit of the chicken auditory brainstem. We explored how this cell group processes sound information by examining the topographic organization of neuronal properties important for auditory processing. The quantitative 3D map of SON provides a powerful tool for studying this auditory system. Moreover, these analytical methods will be broadly applicable to map other sensory and motor structures.

1.2 Long-range inhibitory projections in the nervous system

Topography is mainly studied in excitatory pathways, in which a number of principles underlying sensory perception and circuit construction have been revealed. In addition, some inhibitory topographic projections have been identified and examined. The anatomical organization of inhibitory projections determines how they shape the output of the neuronal circuit. As an example, the inhibitory connection from the deep cerebellar

nucleus (DCN) to the inferior olive (IO) follows a precise topographic arrangement such that a closed loop is formed among neurons of the IO, DCN, and cerebellar cortex (Hesslow, 1986; Nelson et al., 1989). This arrangement forms independent inhibitory feedback loops that each regulates the background activity of a microzone of Purkinje cells to modulate cerebellar learning.

A second example of a long-range inhibitory pathway is the commissural projection between the two superior colliculi (SC). This GABAergic projection follows a heterotopic organization: the medial SC contacts neurons in the lateral region of the contralateral SC and the lateral SC projects to the medial contralateral SC (Takahashi et al., 2007). This heterotopic arrangement allows regions of the SC representing upward eye movements to inhibit contralateral regions representing downward eye movements and vice versa.

Other examples of long-range projections are hippocampal GABAergic neurons sending axons to the inferior hippocampal formation, medial septum (Alonso and Köhler, 1982), cingulate cortex and contralateral dentate gyrus (Losonczy et al., 2002; van Groen and Wyss, 2003; Jinno et al., 2007; Miyashita and Rockland, 2007; Jinno, 2009). And, some of these GABAergic neurons project to multiple targets, such as the medial septum and the inferior hippocampal area (Jinno et al., 2007). This long-range GABAergic projection system may coordinate patterns of rhythmic activity in widespread but functionally related areas (Klausberger and Somogyi, 2008).

The mammalian auditory system possesses a wealth of well-studied inhibitory projection pathways. Three examples are the projection from the dorsal nucleus of the lateral lemniscus (DNLL) to the inferior colliculus (IC) (Shneiderman et al., 1988;

Henkel et al., 2003), the projection from the medial nucleus of the trapezoid body (MNTB) to the lateral superior olive (LSO; Figure 1) (Boudreau and Tsuchitani, 1968; Sanes and Rubel, 1988) and the projection from the MNTB to the medial superior olive (MSO; Figure 1) (Grothe and Sanes, 1993, 1994). A prominent inhibitory input to the IC arises bilaterally from GABAergic neurons in DNLL, whose axons terminate in the IC in a characteristic stripe-like pattern (Shneiderman et al., 1988). Inhibitory stripes from the ipsilateral and contralateral DNLL interdigitate to create aural dominance bands. Both the MNTB-LSO and MNTB-MSO inhibitory pathways are in sound localization circuits and show precise topographic organizations matching the precision of the excitatory inputs from cochlear nuclei to LSO and MSO (Werthat et al., 2008). This organization allows neurons in the LSO and MSO to integrate timing information from multiple inputs at specific frequencies.

How inhibitory projections regulate activity of excitatory circuits to modulate sensory processing is not fully understood. The sound localization circuit in the chicken auditory brainstem is well-suited to address this question. First, the excitatory circuit is precisely organized and quantitatively described (Rubel and Parks, 1975; Young and Rubel, 1983). Second, the computations performed by the circuit to localize and segregate sounds are well-studied (for review, see Hyson, 2005). In addition a long-range projection provides the majority of inhibitory input to this circuit, and some physiological functions of the inhibitory input in sensory processing have been demonstrated (Nishino et al., 2008; Fukui et al., 2010). But, the anatomical organization of the inhibitory projection remains to be determined. We examined the topography of this inhibitory

projection, contrasted it to the topography of excitatory pathways in the circuit, and related the anatomy to physiological functions of this inhibitory input (Chapter 3).

1.3 Avian auditory brainstem

Binaural hearing provides important perceptual information for localizing sound and detecting signals in noisy environments. Submillisecond differences in the arrival time of sounds to the two ears, interaural time differences (ITDs), are important binaural cues for localizing their sources. Processing of these cues is optimized by both morphological and physiological specializations in binaural coincidence-detecting neurons in MSO of mammals and NL of birds (Goldberg and Brown 1969; Yin and Chan 1990; Carr and Konishi 1990; Overholt et al. 1992). In birds, ITD sensitivity is maintained in NL over a large range of sound levels (~50-dB) (Peña et al., 1996; Nishino et al., 2008). One mechanism important for maintaining ITD sensitivity is sound-level-dependent inhibition. Below we will first review the anatomy of the circuit that processes binaural stimuli, then summarize the neuronal mechanisms that enable accurate detection of coincident synaptic inputs essential to ITD processing, and finally discuss how inhibitory circuits improve ITD processing in a sound-level-dependent manner.

1.3.1 Anatomy of the avian auditory brainstem

In birds, the auditory brainstem circuit that processes ITDs is composed of one inhibitory (GABAergic and possibly glycinergic) and three excitatory (glutamatergic) cell groups (Figure 2A). Auditory nerve fibers from the avian cochlea enter the brainstem, branch, and innervate two excitatory cochlear nuclei: nucleus angularis (NA) and nucleus magnocellularis (NM) (Ramón y Cajal, 1908; Boord and Rasmussen, 1963; Parks and Rubel, 1978; Carr and Boudreau, 1991). NA comprises a diverse array of cell types with

distinct response properties and is involved in processing multiple features of sound (Soares et al., 2002; Fukui and Ohmori, 2003; Köppl and Carr, 2003). NM comprises a homogenous population of large, round neurons arranged in a precise tonotopic map with low frequencies represented caudolaterally and high frequencies represented rostromedially (Rubel and Parks, 1975). NM axons bifurcate to innervate NL bilaterally (Parks and Rubel, 1975; Jhaveri and Morest, 1982; Young and Rubel, 1983).

In chicken, NL comprises a monolayer of bitufted excitatory neurons receiving ipsilateral and contralateral NM inputs segregated to the dorsal and ventral dendrites, respectively (Parks and Rubel, 1975; Smith and Rubel, 1979; Young and Rubel, 1983). Neighboring NM neurons innervate neighboring narrow arrays of NL, creating a precise caudolateral-to-rostromedial (low-to-high frequency) tonotopic map (Rubel and Parks, 1975; Young and Rubel, 1983). The NM projection to the contralateral NL forms a delay line that compensates for the ITD created outside the head (Young and Rubel, 1983; Seidl et al., 2010). Myelination thickness and axon diameter systematically varies along NM axons to adjust the conduction velocity and enhance the accuracy of coincidence detection of bilateral action potentials (Carr and Konishi, 1990; Seidl et al., 2010). Physiological studies have demonstrated that individual NL neurons are sensitive to changes in ITDs, responding maximally when input from the ipsilateral and contralateral NM arrives at the two dendritic arbors simultaneously (Carr and Konishi, 1988, 1990; Overholt et al., 1992; Joseph and Hyson, 1993; Köppl and Carr, 2008). Orthogonal to its tonotopic map, NL is arranged by preferred ITD such that neighboring neurons have adjacent receptive fields along the azimuth (Parks and Rubel, 1975; Young and Rubel, 1983; Köppl and Carr, 2008).

NA and NL axons projecting to the pons and midbrain send collateral branches to innervate the ipsilateral inhibitory SON. SON neurons densely express GABA and its synthesizing enzyme glutamic acid decarboxylase (Carr et al., 1989; Code et al., 1989; von Bartheld et al., 1989; Lachica et al., 1994), and many SON neurons may also contain glycine (Coleman et al., 2011). Like NA, SON comprises a heterogeneous population of cells with diverse response patterns to tone stimulation (Moiseff and Konishi, 1983; Coleman et al., 2011). Individual SON neurons project to multiple ipsilateral brainstem nuclei (NA, NM and NL) providing the predominant source of inhibition in this brainstem circuit (Yang et al., 1999; Monsivais et al., 2000; Burger et al., 2005). In addition, a separate population of SON neurons projects to the contralateral SON (Monsivais et al., 2000; Burger et al., 2005). SON neurons also project to auditory structures in the pons and midbrain (Conlee and Parks, 1986; Westerberg and Schwartz, 1995).

The functional properties of the inhibitory connections have been reviewed recently (Burger et al., 2011). In summary, each side of the auditory brainstem contains an inhibitory feedback loop; the output of NA and NL drives activity in SON, which provides inhibitory feedback to NA, NM and NL (Figure 2B). In addition, the reciprocal projection between the two SONs negatively couples these feedback loops. This circuit organization enables SON to influence both monaural and binaural processing.

1.3.2 Frequency-dependent specializations in NL enable ITD processing

The brainstem circuit has numerous specialized features for accurate ITD computation. Because the requirements for ITD processing vary across sound frequencies, many of these specialized features also vary in a similar manner. Here we focus on properties of

NL neurons that vary as a function of characteristic frequency (CF), a measure of frequency tuning defined as the sound frequency at which an auditory neuron has the lowest response threshold.

Recordings from brainstem slices of the chicken NL revealed that coincidence detection varies systematically with tonotopy. The precision of coincidence detection was found to be proportional to the time course of excitatory postsynaptic potentials (EPSPs) (Kuba et al., 2005). When two electrical stimuli with a varying time interval were applied to the bilateral inputs from NM, responses to the two stimuli were summed in individual NL neurons. When the intervals were short, EPSPs were summed to produce a suprathreshold response but when the intervals were longer, EPSPs remained subthreshold. The precision of coincidence detection (inversely proportional to the time window that induced suprathreshold responses) was dependent on the CF of neurons; the average time window was smallest in neurons located in the middle CF region, followed by the high CF region, and was most broad in the low CF region (Kuba et al., 2005). Similarly, the time windows measured *in vivo* from NL neurons of the barn owl were smaller in middle and high CF neurons than in low CF neurons (Carr and Konishi, 1990).

Low-voltage-gated K^+ channels abbreviate the falling phase of EPSPs and immuno-detection of these channels was most dense in the middle and high CF regions of NL and less dense in the low CF region (Kuba et al., 2005). This immunolabeling pattern of K^+ channels was approximately reciprocal to the distribution of the time window for coincidence detection and may largely determine the accuracy of coincidence detection in NL. The frequency dependence of coincidence detection in slices has behavioral correlations in studies of sound localization (Knudsen and Konishi, 1978, 1979; Klump,

2000). As a result, most animals have the highest accuracy in the middle CF region within the hearing range inherent to that species.

1.3.3 Modulation of ITD tuning by sound-level-dependent inhibition

Studies in chickens and owls have shown ITD selectivity by NL neurons is stable across a wide range of sound intensities (Peña et al., 1996; Nishino et al., 2008). Several interrelated mechanisms contribute to this stability, including synaptic depression at the NM-NL synapse (Kuba et al., 2002; Cook et al., 2003), nonlinear summation of inputs in dendrites (Agmon-Snir et al., 1998), abundance of low-voltage-gated K^+ channels (Reyes et al., 1996; Kuba et al., 2005), and sound-level-dependent inhibition (Peña et al., 1996; Burger et al., 2005, Dasika et al., 2005; Nishino et al., 2008). SON-dependent inhibition shapes activity in NL indirectly by influencing NM neuronal activity, and directly by forming synapses on NL neurons. Inhibitory input to NL influences ITD processing in three ways: (1) shifting action potential threshold (i.e. inactivating voltage gated Na^+ channels), (2) speeding kinetics of EPSPs, and (3) reducing the duration of the coincidence window. GABAergic signaling in NL (and NM) is depolarizing (Hyson et al., 1995) evoking both Cl^- and K^+ conductances (low-voltage-gated K^+ channels) to enhance coincidence detection.

Using a slice preparation, Funabiki et al. (1998) examined the physiological effect of GABAergic input to NL by pairing intracellular depolarizing current with unilateral afferent stimulation of NM inputs. The timing between the two stimuli was varied to determine the precision of coincidence detection. When exogenous GABA was applied to the preparations the coincidence detection window was decreased by ~50%, enhancing computational precision. These observations demonstrated that the effect of GABA

signaling in NL enhances ITD encoding by reducing the temporal window over which convergent excitatory inputs from each NM can sum to evoke a suprathreshold response. In addition, GABA signaling potently inhibits spike generation when excitatory postsynaptic potentials arrive just outside that window (Howard and Rubel, 2010).

Simulations of the excitatory auditory brainstem pathway indicated that loud sound reduces the contrast between the peak and trough of the ITD-tuning curve (i.e. selectivity) (Burger et al., 2005; Dasika et al., 2005). But *in vivo* recordings from birds showed ITD selectivity was maintained rather than reduced at high sound levels (Peña et al. 1996; Nishino et al., 2008). Peña et al. (1996) proposed that inhibition from SON controls ITD tuning in NL, making it stable across a wide range of sound levels.

Nishino et al. (2008) demonstrated ITD tuning in NL is under sound-level-dependent control by SON. By recording *in vivo* from single NL neurons in the chicken, ITD tuning was found to depend both on the frequency and level of sounds (Nishino et al., 2008). The ITD selectivity in middle-high CF neurons was maximal at intermediate sound levels, and lost at very high sound levels (>90 dB). In contrast, low CF neurons became more selective to ITDs as the sound became louder. Electrical lesion of SON reduced ITD selectivity at high sound levels in low CF neurons (Nishino et al., 2008). Remarkably, silencing SON did not alter the sound-level-dependence of ITD selectivity level of middle-high CF neurons. These observations demonstrated that SON inhibition enables low CF NL neurons to maintain sensitivity to ITDs across a wide range of sound levels. Anatomically, Nishino et al. (2008) observed the GABAergic projection from SON to NL was robust in the low CF region of NL but became less prominent toward the

high CF region, suggesting the dense inhibitory projection from SON to NL regulates ITD tuning in NL (Nishino et al., 2008).

In addition, Nishino et al. (2008) found that eliminating SON input strongly influenced the phase selectivity of NL neurons. In the control condition, NL neuron phase selectivity was stable, reflecting the summation of coincident phase delays between bilateral NM input spikes. Following SON lesion, the NL neurons' best phase shifted with ITD mirroring the stimulus phase at the ipsilateral ear. This finding suggested that silencing the ipsilateral SON caused an imbalance between the activity levels of the bilateral excitatory inputs to NL, allowing input from the ipsilateral NM to dominate NL responses. This illustrates a second function of SON circuitry: to balance activity levels between the two NMs.

1.3.4 SON circuitry for balancing binaural inputs to NL

In addition to its direct inhibitory input in NL, SON indirectly impacts NL through its interactions with NM inputs, modulating frequency selectivity, phase locking, and bilaterally coupling activity in the two NMs to reduce firing rate differences between them. These bilateral influences of SON are mediated through the reciprocal projections between SONs. This coupling is thought to be important for ITD processing in NL (Monsivais et al., 2000; Burger et al., 2005; Dasika et al., 2005; Nishino et al., 2008; Fukui et al., 2010).

In addition to maintaining ITD selectivity over a wide range of sound levels, the auditory brainstem must maintain ITD selectivity when sound levels at the two ears are different. This situation occurs when sound sources are located to the sides of the head because (1) the head shadows sound waves reaching the contralateral ear and (2) an air-

filled canal acoustically couples the middle ears in birds, inducing sound level differences at the tympanic membranes (Hyson et al., 1994), and generating large differences in firing rates between the two NMs. This bilateral asymmetry in firing rates of presynaptic terminals generates a computational challenge for NL: to distinguish between an intense monaural input and ideally timed binaural inputs. The contralateral projections between the two SONs seem well-suited to eliminate bilateral imbalances between activity levels in the two NMs. In fact, a recent *in vivo* study demonstrated that a single SON inhibits the ipsilateral NM while simultaneously disinhibiting the contralateral NM (Fukui et al., 2010).

Fukui et al. (2010) recorded responses from individual NM neurons *in vivo* while pharmacologically silencing the ipsilateral or contralateral SON. In control experiments, the input-output functions of NM neurons were generally monotonic but with a mild depression for high-intensity stimuli (Fukui et al., 2010). After pharmacological lesion of the ipsilateral SON, NM firing rates increased suggesting that the ipsilateral SON suppressed neuronal activity during intense stimulation (Fukui et al., 2010). In contrast, after pharmacological lesion of the contralateral SON, which silenced its input to the ipsilateral SON feedback circuit, the activity in NM was suppressed compared with controls (Fukui et al., 2010). These experiments suggest that SONs function to balance neuronal activity levels between the two NMs. When sound stimuli favor one ear, the balance of inhibition is shifted toward that ear by increased activity in the ipsilateral SON-NM projection, and decreased activity in the contralateral SON-NM projection. This process balances the activity levels of bilateral inputs contacting NL neurons, improving ITD computation (Nishino et al., 2008; Fukui et al., 2010; Burger et al., 2011).

1.4 Questions addressed in this work

Investigating topographic maps has led to countless insights on the development and function of the nervous system. Yet, how inhibitory projections modulate excitatory maps to shape sensory perception is not fully understood. To address this question we determined the organization of inhibitory projections in a sound localization circuit of the chicken auditory brainstem and compared our findings to the pattern of excitatory connections. These results improve our understanding of how inhibition is organized to regulate the output of the sound localization circuit.

Physiological and computational studies have demonstrated a critical role for inhibitory long-range projections in binaural hearing; however, the anatomical substrate shaping the circuitry remains to be determined. We thus examined the spatial organization of inhibition in multiple levels of analyses (Figure 3). First, we demonstrated the topographic organization of SON in 3D using quantitative mapping methods (Chapter 2). We addressed the questions: (1) Is the tonotopic organization of the brainstem auditory pathway preserved in SON? Past studies in the owl (Moiseff and Konishi, 1983) and chicken (Lachica et al., 1994) have suggested that sound frequency may be systematically represented in SON, but as yet this has not been directly accessed. (2) Are the diverse classes of inhibitory neurons composing SON segregated in separate organizations in SON? Although physiological studies showed SON contains a heterogeneous mixture of response patterns to tone stimulation (Moiseff and Konishi, 1983; Coleman et al., 2011), a detailed topographic map of these response features remained to be determined.

Second, we examined whether the organization of SON is preserved in its projection to NL (Chapter 3). We asked: (1) Does the topography of the SON-NL projection indicate SON is regulating NL in a sound frequency-specific manner? We compared the patterns of inhibitory and excitatory projections to NL to explore the role of SON in sharpening NL frequency tuning through lateral inhibition. (2) Is the SON-NL loop reciprocal, such that an NL region receives inhibitory feedback from the same SON region that it drives? Studies of other long-range inhibitory projections demonstrated that reciprocal projections act to regulate the activity level of the circuit (e.g. inhibitory connection from DCN to IO) (Hesslow, 1986; Nelson et al., 1989).

Finally, we present preliminary findings of our ongoing study to explore the axonal arborization pattern of individual SON neurons in NL (Chapter 4). Experiments address the questions: (1) What is the size and shape of a axonal arborization of a single SON neuron projecting to NL? (2) What is the distribution of inhibitory synaptic sites between individual SON axonal arborizations and NL? We compare the inhibitory axonal arborization patterns with the excitatory axons innervating NL, to better understand how inhibition shapes neuronal activity and influences binaural hearing.

Together the three studies provide data to better understand the neuronal circuitry underlying how sound-level-dependent inhibition from SON helps NL maintain ITD sensitivity across a wide range of sound levels. We demonstrated a relatively coarse tonotopic map in SON and a broad topographic pattern of SON axons to NL. These findings suggest NL neurons do not receive precise frequency-selective information but instead a representation of the overall sound level of the environment from SON.

Futhermore, the SON projection may provide lateral inhibition to sharpen ITD tuning and frequency selectivity in NL.

1.5 Figures

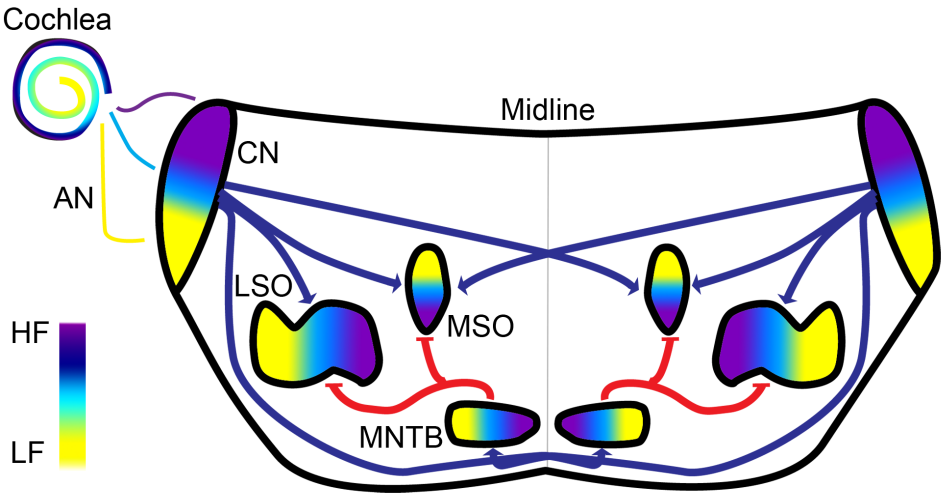

Figure 1. Schematic of mammalian auditory brainstem.
Tonotopic organization (represented with color gradient) is established in the cochlea and preserved in brainstem auditory structures. Red lines indicate two well-studied inhibitory projections in the mammalian auditory brainstem; the mntb-lso and the mntb-mso pathways. Blue lines indicate excitatory projections in the brainstem. Abbreviations: an, auditory nerve; cn, cochlear nucleus; hf, high frequency; lf, low frequency; lso, lateral superior olive; mntb, medial nucleus of the trapezoid body; mso, medial superior olive.

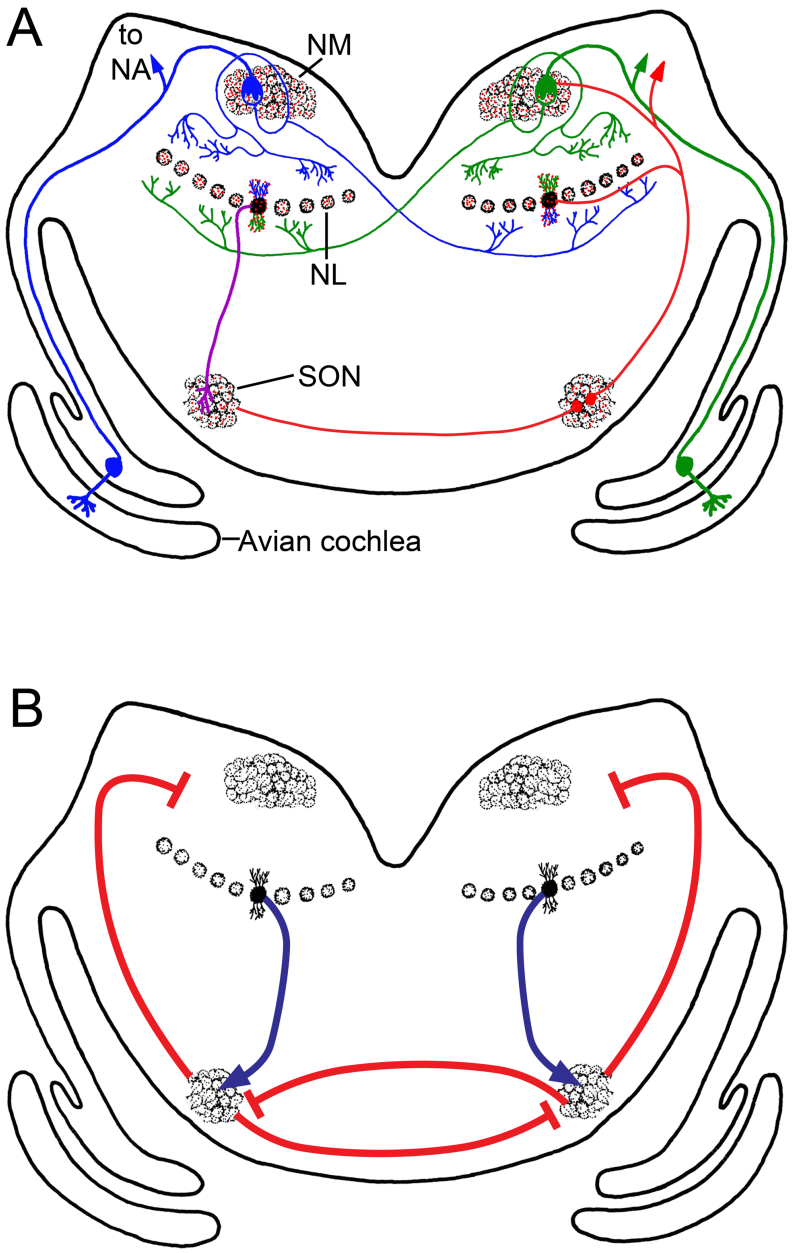

Figure 2. Schematic coronal view of the auditory brainstem in chickens.
A. Auditory stimuli are encoded in the avian cochlea and transmitted to nucleus magnocellularis (NM) and nucleus angularis (NA, not shown) in the brainstem. NM axons bifurcate and innervate bilaterally nucleus laminaris (NL). Thus, NL receives excitatory inputs from left (blue) and right (green) ears segregated to the dorsal and ventral dendritic lamina. Inhibition arises from the superior olivary nucleus (SON) (red). SON receives excitatory input from the ipsilateral NA and NL (purple) and provides inhibition to the ipsilateral NA, NM and NL. In addition, SON projects to the contralateral SON. **B.** Each side of the auditory brainstem contains a feedback loop; NA and NL drive SON, which provides inhibition to NA, NM and NL. The reciprocal projection between SONs negatively couples the feedback loops. Inhibitory pathways are represented in red, excitatory pathways in blue.

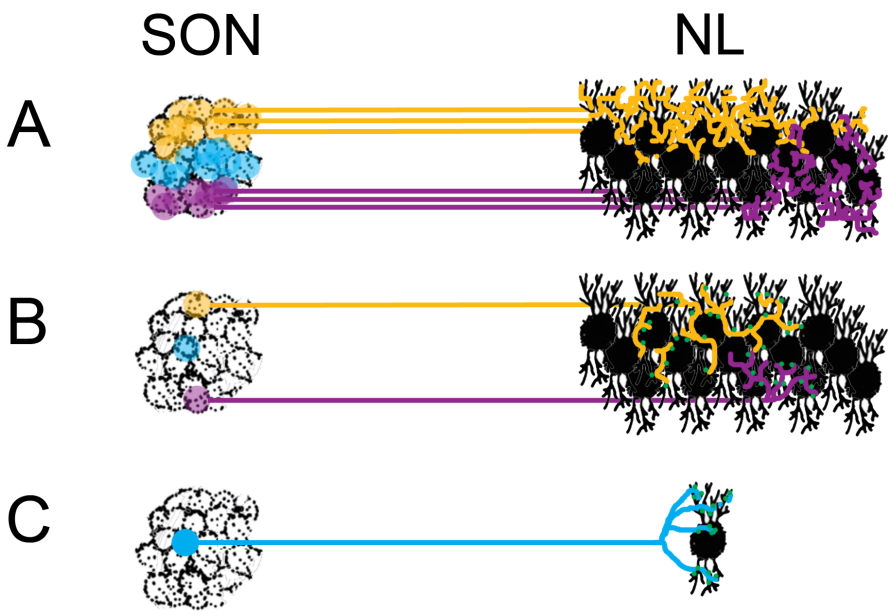

Figure 3. Multiple levels of analyses of inhibitory projection topography.
A. Population level: In Chapter 2 we quantitatively analyze the organization of SON and in Chapter 3 we examine the topography of projections from small regions of SON to NL. **B.** Single neuron level: In Chapter 4 we demonstrate the connectivity patterns of single SON axonal arborizations in NL (divergence). **C.** Single presynaptic and postsynaptic neuron level: One future avenue of exploration is to determine the pattern of connectivity between one presynaptic SON neuron and one postsynaptic NL neurons.

Chapter 2
TONOTOPIC ORGANIZATION OF THE SUPERIOR OLIVARY NUCLEUS IN THE CHICKEN AUDITORY BRAINSTEM

2.1 Abstract

Topographic maps are salient features of neuronal organization in sensory systems. Inhibitory components of neuronal circuitry are often embedded within this organization, making them difficult to isolate experimentally. The auditory system provides opportunities to study the topographic organization of inhibitory long-range projection nuclei, such as the superior olivary nucleus (SON). We analyzed the topographic organization of response features of neurons in the SON of chickens. Quantitative methods were developed to assess and communicate this organization. These analyses led to three main conclusions: 1) sound frequency is linearly arranged from dorsal (low frequencies) to ventral (high frequencies) in SON; 2) this tonotopic organization is less precise than the organization of the excitatory nuclei in the chicken auditory brainstem; and 3) neurons with different response patterns to pure tone stimuli are interspersed throughout the SON and show similar tonotopic organizations. This work provides a predictive model to determine the optimal stimulus frequency for a neuron from its spatial location in the SON.

2.2 Introduction

Topographic organization is a robust and salient feature of sensory and motor areas in the vertebrate brain. Anatomic and physiologic topography is thought to provide a neuronal substrate critical for processing sensory information. For example, location of a visual stimulus is encoded at the retina and then represented in ‘‘retinotopically’’ organized structures throughout the visual pathways. Similarly, in the auditory system, sound

frequency encoded along the sensory epithelium gives rise to ‘‘tonotopic’’ maps throughout the central auditory pathways. Descriptions of maps provide information to understand how an external stimulus is represented and processed in the nervous system. Moreover, quantitative maps provide predictive tools to determine the optimal stimulus for a particular neuron based on its location in the tissue. Using this information investigators can 1) relate anatomical, biophysical, and pharmacological characteristics of a neuron to sensory processing based on stimulus selectivity (Smith and Rubel, 1979; Kuba et al., 2005); and 2) compare the precision of processing across sensory areas or across species.

Inhibitory components of many neuronal circuits comprise interneurons residing alongside principal neurons (Huang et al., 2007). Thus, independent evaluation of the organizing features of these circuit components is difficult. However, in the auditory brainstem, inhibitory neurons often reside in nuclei that project to one or more targets, thus providing opportunities to study sensory mapping in inhibitory long-range projection nuclei (Tsuchitani and Boudreau, 1966; Sanes and Friauf, 2000; Kim and Kandler, 2003). In the current study we use a quantitative strategy to describe the 3D tonotopic organization of the superior olivary nucleus (SON) in chicken. The avian SON comprises inhibitory neurons that provide long-range γ-aminobutyric acid (GABA)ergic and possibly glycinergic inhibition to other auditory nuclei in the brainstem (Yang et al., 1999; Kuo et al., 2009; Coleman et al., 2011). Inhibition from the SON expands the dynamic range and sharpens temporal coding of auditory neurons to enable sound localization (Burger et al., 2005; Nishino and Ohmori, 2009; Fukui et al., 2010).

The goal of the current study is to analyze the topographic organization of 1) sound frequency and 2) physiologically identified cell types. Specifically, is the tonotopic organization of the brainstem auditory pathway preserved in the SON? Past studies in the owl (Moiseff and Konishi, 1983) and chicken (Lachica et al., 1994; Tabor et al., 2011) have suggested that stimulus frequency may be systematically represented in the SON. Furthermore, the SON contains a heterogeneous mixture of response patterns to tone stimulation (Moiseff and Konishi, 1983; Tabor et al., 2011; Coleman et al., 2011). However, a detailed topographic map of these response features remains to be determined.

In addition to the physiological heterogeneity in SON, anatomical evidence suggests that the SON contains functionally distinct classes of neurons. Anatomically, multiple auditory pathways converge in the SON. One major input arises from the binaural coincidence detecting neurons in the nucleus laminaris (NL), whereas another arises from the ipsilateral nucleus angularis (NA) (Moiseff and Konishi, 1981, 1983; Takahashi et al., 1984). Also, distinct populations of SON neurons give rise to two projections, one to ipsilateral targets and the other to the contralateral SON and higher order centers (Conlee and Parks, 1986; Westerberg and Schwartz, 1995; Burger et al., 2005). Whether the physiologically distinct cell types correspond to the apparent functional classes of SON neurons revealed by anatomical projections remains unknown. Because SON neurons provide the majority of inhibition to all auditory nuclei in the dorsal brainstem (Lachica et al., 1994; Yang et al., 1999; Burger et al., 2005), it is important to understand how auditory information is processed in the SON.

Using *in vivo* single- and multiple-unit recordings we classified the characteristic frequency (CF), frequency selectivity, threshold, and response patterns of SON neurons. 3D reconstructions and quantitative analyses determined that CF is linearly mapped in the SON. This tonotopic organization is less precise than that of other auditory nuclei in the avian brainstem (Rubel and Parks, 1975). In addition, we found that SON neurons with onset and sustained response patterns are interspersed throughout the entire structure of the SON, and that both types show similar tonotopic organizations. These results suggest that both phasic and tonic SON responses are generated for all sound frequencies processed in the chicken auditory system. The quantitative 3D tonotopic map of the SON provides a powerful tool for future studies of neuronal circuitry in this system. These analytical methods will be broadly applicable to other sensory and motor system circuitry.

2.3 Methods and Materials

Experiments were conducted on white leghorn chicken hatchlings (*Gallus gallus domesticus*) 7–15 days old. All procedures were carried out in accordance with the National Institutes of Health Guide for the Care and Use of Laboratory Animals and approved by the Lehigh University Institutional Animal Care and Use Committee. All efforts were made to minimize pain and discomfort of the animals used and to minimize the animal number. Detailed experimental methods were reported previously (Coleman et al., 2011).

2.3.1 Surgery

Chickens (54–157 g) were anesthetized with an intramuscular injection of ketamine (80 mg/kg; Ketaset, Fort Dodge Animal Health, Fort Dodge, IA), an intraperitoneal injection

of pentobarbital (80 mg/kg; Sigma-Aldrich, St. Louis, MO), and an intramuscular injection of urethane (4, 0.625 g/kg doses separated by 20–30 minutes; Sigma-Aldrich). Additional urethane (0.625 g/kg) was injected in some cases to maintain the level of anesthesia. The bird's body temperature was maintained at 40°C throughout all procedures by using a heating pad. A tracheotomy was performed to facilitate breathing during the experiment. The head was fixed to a stereotaxic stage and a brass rod was fastened to the top of the cranium with dental cement. After the cement cured, the animal was transferred to a customized stereotaxic apparatus inside a sound attenuation booth. The skin covering the skull was removed, and the skull was opened to expose the cerebellum. A slit was made in the dura mater for electrode penetration. Care was taken not to injure the large venous sinus.

2.3.2 Sound presentation and data acquisition

Freely available software (Spike; Brandon Warren, University of Washington) controlled acoustic stimuli generation and data acquisition. Sound stimuli were output through an HB7 Headphone Driver (Tucker-Davis Technologies, Alachua, FL) to an Eartone 3A Insert earphone coupled to the ipsilateral ear with a tube insulated with acoustic foam (Etymotic Research, Elk Grove Village, IL). The sound pressure level (SPL) was calibrated using a ¼'' free-field microphone (model 2520; Larson-Davis, Provo, UT) and microphone preamp (model 221; Larson-Davis). The maximum sound intensity was 90 dB SPL, and the sound frequency range was 50–6,000 Hz. Tone duration was 20 or 40 ms with a 5-ms rise and fall time for a triangle-shaped envelope.

2.3.3 In vivo recording

Tungsten recording electrodes (5–8 MΩ; no. 575300, AM Systems, Sequim WA) were inserted 2.1–2.3 mm lateral and 0.0–0.5 mm rostral to the venous sinus. SON neuronal units were located by presenting a white-noise stimulus (65–70 dB SPL, 50-ms duration, 3 pulses/s) to the ipsilateral ear while advancing the electrode using a remotely driven actuator (MC1000e-1 Controller; Siskiyou Design Instruments, Grants Pass, OR). Neuronal action potentials were bandpass-filtered between 300 Hz and 3 kHz (model 3362 filter; Krohn-Hite, Brockton, MA) and amplified with a Neuroprobe Amplifier Model 1600 (A-M Systems, Carlsborg, WA). Both analog voltage traces and action potential event times were simultaneously recorded. Analog traces were collected with 12-bit resolution at 50-kHz sampling frequency. Action potential event times were recorded by using a voltage window discriminator (model 121; World Precision Instruments, Sarasota, FL). Both signals were processed by an RX6 Multifunction Processor (Tucker-Davis Technologies).

After isolation of a neuronal unit or cluster from background noise, the frequency tuning of the neuronal response was coarsely mapped to determine whether the unit responded to low-, middle-, or high-frequency acoustic stimuli. A high-resolution frequency response function was derived by presenting a series of low (0.05–2 kHz), middle (1–4 kHz), or high (2–5 or 6 kHz) tone stimuli (12 logarithmic steps, 20- or 40-ms duration, 10 pulses/s) at levels ranging from 0 to 90 dB SPL (10-dB steps). If responses from a neuronal unit spanned two frequency ranges, both stimulus sets were presented. Each stimulus was presented 20 times in a pseudo-randomized sequence. After recordings, small electrolytic lesions (~100 μm in diameter, 15 μA, 20 seconds to 1

minute) were made to mark the position of the electrode penetrations (see Fig. 4B) and to facilitate 3D reconstruction of SON.

2.3.4 Analysis of electrophysiological data

Single- and multiple-unit activity were sorted by using a freely available PostHawk program (David Schneider, Woolley Lab, Columbia University, New York, NY) written in MatLab (Mathworks, Natick, MA). Spike counts were obtained from a time window equal to the duration of the stimulus and adjusted to the minimum first latency of the response. For multiple-unit recordings, neuronal events were counted when the voltage trace exceeded two-thirds the peak voltage of the recording. We used event counts to calculate the rates of multiple-unit activity. Response threshold was defined as the intensity at which the spike rate (or rate of multiple-unit activity) during the stimulus time exceeded the average spontaneous rate by two standard deviations (SDs). Characteristic frequency (CF) was defined as the frequency with the lowest response threshold. Response patterns of neurons were classified from post-stimulus time histograms to tones of CF presented 20 dB above response threshold (Fig. 1). Frequency tuning curves were assessed by analyzing Q10, defined as the CF divided by the response bandwidth 10 dB above threshold.

2.3.5 Nissl staining

Following electrophysiological recording, animals were transcardially perfused with phosphate-buffered saline (PBS; 0.1 M, 7.2–7.4 pH) followed by chilled 4% paraformaldehyde in PBS. The brains were removed from the skull and postfixed overnight in the paraformaldehyde solution. Each brain was cut coronally at 40 μm on a

freezing stage of a sledge microtome, and each section was collected in PBS. Sections were maintained in order and stained for Nissl with thionin.

2.3.6 Imaging and 3D reconstruction

Brightfield images were captured by using a Zeiss Axioplan 2ie microscope (Carl Zeiss Microimaging, Thornwood, NY) equipped with a 4x (NA 0.09) objective and a CoolSnap HQ monochrome digital camera (Princeton Instruments, Trenton, NJ) and collected in Slidebook (version 4.0.2.8; Intelligent Imaging Innovations, Denver, CO). Selected images were further processed in Adobe Photoshop (Adobe Systems, Mountain View, CA) to enhance contrast and alter brightness for inclusion in figure illustrations. Images of all brainstem sections containing the right SON were aligned to form a z-stack using freely available stackreg plugin (Thevenaz et al., 1998) for ImageJ software (W.S. Rasband; NIH, Bethesda, MD). SONs were reconstructed in 3D from the aligned image stack by using Amira software (Visage Imaging, Berlin, Germany).

For each case, coordinates of electrolytic lesions and electrode tracks in the aligned image stack were compared with stereotaxic coordinates taken at the brain surface for each electrode penetration in order to map recording sites in the reconstructed SON (see Fig. 4). Multilinear regression analysis (MRA) with linear and log equations was used to examine the tonotopic organization of each case (Table 1).

For each SON reconstruction, we determined the ratio of lengths of the medial-lateral to dorsal-ventral to anterior-posterior axes (mean ± SD, 0.70 ± 0.07 to 0.59 ± 0.05 to 1). Also, we determined the orientation of the major axis of each SON reconstruction. For all cases, the anterior ends of the major axes pointed 17 ± 10° medial and 9 ± 6° ventral to the anterior-posterior axis.

We created a standardized SON containing all recording sites of 19 reconstructed SONs by using three steps. First, we translated the reconstructed SONs to overlay their centroids. Second, we rotated the reconstructed SONs to align their major axes to the mean orientation of the population (see above). Third, we normalized the lengths of the medial-lateral, dorsal-ventral, and anterior-posterior axes of all reconstructed SONs. All analyses of the combined dataset containing all recording sites used these normalized anatomical coordinates ranging from 0 to 1 along each axis. However, to visualize the standardized SON and its topographic organization, the lengths of the medial-lateral, dorsal-ventral, and anterior-posterior axes were scaled by the mean ratio of the population (0.7 to 0.59 to 1; see above) to preserve the anatomical shape of SON.

Principle component analysis (PCA) and MRA were used to determine the major tonotopic axis across the standardized SON. Three key steps were used to apply PCA to our experimental dataset. First, we organized the combined dataset into a 4 x 659 matrix. Each of the four rows contained one measurement type (medial-lateral coordinate, dorsal-ventral coordinate, anterior-posterior coordinate, CF) and each column contained data from one recording location. Second, we subtracted the mean and normalized the range of each measurement type, or row of the matrix. Third, we computed the eigenvectors and eigenvalues of the covariance matrix to determine the principal components. The orientation of the first principal component was visualized in three spatial dimensions by using the first three values of the eigenvector associated with the medial-lateral, dorsal-ventral, and anteior-posterior dimensions, respectively.

MRA was performed on the combined dataset by using linear and log equations. The data were best fit by the multilinear regression function:

$$CF = 0.01 + 0.32l + 4.09v - 0.55a \quad (1)$$

where CF is the characteristic frequency in kHz, l is the normalized medial-lateral coordinate (lateral edge is 1.0), v is the normalized dorsal-ventral coordinate axis (ventral edge is 1.0), and a is the normalized anterior-posterior coordinate (anterior edge is 1.0).

To visualize the tonotopic dimensions (see Figs. 5, 6, and 8), we show the orientations of the first principal component and the multilinear regression equation with arrows passing through the ‘‘center of mass’’ of the recording sites. The center of mass of recording sites was defined as the mean of their positions in 3D.

For isolated neuronal responses, the spatial distributions of two physiological types of neurons (sustained and onset) were visualized and analyzed in the standardized SON. The tonotopic organization of each type was examined by using MRA (Table 1).

Statistical evaluations were made by using Student’s t-test or r^2 correlation, and statistical significance was achieved when $P < 0.05$. All data are presented as mean ± SD.

2.4 Results

The results are presented in three main sections. First, we characterize several properties of SON neurons important for auditory processing: response patterns, frequency tuning and selectivity, and response threshold. Second, the 3D spatial organization of frequency tuning is reconstructed for each individual SON. Finally, these representations are projected onto a 3D standardized SON to provide a predictive tonotopic map and examine the spatial distribution of two neuronal response patterns in the SON.

2.4.1 Response patterns, frequency tuning and selectivity, and response threshold

Using *in vivo* recordings, we characterized the response properties of neurons in the SON to ipsilateral tones. Response patterns, CFs, widths of tuning curves, and response thresholds varied widely between SON neurons.

Figure 1 illustrates the response patterns of isolated single SON neurons to ipsilateral tones of CF presented at 20 dB above response threshold. Seventy-three percent of isolated neurons generated sustained responses, either primary-like (Fig. 1A) or pauser-like patterns (Fig. 1B), 25% of isolated neurons produced onset response patterns (Fig. 1C), and 2% suppressed activity in response to ipsilateral tones (Fig. 1D). These activity patterns, and the relative proportion of each response type are consistent with our previous characterization of the SON in chickens (Coleman et al., 2011). Complexity and diversity of SON neuronal responses may derive from their multiple inputs. SON responses resemble the varied response types observed in NA neurons (Sachs et al., 1978; Carr and Soares, 2002; Koppl and Carr, 2003). Additionally, sustained responses in SON may also be evoked by sustained NL neuron inputs, which are weakly driven by monaural stimulation (Peña et al., 1996).

To examine frequency tuning of SON neurons, we constructed their frequency-level response maps. The patterns of excitatory and suppressed response regions of tuning curve plots differed widely between neurons. Representative tuning profiles are shown in Figure 2. Figure 2A shows a response map of an isolated neuron with a V-shaped excitatory region (gray lines) and suppressed responses to neighboring frequencies (red line). Figure 2B shows tones at CF driving excitatory responses of a neuron at intensities above response threshold, but suppressing responses of this neuron

at lower sound levels. Figure 2C illustrates an example of a suppressed responder, which reduced its spike rate to a range of frequencies but showed no excitatory response areas.

To compare tuning and selectivity of these neurons, we measured their CF, Q10s, and response thresholds. Figure 3 shows the distributions of response properties of SON neurons to ipsilateral tones. Among the 310 multiple-units and 349 isolated neurons recorded in the SON, CF ranged from 90 to 5,000 Hz (Fig. 3A; see Fig. 3 legend for statistics). CF distributions of isolated neurons with sustained or onset response patterns represented the entire frequency range of hearing in chicken (Fig. 3B; Gray and Rubel, 1985; Saunders and Salvi, 1993). Next we measured the response thresholds at CF in the SON. Thresholds of multiple-unit responses tended to be slightly higher than the thresholds of isolated neuronal responses ($P < 0.01$; Fig. 3C). This increase reflects multiple-unit recordings with neuronal waveforms that individually were not detected by using our threshold criterion, but summed to form detectable waveforms at higher sound intensities. For isolated neurons, thresholds of both sustained and onset responders increased with CF (Fig. 3C,D). For example, average thresholds of sustained responders increased ~20 dB between CF of 100 and 5,000 Hz (Fig. 3D, bottom). Caution should be used when comparing thresholds between sustained and onset responders because the spike rate criterion used to determine response threshold (see Materials and Methods) may not be equally sensitive between categories of responders.

Finally, we assessed frequency selectivity of SON neurons by measuring Q10, which increases with selectivity and CF ($r^2 = 0.50$, $P < 0.01$). Sustained responders showed higher frequency selectivity, i.e., narrower tuning curves, than onset responders ($P < 0.01$; Fig. 3E). In summary, Figure 3 shows that CF, threshold, and Q10

distributions in the SON resemble other auditory brainstem nuclei in this species (Sachs et al., 1978; Warchol and Dallos, 1990).

2.4.2 3D reconstructions of SON and recording sites

Figure 4 illustrates how individual SONs and recording F4 sites were reconstructed in 3D. Figure 4A shows coronal sections through the SON stained for Nissl. Consecutive sections containing the SON were aligned as described in Materials and Methods. By using the coordinates of the electrolytic lesions, approximately 100 μm in diameter (Fig. 4B, double arrowheads), and the positions of the electrode tracks (Fig. 4A,B, arrows), the recording sites were mapped onto the reconstructed SON for each case (see Materials and Methods). The 3D reconstruction of the SON and locations of recordings are presented in the coronal (Fig. 4C), sagittal (Fig. 4D), and horizontal views (Fig. 4E). Supplemental Movie 1 shows a rotation of this 3D reconstruction (Fig. 4), to visualize the shape of SON and locations of recordings. Table 1 lists the number of recording sites and general region of the SON sampled in each case. We recorded from 12 to 75 sites per animal, and across all cases neuronal responses from all regions of SON were sampled. Because we were able to map recordings to precise locations in 3D SON reconstructions, these datasets could be used to quantitatively analyze the topographic organization of the SON.

2.4.3 Individual SONs are tonotopically organized

Using 3D reconstructions of recording sites in the SON, we performed MRA to determine the tonotopic organization of individual SONs in each animal. In the majority of cases, recording sites were clearly arranged from low CF located dorsally to high CF located in the ventral SON. Figure 5 shows tonotopic analyses of two individual SONs. Figure 5A shows the case presented in Figure 4 with CFs of recording sites indicated by

colored dots. We tested for a relationship between location and CF by using both linear and log regression functions. In 15 cases, including the two shown in Figure 5A and B, a linear relationship best predicted the tonotopic organization. In two cases a log equation better fit the data, and in two cases no relation was observed (Table 1). These results are comparable to the linear representation of frequency in other auditory brainstem nuclei in chickens (Rubel and Parks, 1975). In the case shown in Figure 5A, the coefficient of determination (r^2) indicated that 85% of the variation in CF could be accounted for by the location of the recording within SON. The case illustrated in Figure 5B had an r^2 value of 0.62 (see Table 1 for all r^2 values). The tonotopic axes, determined by the regression functions, are represented with arrows drawn through the center of mass of the recording sites and pointing to high CF (Fig. 5A,B).

To visually compare the tonotopic organization between cases, all statistically significant tonotopic axes (17 of 19 cases) were overlaid on a single 3D reconstruction of the SON (Fig. 5C). Here, the lengths of the arrows approximate the extent of the SON in that direction sampled in each case. Also, we measured the angles between the dorsal-ventral axis and the tonotopic axes in the medial-lateral (mean ± SD, Θ_{ML}: -4 ± 38) and anterior-posterior (Θ_{AP}: 12 ± 24) dimensions (Table 1). In 14 cases the CF was predominantly mapped along the dorsal-ventral axis of the SON; from lower CF in the dorsal SON to higher CF in the ventral SON (Fig. 5C, left and center). This trend was apparent whether recording sites were concentrated in the anterior, posterior, medial, or lateral region of the SON (Fig. 5A,B, Table 1).

2.4.4 Standardized SON is tonotopically organized

Above we demonstrated that individual SONs were tonotopically organized. However, in most subjects we sampled a limited region of the SON. In order to map the tonotopic organization of the entire SON, we standardized the reconstructed SONs and the locations of the neuronal recordings and analyzed this combined dataset. To combine data from all 19 reconstructed SONs, locations of the recording sites were converted into normalized distances along three orthogonal axes in the SON (see Materials and Methods). These normalized coordinates allowed all recording sites to be mapped in a standardized SON.

Because the presence and arrangement (linear or nonlinear, single or multiple gradients) of the tonotopic organization in SON were unknown, we performed principal component analysis (PCA) on the combined dataset to determine the appropriate dimension(s) to observe the possible tonotopic organization. The first principal component accounted for 72% of the variance in the data (Fig. 6D). Visualizing this component in three spatial dimensions (Fig. 6A–C, gray arrows) revealed that it was dorsoventrally oriented and followed the gradient of CFs in the SON. These results suggest that frequency is organized in a gradient along one dimension in the SON.

To quantitatively model the tonotopic organization in the combined dataset, we performed MRA by using both linear and log equations. A linear equation (Eq. 1) best fit the combined dataset, finding a significant but not strong correlation ($r^2 = 0.62$, $P < 0.01$) between CF and location within the SON. The regression function suggests a predominantly dorsoventrally oriented tonotopic axis in SON (Fig. 6A–C, black arrow). Supplemental Movie 2 shows the 3D standardized SON with CF of recording sites and the orientations of the first principal component and regression function, rotating around

the dorsal-ventral axis. Comparing the predicted and measured CFs, we found that error magnitude ($|CF_{predicted} - CF_{measured}|$) varied widely at each position along the calculated tonotopic axis (Fig. 6E). We performed these same analyses on a dataset including only isolated neuronal recording sites (Fig. 6D,E, red). The results of both PCA and MRA were similar to the results obtained from the complete dataset. Both the large error magnitude and the relatively low r^2 value suggest that the frequency map in the SON is not as precise as the tonotopic organization in other brainstem auditory nuclei in the same species (Rubel and Parks, 1975).

Next, we examined the possibility that the relatively low r^2 values reflected particular regions of the SON that did not match the predicted frequency organization. To address this possibility, the standardized SON was sliced into five sections containing approximately the same number of recording sites using isofrequency planes (inset in Fig. 6F). Sections were collapsed along the tonotopic axis into 2D, and MRA showed no significant relation between these 2D locations of recordings and CF ($P > 0.05$ for MRA of all slices). Also, CF was not correlated with medial-lateral (Fig. 6F) or anterior-posterior (Fig. 6G) location in these sections, but varied widely throughout these slices. Because we did not detect a pattern to the distribution of error across SON we did not pursue nonlinear analyses.

To compare the location of regions of SON involved in processing different ranges of stimulus frequencies, we visualized the location of low (CF<1120 Hz, n = 219), intermediate (1120 Hz < CF < 2,460 Hz, n = 233) and high (CF > 2,460 Hz, n = 207) CF neuronal responses (Fig. 7). As expected from the analyses of the tonotopic organization, the low CF sites were densely distributed in the dorsal SON (Fig. 7A), whereas the high

CF sites were densely distributed in the ventral SON (Fig. 7C). Intermediate CF sites were densely distributed in a band through the middle of the SON (Fig. 7B). When viewed in the horizontal plane (Figs. 6C, 7, bottom) the CF distribution within these three broad divisions of CF appeared quite random.

2.4.5 Distribution patterns of response patterns in SON

We examined the spatial distribution patterns of isolated neurons with onset or sustained response patterns. Suppressed responders were encountered too infrequently to assess their spatial distribution. As shown in Figure 8A, both onset and sustained responders were located throughout SON. In addition, the distributions of onset and sustained responders were similar across the tonotopic axis derived from the regression function (Fig. 8B). By using MRA, we examined the tonotopic organization of onset and sustained responders separately. Both neuronal types showed a dorsal (low CF) to ventral (high CF) tonotopic organization (Fig. 8C, Table 1). These results suggest that onset and sustained types of neuronal responses are not distributed in separate regions or patterns, but instead are interspersed throughout SON.

2.5 Discussion

We investigated the tonotopic organization and neural response properties in the SON, the primary source of inhibitory inputs to auditory nuclei in the avian dorsal brainstem. We generated a quantitative 3D map of the relationship between the characteristic frequency (CF) and anatomical coordinates by using predictive statistical methods. This map is required for future investigation of functional roles of the SON, in particular those involving interactions between frequency representation and coding of other acoustic features. This map contains three main observations: 1) sound frequency is linearly

mapped approximately dorsal-ventral across SON; 2) this tonotopic organization is less precise than that of the other nuclei in the auditory brainstem, suggesting that inhibitory function in this avian auditory circuitry does not depend on precise tuning; and 3) neurons with sustained or onset response patterns are interspersed throughout the SON in all CF regions. These findings are consistent with proposed roles of the SON in regulating firing rate and frequency tuning of its targets. In the sections below, we first compare the quantitative mapping methods used in the current study with other quantitative methods that have been applied in topographical mapping. Next we compare physiological properties of SON with other auditory centers in birds in relation to their role in auditory information processing. Finally, we relate SON circuitry to inhibitory function in mammalian auditory brainstems.

2.5.1 Comparison of quantitative mapping methods

This work follows a long history of studies attempting to map frequency tuning and other physiological features of auditory structures (Clopton et al., 1974; Rubel and Parks, 1975; Sanes et al., 1989; Bajo et al., 1999; Cohen and Knudsen, 1999). In these studies, 3D auditory structures were often collapsed along assumed inconsequential dimensions into lower (one or two) dimensional projections from which all analyses were performed. Laminar structures such as sensory epithelium and cortical areas are usually suited for 2D analyses. However, sensory centers in other regions of the brain more often have complex 3D structures. Traditional analyses based on 2D projections of these complex structures are not able to provide complete and accurate knowledge of their organization. Quantitative constructions of topographic maps in 3D, such as the approach we adopted to map the SON, offer a number of advantages: 1) no loss of information from dimension

reduction; 2) visualizing the dataset and model in 3D; 3) creating an expandable database; and 4) comparing structures between experimental groups or between species.

We used two complementary methods, PCA and MRA, to analyze the topography of SON features. Both methods produced similar results from the standardized dataset. A key application of PCA is data analysis of an unknown, but potentially low-dimensional system. In the current study, PCA produced low-dimensional reductions of the tonotopic organization from seemingly complex data collected in the SON, when equations governing this organization were not known.

In addition to PCA, we used MRA to examine the relation between location and frequency tuning in the SON. Generally, in different auditory nuclei this relationship can be best described by different regression functions, such as linear, log, or power (Clopton et al., 1974). Our results demonstrated that the tonotopic organization of SON was best fit by linear functions, similar to other studied auditory nuclei in chicken (Rubel and Parks, 1975; Heil and Scheich, 1985). This linear relationship, as opposed to a log relationship often observed in auditory centers, is probably a consequence of the limited frequency range of hearing in chickens (Gray and Rubel, 1985; Saunders and Salvi, 1993) relative to most mammals (Masterton et al., 1969).

2.5.2 3D tonotopic map of SON

Most individual cases showed recording locations organized tonotopically from low frequencies in the dorsal SON to high frequencies in the ventral SON. The analyses of two cases showed no tonotopic organization, probably due to a limited number of recording sites in one case (100810) and a few aberrant recording sites in the other case (110228). When the standardized SON was analyzed, the multilinear regression function

accounted for 60% of the variability in the dataset, an indicator of the precision of this topographical map. This degree of precision is notably less than the coefficient of determination (r^2), calculated from the basilar papilla, NL, nucleus magnocellularis (NM), and Field L in chickens (Rubel and Parks, 1975; Ryals and Rubel, 1982; Heil and Scheich, 1985; Manley et al., 1987), but similar to those quantified in the lateral superior olive, inferior colliculus, medial geniculate nucleus, and auditory cortex in cat (Clopton et al., 1974) and in Field L complex in canary (Terleph et al., 2006). Finally, we found that neurons with the two most common response types, sustained and onset, are interspersed throughout the SON. Each type forms a complete tonotopic representation, and these maps show similar spatial arrangements. Thus, the SON appears to process at least two types of information in parallel.

Two features common to all auditory nuclei studied in the bird brainstem including the SON are: 1) that only a single frequency representation is found for each nucleus (Rubel and Parks, 1975; Koppl, 2001); and 2) that the tonotopic map preserves the topographic organization of the sensory epithelium without magnification or compression (Ryals and Rubel, 1982; Manley et al., 1987).

2.5.3 Possible functions of SON

Firing patterns of SON neurons to ipsilateral tones appear to be shaped primarily by the inputs from the NA, one of two main excitatory inputs to the SON. First, physiological response patterns of SON neurons closely resemble those of NA neurons. Both nuclei include sustained and onset responders and diverse frequency-level response maps (Sachs et al., 1978; Moiseff and Konishi, 1983; Warchol and Dallos, 1990; Lachica et al., 1994; Carr and Soares, 2002; Soares et al., 2002; Koppl and Carr, 2003; Fukui et al., 2010;

Coleman et al., 2011). Second, response thresholds in SON are similar to CF-matched NA neurons, whereas NM neurons may have slightly higher thresholds (Sachs et al., 1978; Warchol and Dallos, 1990; Coleman et al., 2011). Although the SON most closely resembles the NA physiologically, we cannot exclude contributions from the NL. It is possible that sustained responders in the SON may derive their responses from NL inputs. NL neurons, in turn, inherit their monaural physiological characteristics from NM neurons, which include primary-like response patterns and simple V-shaped tuning curves. Also, we did not assess the binaural response properties of SON neurons in this study, which could reveal a currently unexplored contribution from NL's projection to SON response properties.

One proposed function of the SON is lateral sharpening of frequency tuning in its target neurons within the NM, NA, and NL. An *in vivo* physiological study revealed that inhibitory input to the NM is more broadly tuned than excitatory input to the NM (Fukui et al., 2010). Whether this broadly tuned inhibition results from a few broadly tuned SON inputs or the convergence of many narrower tuned inputs remains to be determined. Because frequency selectivity (e.g., Q10 dB values) varies widely between SON neurons, encompassing the range of Q10 dB values reported for NA and NM neurons (Warchol and Dallos, 1990), the convergence of SON inputs to the NM accounting for the broad tuning cannot be accurately predicted from the data available. In the NL, the breadth of inhibitory tuning remains unknown; however, anatomical studies demonstrated a broad topographic organization of the SON-NL projection in marked contrast to the NM-NL projections, which innervate highly restricted regions of the tonotopic axis (Young and

Rubel, 1983; Tabor et al., 2011). This projection pattern suggests an anatomical substrate for lateral sharpening of frequency tuning in NL neurons.

How the diverse response properties of SON neurons to pure tone stimuli affect the neuronal activity in this circuit remains unknown. The majority of SON neurons show a sustained response to tones with their firing rate reflecting stimulus intensity. This pattern is well suited to regulate the gain of the circuit, a function that has been implied for SON (Peña et al., 1996; Burger et al., 2005; Dasika et al., 2005). In addition, many neurons with sustained responses show phase-locking, which may provide temporally patterned inhibition to the network (Coleman et al., 2011). Timed inhibition is important for computing interaural timing differences in the gerbil medial superior olive (MSO) (Brand et al., 2002; Grothe, 2003); however, its role in the avian auditory brainstem has not been tested.

2.5.4 Comparison with mammals

The mammalian auditory system does not appear to have an exact homolog or analog to the SON. Instead, mammals have multiple nuclei that provide inhibition to the auditory brainstem and the inner ear. These nuclei, which may include the medial nucleus of the trapezoid body (MNTB) and a number of periolivary nuclei, provide a similar range of functions to the SON in birds. Our current view is that the SON enables binaural balancing of neural activity (Burger et al., 2005; Dasika et al., 2005; Fukui et al., 2010; for review, see Burger et al., 2011) that is essential for brainstem processing of low-frequency binaural information used for sound localization. In addition, the SON provides feedback inhibition to the NL and the cochlear nuclei (Lachica et al., 1994; Yang et al., 1999; Monsivais et al., 2000; Burger et al., 2005), and feed-forward

inhibition to the lateral lemniscus (LL) and midbrain (Conlee and Parks, 1986; Westerberg and Schwarz, 1995; Wild et al., 2009). In rodents, binaural balancing is performed by the lateral olivocochlear efferents (Groff and Liberman, 2003; Darrow et al., 2006).

Feedback inhibition to all subdivisions of the mammalian cochlear nucleus is provided by glycinergic and GABAergic input from periolivary regions, in particular, the contralateral ventral nucleus of the trapezoid body, and the ipsilateral MNTB and lateral nucleus of the trapezoid body (LNTB) (Adams, 1983; Spangler et al., 1985; Schofield, 1994; Warr and Beck, 1996; Ostapoff et al., 1997). Inhibition to MSO (analogous to NL) is provided by MNTB and LNTB (Cant and Hyson, 1992; Grothe and Sanes, 1993). Feed-forward inhibition to LL and the auditory midbrain is provided by a combination of the various nuclei, including the MNTB, LNTB (Yavuzoglu et al., 2010), and superior periolivary nucleus (also named the dorsomedial periolivary nucleus) in mammals (Kadner and Berrebi, 2008; Saldana et al., 2009; Kopp-Scheinpflug et al., 2011). The comparatively simple organization of inhibition in the avian auditory brainstem makes this an appealing model for studying the roles of inhibition in auditory processing in vertebrates.

2.6 Figures and Tables

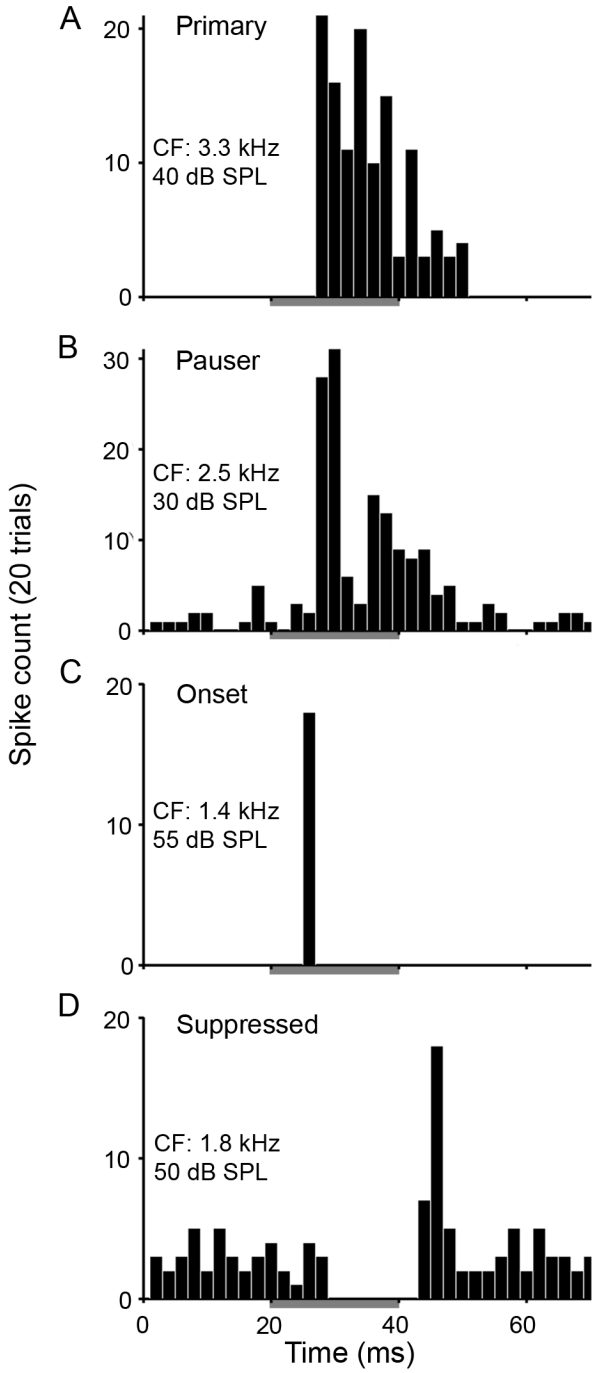

Figure 1. SON neurons show three classes of response patterns to ipsilateral tones. Post-stimulus time histograms constructed from responses to 20 presentations of CF tones at 20 dB above response threshold. See histograms for CF of neurons and stimulus intensity. **A–D:** Histograms show sustained (including primary-like [A] and pauser-like [B] types), onset (C), and suppressed (D) firing patterns. Gray bars indicate 20-ms tone presentations with 5-ms rise and fall times for triangle-shaped envelopes. Binwidth: 2 ms.

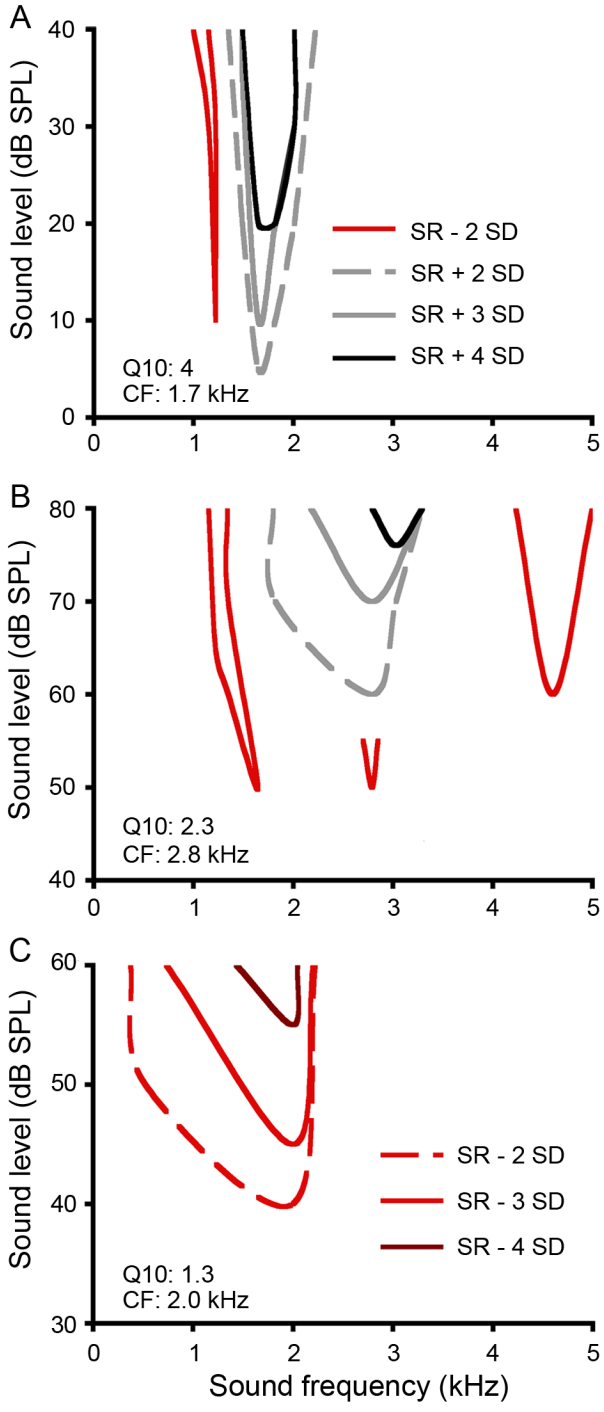
A
Sound level (dB SPL)
40
30
20
10
0
0
1
2
3
4
5
SR - 2 SD
SR + 2 SD
SR + 3 SD
SR + 4 SD
Q10: 4
CF: 1.7 kHz
B
Sound level (dB SPL)
80
70
60
50
40
Q10: 2.3
CF: 2.8 kHz
C
Sound level (dB SPL)
60
50
40
30
SR - 2 SD
SR - 3 SD
SR - 4 SD
Q10: 1.3
CF: 2.0 kHz
Sound frequency (kHz)

Figure 2. SON neurons show complex frequency response maps to ipsilateral tones. **A,B:** Response maps of two sustained responders. Contours represent boundaries of excitatory responses 2 SD above spontaneous firing rate (SR) indicated by gray dashed lines (the criterion used to determine response threshold at CF), 3 SD above SR (gray solid lines), and 4 SD above SR (black lines). Complex patterns of frequency or level-dependent suppression of responses are indicated by red lines (2 SD below SR). **C:** Response map of a suppressed responder. Contours represent boundaries of suppression 2 SD below SR (red dashed line; the criterion used to determine response threshold at CF), 3 SD below SR (red solid line), and 4 SD below SR (dark red line). All responses were assessed with 20- or 40-ms tones with 5-ms rise and fall times for triangle-shaped envelopes. Abbreviations: CF, characteristic frequency; SR, spontaneous firing rate.

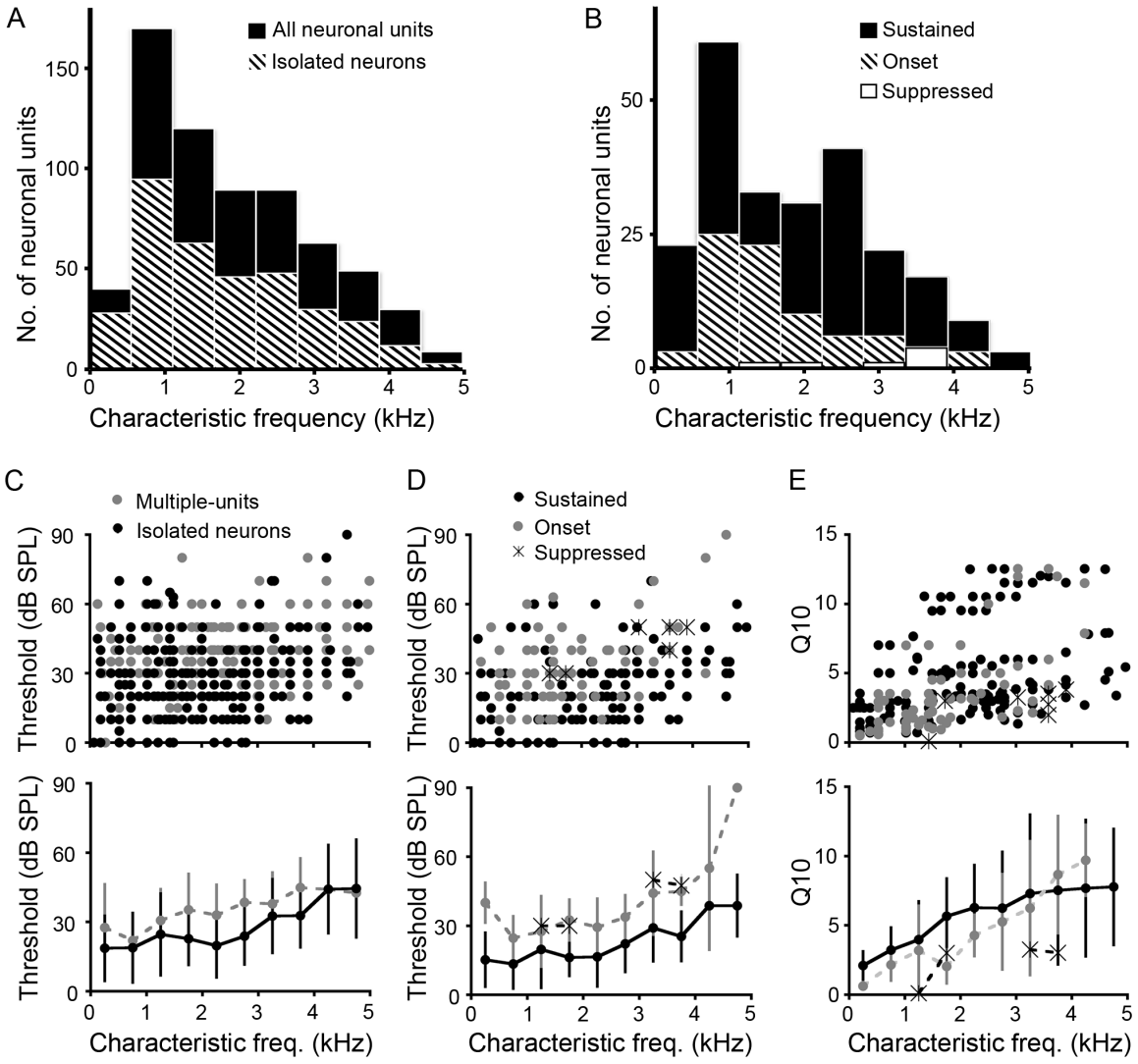

Figure 3. Heterogeneity of response properties to ipsilateral tones is expressed across CF in SON.

A: Histogram of CFs for all neuronal responses (black) (mean ± SD, CF: 1,947 ± 1,198 Hz, n = 659) and isolated neuronal responses (striped; 1,834 ± 1,170 Hz, n = 349). **B:** Histogram of CFs for sustained (black; 1,870 ± 1,214 Hz, n = 233), onset (striped; 1,690 ± 1,031 Hz, n = 80), and suppressed (white; 2,975 ± 994 Hz, n = 7) isolated neuronal responses (binwidth: 600 Hz). **C:** Scatterplot showing response threshold as a function of CF for each recording site (top panel) and mean thresholds shown below for both multiple units (gray) and isolated neurons (black; multiple-unit threshold: 34 ± 15 dB, n = 310; isolated neurons: 24 ± 16 dB). **D:** *Top panel*, scatterplot showing distribution of thresholds as a function of CF for sustained (black dots), onset (gray dots), and suppressed (asterisks) neurons. *Bottom panel* shows that overall, mean thresholds for both onset and sustained neurons increase with CF. **E:** Scatterplot (top) and mean ± SD (bottom) Q10 values showing a mild increase as a function of CF for each response type (Q10 values: sustained, 5 ± 3.6; onset, 3.7 ± 3.4; suppressed, 2.6 ± 1.3). C–E bottom, binwidth: 500 Hz.

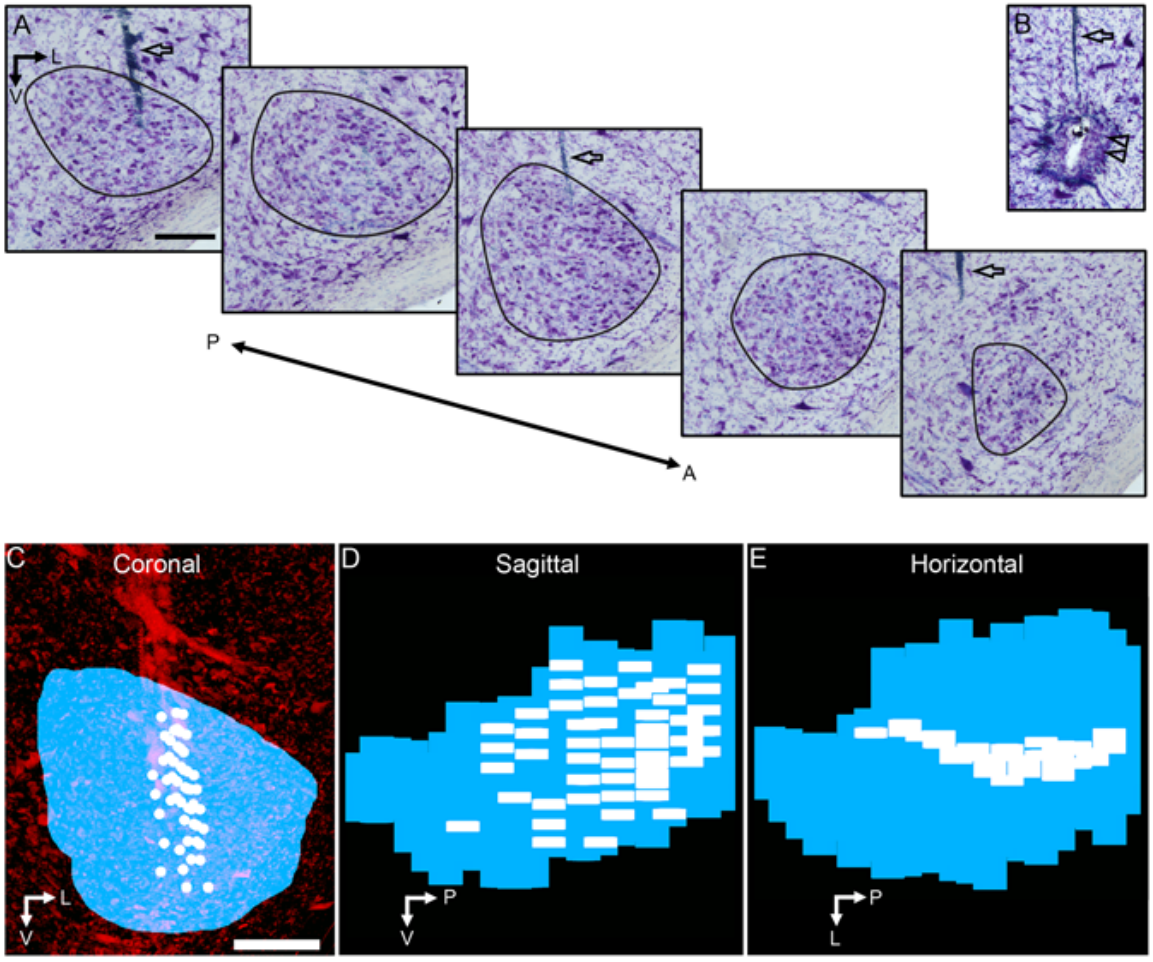

Figure 4. 3D reconstruction of the SON and locations of neuronal recordings.
A: Series of Nissl-stained sections through the SON; black lines define SON borders. **B:** Electrolytic lesion site (double arrowheads) used to map recording sites to tissue. Open arrows (in A and B) indicate electrode tracks. **C–E:** 3D reconstruction of the SON (blue) and location of neuronal recordings (white) shown in coronal (C), sagittal (D), and horizontal (E) views. C shows the ventral brainstem stained for Nissl substance (red). Abbreviations: A, anterior; L, lateral; P, posterior; V, ventral. Scale bars = 200 μm in A (applies to A, B); in C (applies to C–E).

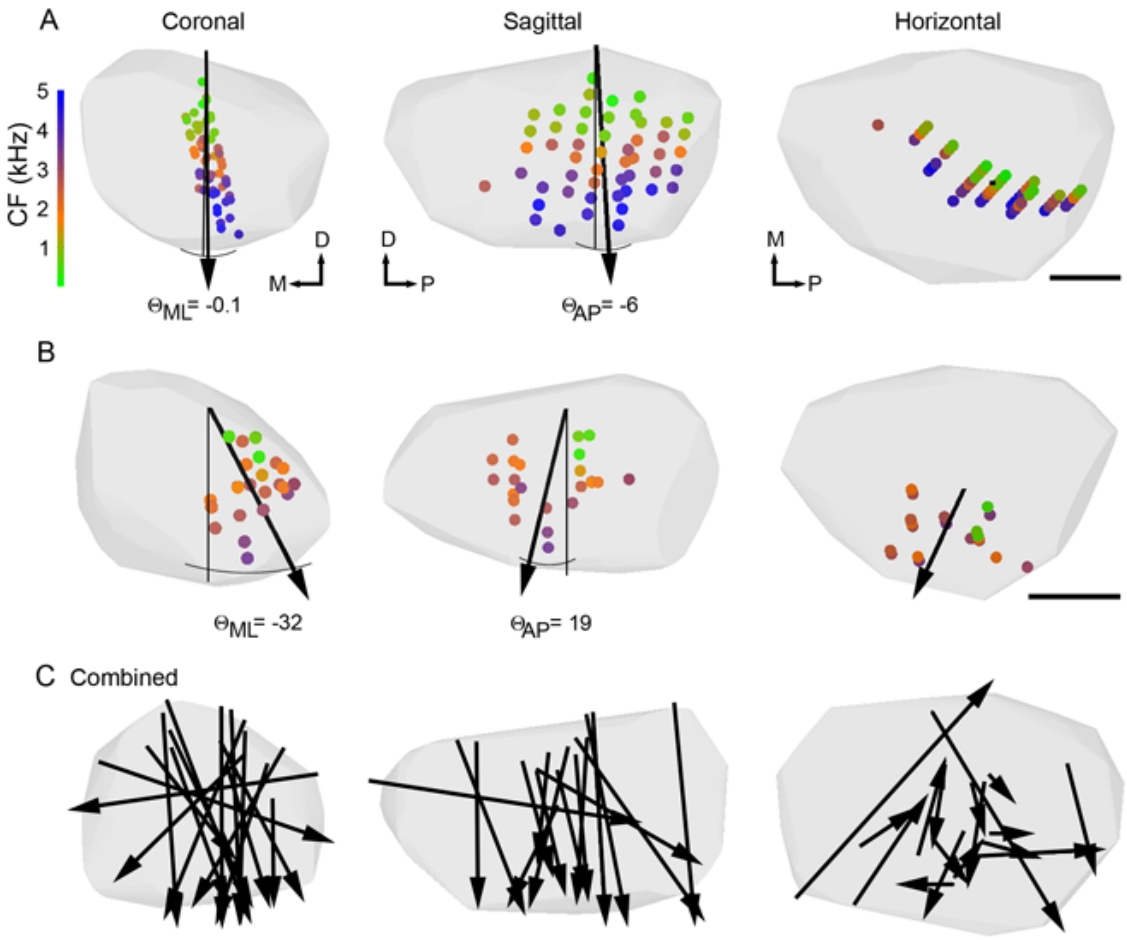

Figure 5. Individual SON reconstructions show tonotopic organization.
Coronal, sagittal and horizontal views of individual SON reconstructions indicated by the gray hulls. **A,B:** Small circles show locations of neuronal recordings color-coded to represent CF (color scale at left). Black arrows show orientation of tonotopic axes derived from MRA. Arrowheads point toward high CFs. Angles between the dorsal-ventral axes (thin black lines) and tonotopic axes in the medial-lateral (θ_{ML}) and anterior-posterior (θ_{AP}) dimensions are indicated. θ values for all cases are listed in Table 1. A shows case 100811 with 51 recordings sites, the same SON reconstruction presented in Figure 4. B shows case 100729 with 24 recordings sites. **C:** Coronal, sagittal, and horizontal views with arrows indicating predicted tonotopic axes from individual SONs (n = 17 of 19) combined on a single SON reconstruction. Each arrow intersects the center of mass of the recording sites in its case. Lengths of arrows approximate the extent of the SON in that direction sampled in each case. Abbreviations: CF, characteristic frequency; D, dorsal; M, medial; P, posterior. Scale bar = 200 μm in A,B.

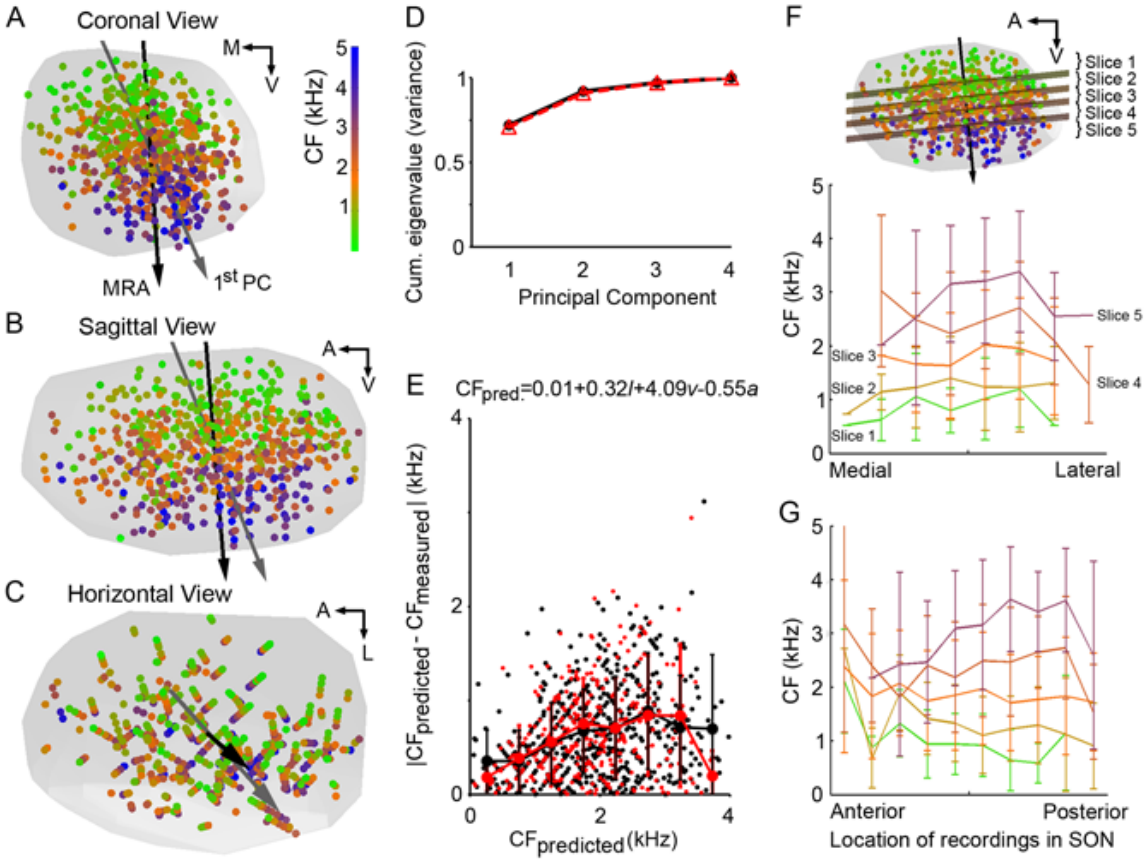
A
Coronal View
M
V
CF (kHz)
5
4
3
2
1
MRA
1st PC
B
Sagittal View
A
V
C
Horizontal View
A
L
D
Cum. eigenvalue (variance)
1
0.5
0
1
2
3
4
Principal Component
E
CFpred=0.01+0.32l+4.09v-0.55a
|CFpredicted - CFmeasured| (kHz)
4
2
0
0
2
4
CFpredicted (kHz)
F
A
V
Slice 1
Slice 2
Slice 3
Slice 4
Slice 5
CF (kHz)
5
4
3
2
1
0
Slice 5
Slice 4
Slice 3
Slice 2
Slice 1
Medial
Lateral
G
CF (kHz)
5
4
3
2
1
0
Anterior
Posterior
Location of recordings in SON

Figure 6. Standardized SON with all recording sites superimposed shows a linear tonotopic organization.
A–C: Recording sites (circles) from 19 animals combined on a standardized SON (gray hull) and presented in coronal (A), sagittal (B), and horizontal (C) views. Sites color-coded by CF (color scale in A). Orientation of regression function (black arrows) and first principal component (gray arrows) pointing to high CF regions. Both analyses show dorsal-ventral tonotopic organization across the SON. **D:** Cumulative eigenvalues from PCA performed on complete set of recordings sites (solid black line) or sites of isolated neuronal recordings (triangles, dashed red line). The first principal component accounts for 72% (all sites) or 71% (isolated neuronal sites) of the variance of these distributions. **E:** Magnitude of error of estimate ($|CF_{predicted} - CF_{measured}|$) versus predicted CF determined by MRA. MRA performed on all recording sites (black circles) and isolated neuronal sites (red circles). Mean ± SD shown as a function of predicted CF (binwidth: 500 Hz). Black lines connect mean errors of all recordings. Red lines connect mean errors of isolated neuronal recordings. See E for multilinear regression equation, where $CF_{pred.}$ is the characteristic frequency in kHz, *l* is the normalized medial-lateral coordinate (lateral edge is 1), *v* is the normalized dorsal-ventral coordinate (ventral edge is 1), and *a* is the normalized anterior-posterior coordinate (anterior edge is 1). **F,G:** Planes orthogonal to the multilinear regression function dividing SON sites into five slices (see inset in F) encompassing the following CF ranges: 1) $CF_{predicted} < 1{,}204$ Hz, n = 132 sites; 2) 1,204 Hz < $CF_{predicted} < 1{,}698$ Hz, n = 131; 3) 1,698 Hz < $CF_{predicted} < 2{,}129$ Hz, n = 131; 4) 2,129 Hz < $CF_{predicted} < 2{,}632$ Hz, n = 131; 5) 2,632 Hz < $CF_{predicted}$, n = 134. CF versus medial-lateral (F) or anterior-posterior (G) location in the SON plotted for each slice. Mean ± SD shown for bins of 10% of total dimensional distance. Abbreviations: CF, characteristic frequency; A, anterior; L, lateral; M, medial; V, ventral.

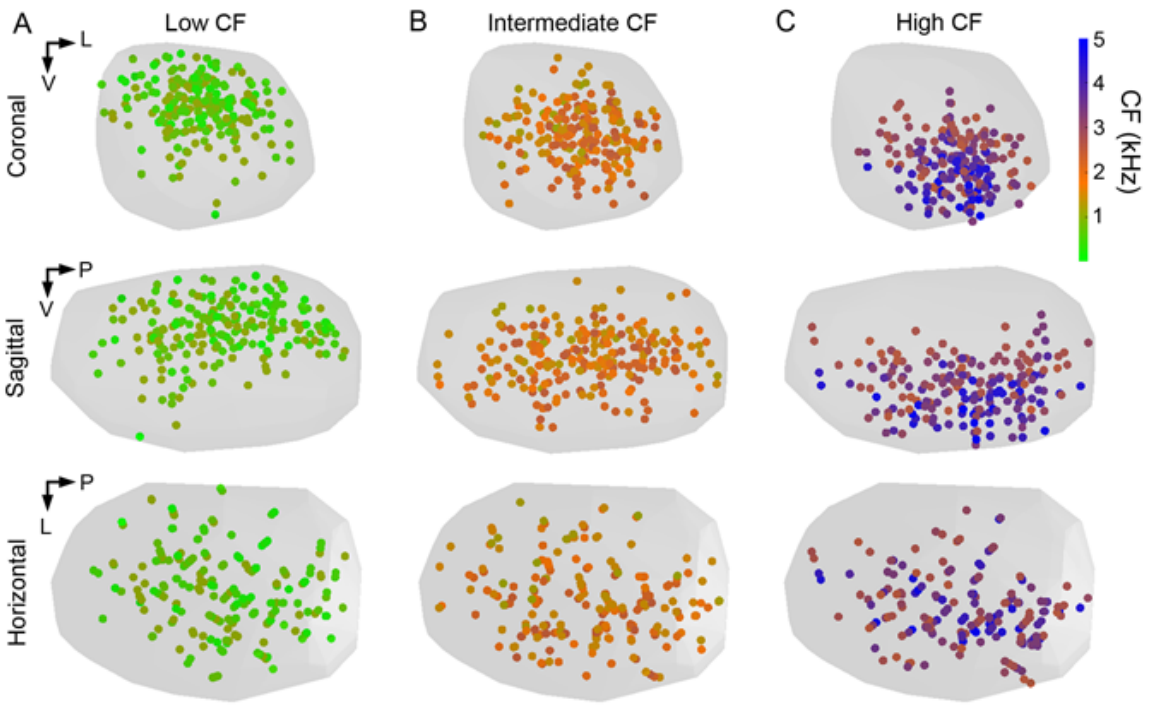

Figure 7. Distributions of low, intermediate, and high CF recording sites are separated in the standardized SON.
Circles show locations of neuronal recordings color-coded to represent CF (color scale at right). **A:** Standardized SON populated with the locations of low CF (CF < 1,120 Hz, n = 219) recording sites shown from the coronal (top), sagittal (middle), and horizontal (bottom) views. **B,C:** Locations of intermediate CF (1,120 Hz < CF < 2,460 Hz, n = 233) and high CF (CF > 2,460 Hz, n = 207) recordings sites, respectively. Abbreviations: CF, characteristic frequency; L, lateral; P, posterior; V, ventral.

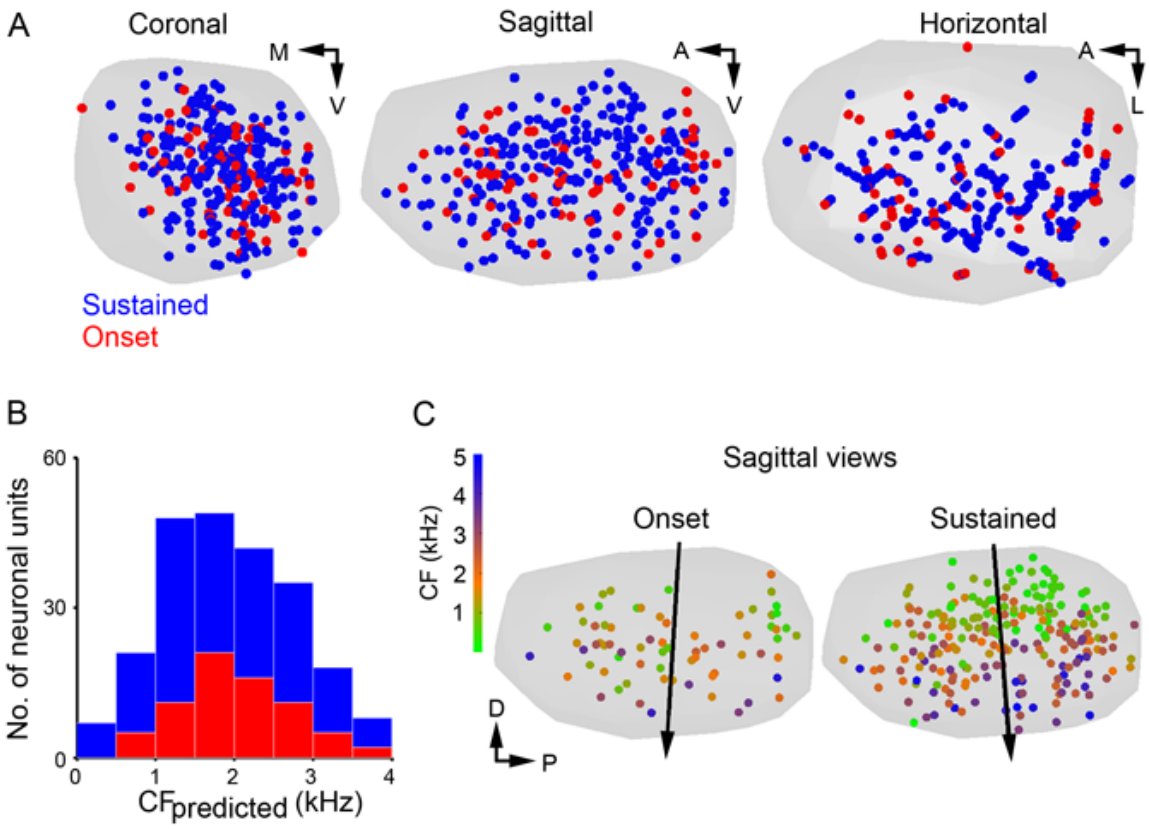

Figure 8. Sustained and onset responders are interspersed throughout the SON. **A:** Coronal (left), sagittal (center), and horizontal (right) views of a standardized SON (gray hull). Locations of sustained (blue circles) and onset response patterns (red circles) for isolated neuron recordings are shown. No differences were observed in the distribution pattern of sustained and onset responders. **B:** Histograms of predicted CF of sustained (blue) and onset (red) responders confirm broad and similar distributions for each type across the tonotopic axis. **C:** Sagittal views of standardized SON (gray) showing locations of neurons with onset (left) and sustained (right) responses color-coded by CF. See color scale at left. Black arrow indicates orientation of tonotopic axes determined by MRA. Both sustained and onset responders share a dorsal (low CF) to ventral (high CF) tonotopic distribution. Abbreviations: CF, characteristic frequency; A, anterior; D, dorsal; L, lateral; M, medial; P, posterior; V, ventral.

Table 1. Individual superior olivary nucleus (SON) reconstructions and standardized SON show tonotopic organization[1]

Case	No. of recording sites	CF mean±SD (Hz)	Sampled region of SON	Regression function type	R^2	F value	*P* value	Θ_{M-L} (°)	Θ_{A-P} (°)
100726	21	1864±800	L	linear	0.51	5.8	<0.01	-0.8	39.8
100727	55	1612±975	A, P & L	linear	0.51	17.7	<0.001	-19.5	-19.9
100729	24	2328±869	L	linear	0.62	10.7	<0.001	-31.5	19.1
100801	59	1475±944	A, P & M	linear	0.6	28.1	<0.001	-42.2	7.7
100803	75	1992±1352	A, P & M	linear	0.61	36.5	<0.001	-28.6	5.6
100804	25	2101±1527	P	linear	0.81	30.6	<0.001	-5.6	-17.8
100810	12	2542±1107	P				>0.05		
100811	51	2478±1453	P	linear	0.85	86.7	<0.001	-0.1	-5.8
100812	67	1770±1228	M	linear	0.58	28.6	<0.001	-4.6	-5.7
100813	28	1493±860	P	linear	0.83	39.4	<0.001	-23.8	-8.4
100816	19	1786±1008	M & L	log	0.49	48	<0.05	51	-6.9
100817	29	1773±1333	P & L	linear	0.69	18.1	<0.001	2.3	-49.8
100818	13	2055±1207	A	linear	0.86	18.5	<0.001	83.1	-52.6
110224	32	2452±1216	P	linear	0.67	18	<0.001	-73.7	-39.5
110226	43	1889±1102	M	log	0.67	26.9	<0.001	-30.8	-3.6
110228	21	2040±1108	A				>0.05		
110301	24	2400±1124	A & L	linear	0.6	9.9	<0.001	34.2	-28.3
110302	30	1847±940	P & L	linear	0.51	8.9	<0.01	19.7	-21
110303	31	2117±1018	A	linear	0.59	7.9	<0.01	17.4	-0.2
Mean±SD	35±19	1992±344			0.65 ±0.13			-4.4 ±38	-12±24
Combined	659	1935±1210	Entire SON	linear	0.62	182	<0.001	-4.5	-7.7
Onset	80	1690±1031	Entire SON	linear	0.45	8.6	<0.01	-5.9	3.5
Sustained	233	1870±1214	Entire SON	linear	0.64	68.3	<0.001	-2.7	-4.4

[1]Statistics presented for the regression function (linear or log) with the greatest r^2 value. Positive Θ_{M-L} values indicate tonotopic axes oriented from dorsolateral to ventromedial compared with dorsal-ventral axis. Positive Θ_{A-P} values indicate tonotopic axes oriented from dorsoposterior to ventroanterior compared with dorsal-ventral axis. F value used to test significance of the MRA. Abbreviations: A, anterior; L, lateral; M, medial; P, posterior.

Chapter 3
TOPOGRAPHY AND MORPHOLOGY OF THE INHIBITORY PROJECTION FROM SUPERIOR OLIVARY NUCLEUS TO NUCLEUS LAMINARIS IN CHICKEN (*GALLUS GALLUS*)

3.1 Abstract

The avian nucleus laminaris (NL) is involved in computation of interaural time differences (ITDs) that encode the azimuthal position of a sound source. Neurons in NL are bipolar, with dorsal and ventral dendritic arbors receiving input from separate ears. NL neurons act as coincidence detectors that respond maximally when input from each ear arrives at the two dendritic arbors simultaneously. Computational and physiological studies demonstrated that the sensitivity of NL neurons to coincident inputs is modulated by an inhibitory feedback circuit via the superior olivary nucleus (SON). To understand the mechanism of this modulation, the topography of the projection from SON to NL was mapped, and the morphology of the axon terminals of SON neurons in NL was examined in chickens (*Gallus gallus*). *In vivo* injection of AlexaFluor 568 dextran amine into SON demonstrated a coarse topographic projection from SON to NL. Retrogradely labeled neurons in NL were located within the zone of anterogradely labeled terminals, suggesting a reciprocal projection between SON to NL. *In vivo* extracellular physiological recording further demonstrated that this topography is consistent with tonotopic maps in SON and NL. In addition, three-dimensional reconstruction of single SON axon branches within NL revealed that individual SON neurons innervate a large area of NL and terminate on both dorsal and ventral dendritic arbors of NL neurons. The organization of the projection from SON to NL supports its proposed functions of controlling the overall activity level of NL and enhancing the specificity of frequency mapping and ITD detection.

3.2 Introduction

Common components of neuronal networks in the central nervous system include long-distance excitatory projections and local inhibitory connections. In addition, inhibition can also be provided by long-range connections between separate nuclei, such as the GABAergic connection from the deep cerebellar nucleus to the inferior olive (Hesslow, 1986; Nelson et al., 1989) and the GABAergic projections from diverse cell populations in the caudal diencephalon and brainstem to the superior colliculus (Appell and Behan, 1990). However, little is known about how long-range inhibitory projections are organized. In the auditory system, a few inhibitory long-range pathways have been studied, including 1) the GABAergic aural dominance bands in the inferior colliculus arising from bilateral projections of the dorsal nucleus of the lateral lemniscus in cat (DNLL; Shneiderman et al., 1988); 2) the well-described precise tonotopic connection from the medial nucleus of the trapezoid body (MNTB) to the lateral superior olive in mammals (LSO; Boudreau and Tsuchitani, 1968; Sanes and Rubel, 1988); and 3) the GABAergic projection from the superior olivary nucleus (SON) to nucleus laminaris (NL) in the chicken brainstem (Lachica et al., 1994; Yang et al., 1999; Burger et al., 2005). The SON projection to NL provides an opportunity to study the organization of inhibitory input in a system in which the excitatory circuit is precisely organized and well characterized. Additionally, understanding the organization of SON inhibition will provide insight into the role of NL neurons in azimuth sound localization. Here, we investigate the topography of the GABAergic projection from SON to NL.

Interaural time differences (ITDs), the submillisecond differences in the arrival time of sound to the two ears, are a critical cue for binaural localization of sound sources.

The avian NL, similar to the mammalian medial superior olive (MSO), is the first neural center to receive excitatory input from both ears. The chicken NL is composed of a compact monolayer of bitufted neurons with segregated dorsal and ventral dendrites. Excitatory input from either the ipsilateral or the contralateral ear is relayed in a phase-locked manner through nucleus magnocellularis (NM) and conveyed to the dorsal or ventral dendritic arbor, respectively (Parks and Rubel, 1975; Smith and Rubel, 1979; Young and Rubel, 1983). Individual NL neurons are sensitive to changes in ITDs, responding maximally when input from the ipsilateral and contralateral NM arrives at the two dendritic arbors simultaneously (Carr and Konishi, 1990; Overholt et al., 1992). In addition, NL is characterized by systematic shifts of frequency representation, tonotopy, along its rostromedial to caudolateral axis (Rubel and Parks, 1975). Orthogonal to its tonotopic map, NL is arranged by preferred ITD such that neighboring neurons have adjacent receptive fields along the azimuth (Parks and Rubel, 1975; Young and Rubel, 1983, 1986; Köppl and Carr, 2008).

A fundamental requirement for NL neurons to localize sound effectively is to remain sensitive to ITDs across a large dynamic range of firing rates of their inputs. The firing rate of NM fibers increases threefold or more with increasing sound level (Warchol and Dallos, 1990). One mechanism that preserves ITD sensitivity in NL across sound levels is inhibitory feedback (Nishino et al., 2008). GABAergic inhibitory inputs are abundant on the cell body as well as both dorsal and ventral dendritic laminae of NL (Carr et al., 1989; Code et al., 1989). The inhibitory input arises from a small population of interneurons in the surrounding neuropil (von Bartheld et al., 1989) and a prominent projection from the ipsilateral SON (Lachica et al., 1994; Yang et al., 1999; Burger et al.,

2005). SON receives excitatory input from the ipsilateral NL and nucleus angularis (NA) and provides inhibition to the ipsilateral NL, NM, and NA (Lachica et al., 1994; Yang et al., 1999; Monsivais et al., 2000; Burger et al., 2005). Using a computational model of the avian auditory brainstem network, previous studies demonstrated that sound-level-dependent feedback inhibition from the SON can significantly expand the dynamic range of the avian ITD coding system and improve ITD sensitivity (Peña et al., 1996; Dasika et al., 2005).

Individual SON neurons project to multiple ipsilateral target nuclei and thus provide an interaction between the auditory pathways specialized for processing temporal features (NM to NL) and the pathways that process other aspects of sound (Burger et al., 2005). In addition, a separate population of SON neurons projects to the contralateral SON, which has been suggested to serve to decrease the effects of level imbalances to the two sides (Burger et al., 2005).

The physiological properties of the SON allow these neurons to integrate inputs over long time periods and to respond to the overall activity level of their inputs, instead of encoding precise temporal information about the stimulus structure. Compared with NM neurons, chicken SON neurons show poor phase locking and relatively long time constants and excitatory postsynaptic potential (EPSP) durations (Lachica et al., 1994; Yang et al., 1999; Kuo et al., 2009). Furthermore, direct stimulation of the SON evokes a GABA-mediated inhibition in NL neurons lasting on the order of tens to hundreds of milliseconds (Hyson et al., 1995; Funabiki et al., 1998; Yang et al., 1999; Monsivais et al., 2000; Lu and Trussell, 2001; Monsivais and Rubel, 2001), in contrast to the rapid glutamatergic responses (Raman et al., 1994). In NL, GABAergic input from the SON

has been shown to reduce the amplitude and shorten the glutamatergic EPSPs, which may facilitate coincidence detection of the bilateral excitatory inputs (Peña et al., 1996; Funabiki et al., 1998; Yang et al., 1999). This slow inhibition of the glutamatergic response by GABAergic input is consistent with the presumed role of the SON in regulating the gain of the network in order to maintain temporal sensitivity in NL, particularly over variations in sound level.

Although physiological and computational studies have established the critical role of inhibition in ITD coding, the neuronal mechanisms remain unknown. Is the SON regulating NL in a frequency-specific manner or an ITD-specific manner? Is the SON-NL loop homotopic, such that an NL neuron receives inhibitory feedback from the same SON neurons to which it projects? Are SON arborizations confined to specific laminae in NL, suggesting independent regulation of input from each ear within this nucleus? Using *in vivo* anterograde and retrograde tract tracing methods, the current study examined the topography of the projection from SON to NL and determined the detailed morphology of SON terminals within NL. Our observations also raise the possibility of a tonotopic representation in SON.

3.3 Materials and methods

White leghorn hatchlings at postnatal days 4–6 were used for all experiments. All procedures were carried out in accordance with the National Institutes of Health *Guide for the care and use of laboratory animals* and were approved by the University of Washington Institutional Animal Care and Use Committee. All efforts were made to minimize pain or discomfort of the animals and to minimize animal numbers.

3.3.1 Surgery preparation

Chickens were anesthetized with an intramuscular injection of 40 mg/kg ketamine and 12 mg/kg xylazine. Throughout recording and injections, the animal's temperature was maintained at 40°C using a heating pad. The head was fixed to a head holder, and a metal rod was attached to the top of the cranium with dental cement. The skull was exposed, and a hole was made above the cerebellum.

3.3.2 In vivo recordings

Free-field sound stimuli were presented, and the sound pressure level was calibrated at the beginning of each experiment. The maximum sound intensity was 110 dB SPL and the sound frequency range was 100–6,000 Hz. Sound calibration and electrophysiological recordings were made in an electrically shielded, double-walled, sound-attenuated room. Acoustic stimuli were either pure-tone or white-noise pulses (200 msec duration, 2 msec rise and fall time for a triangular envelope, 3 pulses/second). The recording electrode was a glass micropipette (2–5 MΩ) filled with 5 mM AlexaFluor 568 dextran (D22913; Invitrogen, Eugene, OR) in 3 M sodium acetate. The recording electrode was inserted vertically 1.8–2.0 mm lateral to the midline and 0–0.5 mm rostral to the middorsal sinus. The SON was located by monitoring neuronal responses to a white-noise stimulus (80 dB SPL) while lowering the electrode into the brainstem using a motor driven micromanipulator (model PMC100; Newport, Irvine, CA). Neuronal action potentials were recorded extracellularly with a neuroprobe amplifier (model 1600; A-M Systems, Carlsborg, WA) and bandpass filtered between 80 Hz and 10 kHz (two-pole). Data were collected at 50 kHz sampling frequency with 12-bit resolution. Customized software (SPIKE; B. Warren, University of Washington, Seattle), written in Python, controlled sound presentation and data acquisition.

After isolating a unit or multiunit cluster from background noise, the best frequency (BF) was obtained. The BF was defined as the sound frequency, presented for 200 msec at 70 dB SPL, that elicited the greatest spike rate. Each stimulus was presented 20–30 times in a randomized sequence. For six cases, we obtained a tuning curve to a series of sound frequencies (15–25 frequencies at logarithmic intervals between 0.1 and 6 kHz, Fig. 1). Firing threshold was defined as the sound intensity that induced spiking greater than 2 SD above the spontaneous firing rate. Characteristic frequency (CF) was defined as the frequency with the lowest threshold. Spike sorting and analysis of frequency tuning curves were performed using customized software written by David M. Schneider (Columbia University, New York, NY) in MatLab (Mathworks; Natick, MA).

3.3.3 In vivo tracer injection

After the BF of a recording site had been determined, 100–500 nl of AlexaFluor 568 dextran was injected using a pressure device (PicoSpritzer III; General Valve, Fairfeild, NJ), followed by ionophoresis (positive current, 250 nA for 15–20 minutes). In early experiments, we observed that the combination of pressure and current injection methods resulted in increased transport of tracer to the distal axonal processes compared with the results of using either method alone. It also appeared that short-duration pressure pulses (<20 msec) resulted in relatively more anterograde labeling whereas longer duration pressure pulses (>100 msec) resulted in more retrogradely labeled NL neurons. After injection, the micropipette was retracted, the wound was closed, and the animal was allowed to recover.

3.3.4 Immunohistochemical staining

After a survival time of 2 days, animals were anesthetized with ketamine and xylazine and transcardially perfused with 0.9% saline, followed by chilled 4% paraformaldehyde (PFA) in phosphate buffer (0.1 M, pH 7.4). The brains were removed from the skull and postfixed overnight in PFA at 4°C.

Microtubulin-associated protein 2 (MAP2), glutamate decarboxylase 65 (GAD65), and gephyrin were immunolabeled using a procedure described by Wang and Rubel (2008). Briefly, brainstems were cut coronally at 60 or 300 μm using a Vibratome (TPI, St. Louis, MO), and sections were collected in phosphate-buffered saline (PBS; 0.01 M, pH 7.4). Free-floating sections were incubated with primary antibody solutions diluted 1:1,000 in PBS with 0.3% Triton X-100 and 5% normal goat serum overnight at 4°C, followed by incubation with AlexaFluor secondary antibodies (1:200; Invitrogen) for 2 hours at room temperature.

After immunohistochemistry, tissue sections were dehydrated in a series of ethanol steps and placed into a clearing solution (3:5 mixture of benzyl benzoate and methyl salicylate) to increase the optical transparency of fluorescently labeled tissue slices and to allow confocal images to be collected from the entire depth of the tissue slice (MacDonald and Rubel, 2008).

3.3.5 Antibody characterization

See Table 1 for a list of all antibodies used.

MAP2

Mouse anti-MAP2 monoclonal antibody (MAB3418; lot LV1486526; clone AP20; Chemicon, Temecula, CA) was raised against bovine brain MAP2 (aa 997–1332). The antibody was characterized by Western blot analysis, which showed that this antibody

stains high-molecular-weight MAP2 isoforms in adult rat of approximately 300 kD (manufacturer's technical information; Matsunaga et al., 1999). MAP2 associates with microtubules, neurofilaments, and actin filaments and is confined to neuronal cell bodies and dendrites, although small amounts were shown to exist in some axons (Caceres et al., 1984). Our staining results from chicken NL produced a pattern of MAP2 immunoreactivity similar to that described from previous studies (Wang and Rubel, 2008).

GAD65

Polyclonal anti-GAD65 (AB5082; lot LV1580833; Millipore, Billerica, MA) was raised in rabbit against human GAD65 from baculovirus-infected cells. According to the manufacturer's product information, this antibody reacts strongly with GAD65-containing nerve terminals and recognizes a 65-kD protein corresponding to GAD65 by Western blot of mouse brain extract. GAD65 is responsible for catalyzing the production of GABA from L-glutamic acid and is localized to the presynaptic cell membrane. The GAD65 immunolabeling pattern we observed in chicken NL is similar to the distribution pattern previously described for GABAergic synapses in chicken and owl NL; GAD65-positive puncta were located throughout NL and appeared densely distributed on the cell body and proximal dendritic laminae (Carr et al., 1989; Code et al., 1989; Code and Churchill, 1991; Nishino et al., 2008).

Gephyrin

Mouse monoclonal anti-gephyrin (147011; lot 147011/21; clone mAB7a; Synaptic Systems, Goettingen, Germany) was raised against purified rat gephyrin. By Western blot, this antibody stains the brain-specific 93-kD splice variant and was shown to detect

the N-terminus of gephyrin (manufacturer's technical information; Pfeiffer et al., 1984). Gephyrin is a postsynaptic scaffolding protein essential for synaptic clustering of inhibitory neurotransmitter receptors. Our staining results from chicken NL produced a pattern of gephyrin immunolabeling similar to the pattern of GAD65 immunostaining (see Fig. 9A) and the distribution pattern previously described for GABAergic synapses in chicken NL (Code et al., 1989; Code and Churchill, 1991; Nishino et al., 2008).

3.3.6 Fluorescence microscopy

Slices were imaged with an Olympus Fluoview FV300 confocal microscope (Tokyo, Japan) with ×25 (NA 0.8; oil) or ×60 (NA 1.4; oil) objectives. To determine the overlap of AlexaFluor 568 dextran and anti-GAD65 labeling, single optical planes (0.594 μm) of confocal images were analyzed offline in MetaMorph (Molecular Devices; Sunnyvale, CA) and Amira (Mercury Systems; Chelmsford, MA) software. Other image data were collected as z-series of images for offline analyses.

3.3.7 Imaging and data analyses

Four analyses were conducted to measure 1) the volume of the fluorescently labeled injection site in SON (n = 16 animals), 2) the distribution of anterogradely labeled axonal terminals in NL (n = 16 animals), 3) the distribution of retrogradely labeled cell bodies in NL (n = 17 cells), and 4) the morphology of individual axonal arborizations in NL (n = 5 arborizations). These measurements were performed on three-dimensional reconstructions of the nuclei, labeled terminals and neurons from serial confocal z-stack images containing SON or NL.

3.3.8 Reconstruction

Injection site

Serial z-stack images of the entire ipsilateral SON were aligned by using anatomical markers such as blood vessels and fluorescently labeled processes that crossed successive slices. The borders of an injection site were operationally defined by the coalesced appearance of labeling. Contours were traced around the injection site in the coronal plane at 10-μm intervals. Labeled cell bodies within SON but outside the injection site were observed occasionally and marked individually. Contours were concatenated to reconstruct the injection site volume in Neurolucida Explorer (MBF Bioscience; Williston, VT). The sizes of injection sites were measured based on the reconstructed volumes.

Terminal fields and cell bodies

Serial z-stack images containing NL were aligned by using anatomical markers as described above. Positions of retrogradely labeled cell bodies within NL were individually marked. The drawings were edited in Adobe Illustrator and Adobe Photoshop software (Adobe Systems, Mountain View, CA). Axon labeling in NL was reconstructed in three dimensions in Amira software. Occasionally we observed sparsely distributed, small satellites of anterograde label. We did not include these small satellites in calculations relating the positions of injections to the positions of terminal arbors. Examples of these small satellites are seen on the 2-kHz line and the 1-kHz line in Figure 2A,B, respectively. With this exception, all voxels included in the reconstructed images were weighted equally to calculate the center of mass of the labeled terminal distributions within NL. The area and tonotopic spread of the terminal labeling were based on planar projections reconstructed for each case.

To compare across animals, labeled terminal fields were transformed to fit a template of the NL planar projection. We represented the labeled terminal field within NL by drawing a contour circumscribing the terminals. Sparsely distributed, small satellites of anterograde label were not included inside this boundary. Transforming planar projections to the template caused a shift in the predicted CF range spanned by the terminal field (<200 Hz) that was less than the standard error of estimate calculated for the linear regression equation (281 Hz; Rubel and Parks, 1975; see below).

Calculating characteristic frequency from location within NL

The CFs of NL neurons were predicted from the linear relationship between CF and the mediolateral and rostrocaudal location in NL (Rubel and Parks, 1975; see Fig. 4A–C):

$$CF = 0.027r + 0.014m – 0.088,$$

where CF = predicted CF (in kHz) of the NL neuron, r = caudal-to-rostral percentile position in NL, and m = lateral-to-medial percentile position in NL. This regression analysis provides a robust prediction of the CF in NL and has been extensively used to categorize structural and functional properties of NL neurons and determine cellular and physiological specializations that vary across the tonotopic axis (Smith and Rubel, 1979; Smith et al., 1983; Lippe and Rubel, 1985; Parks et al., 1987; Reyes et al., 1996; Person et al., 2004; Kuba et al., 2005; Yamada et al., 2005; Nishino et al., 2008).

Nuclei borders

To calculate the percentage of SON or NL occupied by labeling, we reconstructed the entire nucleus. We traced the contours of the nucleus based on either background fluorescence or MAP2 immunoreactivity. Contours were traced at 10-μm intervals through coronal sections of the entire nucleus. The reconstructed SON volume was

divided by bisecting the mediolateral, dorsoventral, and rostrocaudal dimensions of SON. Only injection sites completely confined to a hemisphere of SON were categorized as medial (n = 8) or lateral (n = 3), dorsal (n = 5) or ventral (n = 4), rostral (n = 4) or caudal (n = 7) and included in the topographic analyses. To analyze the topography of SON projections, labeled terminal distributions in NL were compared between injection site positions in each of these dimensions.

Axonal arborizations

Arborizations of labeled individual SON axonal branches were reconstructed from serial coronal 300-μm sections in Amira software. Cut ends of an axon in one section were connected properly to the corresponding cut ends of the same axon in the successive section. Only axon branches that were well labeled and isolated from other axons were reconstructed.

3.3.9 Image processing

Digital images of selected sections and terminals were acquired using the confocal microscope. Images were further processed in Photoshop to enhance contrast and alter brightness. No corrections were made for tissue shrinkage, because the distribution of labeling, but not the absolute length or volume, was the focus of the current study.

3.3.10 Statistical analyses

Statistical evaluations were made via Mann-Whitney U test, linear regression analysis, and Spearman's ranked correlation coefficient analysis. Values are presented as mean ± SEM. In figures, an asterisk represents a statistical significance of $P < 0.05$.

3.4 Results

Data presented in the current paper resulted from small injections of a bidirectional tracer, AlexaFluor 568 dextran amine, into the SON *in vivo*. The criteria for inclusion of a case in this study were that the injection site resided completely within the boundaries of SON and occupied less than one-eighth of the total volume of SON. Small injection sites were necessary to elucidate whether the SON projections to NL were topographically organized. Among 16 such cases, injection sites were distributed throughout the dorsoventral, rostrocaudal, and mediolateral dimensions of SON. The organization and morphology of the projections from SON to the ipsilateral NL are the main focus of the current study. Observations and analyses of the labeling outside the ipsilateral NL are not presented.

3.4.1 Topographic organization of the SON-NL projection

In three cases, anterograde labeling occupied more than half of the area of NL (99%, 70%, and 60%), suggesting the existence of a nontopographic projection from SON to the ipsilateral NL (see Fig. 6A). In 13 cases, NL received a topographically organized projection from the ipsilateral SON. In these cases, the ipsilateral NL exhibited a relatively confined distribution of anterograde labeling, which occupied less than half of the area of the nucleus. The anatomical location of anterogradely labeled terminals in NL correlated with the location of the injection site in SON. Figure 2 demonstrates the labeling pattern of six representative cases. In all cases (Fig. 2A–F), the data are presented as the left side of the brain, with the lateral aspect to the left and rostral aspect toward the top of the figure. Within each panel, the location of the injection is shown in a series of coronal sections through SON arranged from rostral to caudal (left). The distribution of anterograde labeling in NL is shown both in serial coronal sections

through NL (center) and on planar projections of NL (right). Planar projections were constructed from the series of coronal sections to show a horizontal view of NL. CFs were calculated as described by Rubel and Parks (1975) and are shown in Figure 2A. BFs of the injection sites presented in Figure 2 ranged from 0.5 to 3.29 kHz. Figure 2A illustrates a case with an injection into the rostrodorsomedial SON. The BF recorded at the injection site in the SON was 0.5 kHz, lower than the CF region of NL spanned by labeled SON axons, 1–2 kHz. The predominant anterograde labeling was located in the caudomedial NL; however, a satellite of labeled axons was located more rostrally and laterally in NL. The observed satellite terminals in NL may result from either the main injection site or the labeled SON neurons whose cell bodies reside outside the main injection site. Figure 2B shows a small injection into the caudodorsomedial region of SON (BF 1.04 kHz) and anterograde label restricted to the caudal NL. The spatial position and extent of anterograde labeling were similar to those in Figure 2A. Figure 2C illustrates a case with an injection into the caudomedial SON (BF 1.2 kHz). The majority of anterograde label was located in the lateral NL between 1 and 2.5 kHz. In addition, a smaller satellite of labeled terminals was located more caudally in NL. Figure 2D illustrates a case with an injection into the rostrodorsomedial SON, similar to Figure 2A. In this case, the labeled terminal field was broadly distributed across the rostral NL. The BF of the injection site was 1.45 kHz. Figure 2E,F shows two cases with the injection sites (BF 2.0 kHz and 3.29 kHz, respectively) in the rostroventral SON. Both injections labeled axons innervating the rostral NL, but the case illustrated in Figure 2E showed more extensive labeling, possibly because the injection site, although small, covered more of the dorsoventral extent of SON at its rostral end. The frequency response curves

for the cases in Figure 2B,D,E are shown in Figure 1B,E,F, respectively. We were unable to determine whether SON neurons exhibiting inhibitory and excitatory frequency responses have different projection patterns because of the limited number of injections at locations of frequency-specific suppression (n = 2) and the multiple SON cells labeled by each injection.

To examine the topography of the SON-NL connections better, we compared the position of anterograde labeling in NL between cases in which injections were confined to one half of the SON. For these analyses, the SON was divided in half along the rostrocaudal, mediolateral, and dorsoventral axes, and all cases in which the injection was limited to any one hemisphere were included in the analyses presented in Figure 3. For each case, a contour circumscribing the labeled terminal field in NL was color coded to indicate the location of the injection site within the SON. Each panel of Figure 3 shows contours of terminal fields from all cases meeting the injection site criteria mapped onto a single planar projection of NL (gray). Distribution of terminal fields arising from injections restricted to either the rostral (n = 4) or the caudal (n = 7) half of SON showed no apparent separation, suggesting a lack of topography between the rostrocaudal axis of SON and anterograde terminals in NL (Fig. 3A). Similarly, extensive overlap of contours of terminal fields resulting from injections into either the medial (n = 8) or the lateral (n = 3) half of SON suggests no topography between the mediolateral axis of SON and anterograde terminals in NL (Fig. 3B). On the other hand, terminal fields from injections into either the dorsal (n = 5) or the ventral (n = 4) SON appeared reasonably well segregated, indicating a topographic projection from dorsal SON to caudal NL and from ventral SON to rostral NL (Fig. 3C).

Figure 4 shows quantification of 1) the relationships between the anatomical position of SON injection sites and the CFs of NL spanned by the labeled terminals (Fig. 4A–C) and 2) the relationships between the locations and BFs of injection sites within SON (Fig. 4D–F). These data are derived from the same cases shown in Figure 3. In Figure 3A–C, the lozenges and squares indicate tonotopic positions of the center of mass of the terminal fields. Bars represent the frequency range of NL innervated by labeled SON axons. Consistent with the illustrations in Figure 3, CFs of NL at the center of terminal fields were not significantly different between cases with caudal (average of cases: 1.92 ± 0.23 kHz; lozenges) and rostral (2.39 ± 0.38 kHz; squares) SON injection sites (Fig. 4A) or between cases with medial (1.62 ± 0.19 kHz; lozenges) and lateral (2.03 ± 0.36 kHz; squares) injection sites (Fig. 4B). In contrast, projections from the dorsal (lozenges) SON innervated a significantly lower frequency region of NL (1.56 ± 0.31 kHz) than projections from the ventral (squares) SON (2.72 ± 0.06 kHz; $P = 0.032$, U = 1.5, two-tailed; Fig. 4C). Figure 4D–F shows quantification of the organization of frequency tuning within SON. Lozenges and squares designate BFs at injection sites in SON. The BFs were not significantly different between recordings at caudal (1.46 ± 0.28 kHz) and rostral (1.81 ± 0.58 kHz) injection sites (Fig. 4D) or between BFs recorded from the medial (0.87 ± 0.14 kHz) vs. lateral (1.86 ± 0.71 kHz) SON (Fig. 4E). In contrast, we found a significant difference between the BFs recorded from the dorsal (0.86 ± 0.21 kHz) vs. ventral (2.75 ± 0.30 kHz) SON ($P = 0.016$, U = 0.00, two-tailed; Fig. 4F).

The results from Figures 3 and 4 indicate the SON-NL projections were topographically organized such that neurons of the ventral SON innervated the rostral NL

and neurons of the dorsal SON contacted the caudal NL. In addition, the dorsoventral axis of the SON appeared to be tonotopically organized; SON neurons with higher BFs were located ventrally, and SON neurons with progressively lower BFs were located more dorsally within the nucleus.

To examine further the topographic organization of the SON-NL projection in 15 cases, we ranked the cases by the location of the injection site along the dorsoventral, mediolateral, or rostrocaudal axis of SON. We found significant correlations between the ventral-to-dorsal ranking and the CF at the center of the terminal field ($r^2 = 0.61$, $P = 0.0006$) and between the lateral-to-medial ranking and the CF at the center of the terminal field ($r^2 = 0.37$, $P = 0.016$), but not between the rostral-to-caudal ranking and the CF at the center of the terminal field ($r^2 = 0.03$, $P = 0.532$; Supp. Info. Fig. 1).

3.4.2 Tonotopic organization of the SON-NL projection

To visualize the relationship between frequency tuning of SON neurons and the location of their axonal arbors in NL, Figure 5A shows contours of SON terminal fields (n = 15) mapped onto a single planar projection of NL (gray). One case was excluded from the analysis because it showed anterograde labeling extending across the entire tonotopic axis in NL and no tonotopicity of the SON-NL projection. The color of the contours represents the BF recorded at the injection site using a color scale (Fig. 5A, left). Terminal fields largely occupied the caudal two-thirds of NL following tracer injections in SON locations with low BFs (Fig. 5A, cool colors). In contrast, terminal fields mostly occupied the rostral two-thirds of NL following injections in locations with high BFs (Fig. 5A, warm colors). Figure 5B shows the BF at the injection sites plotted against the frequency range of NL innervated by anterogradely labeled terminals. The CF of NL at

the center of the terminal labeling was correlated with the BF recorded at the injection site in SON ($r^2 = 0.68$, $P < 0.001$, n = 15). The six representative cases illustrated in Figure 2 are indicated with an asterisk in Figure 5B.

The data presented above indicate that the projection from SON to NL is topographically, and tonotopically organized. On the other hand, organization of this inhibitory projection appears to be far less precise than the excitatory pathway from NM to NL (Parks and Rubel, 1975; Young and Rubel, 1983). Although this conclusion agrees with previous findings using retrograde labeling methods (Burger et al., 2005), it could also result from diffusion and uptake of tracer through a much greater volume of SON than we detected. If the extent of the terminal fields in NL was governed largely by the size of the injection site in SON, then there should be a correlation between these parameters. The scatterplots shown in Figure 6 suggest that there was no reliable relationship between the size of the injection sites in SON and the overall area (Fig. 6A) or tonotopic extent (Fig. 6B) of the anterograde labeling in NL. All of the injection sites in SON were relatively small (less than 12.5% volume of SON), yet the spatial extent of anterograde labeling in the ipsilateral NL varied greatly, ranging from 8% to 99% the area of NL. Therefore, the tonotopic organization of the SON projection to NL was not a reflection of the tracer injection methods.

3.4.3 Distribution of retrogradely labeled NL neurons

In vivo tracing methods used in this study were optimized for anterograde transport of tracer; however, in seven cases, we observed retrogradely labeled NL neurons. Eighty-eight percent (15 of 17) of retrogradely labeled NL neurons were positioned within the anterogradely labeled terminal field. Figure 7 is an image of the intermediate CF region

of NL showing a retrogradely labeled NL neuron (open arrowhead) surrounded by labeled SON axonal arbors (solid arrowheads). These observations suggest that NL neurons receive inhibitory input from roughly the same region of SON that they contact.

3.4.4 Morphology of SON axonal arborizations in NL

We confirmed that SON axons innervated the rostrocaudal and mediolateral extent of NL and that these terminals were distributed throughout the dorsal, ventral, and cell body laminae of the nucleus. Figure 8 shows a section through NL double-labeled with AlexaFluor 568 dextran amine (yellow) following an injection into SON, and MAP2 immunolabeling (red) illustrating dendrites and cell bodies of NL neurons. The monolayer arrangement of NL neurons is apparent with the dorsal dendrites above and the ventral dendrites below the cell body lamina. We observed that SON axons enter NL from both the dorsal and the ventral sides and that thin SON axon branches wind through NL, forming large varicosities on all laminae.

SON axonal swellings in NL are GABAergic. In six cases, following *in vivo* injections labeling SON axons projecting to NL, tissue sections were immunostained against GAD65 to visualize the distribution of GABAergic terminals along the labeled SON axonal arbors. To test the specificity of the GAD65 antibody, we colabeled NL using an antibody against the GABAergic postsynaptic marker gephyrin (Fig. 9A). The evident colocalization of GAD65- and gephyrin-positive puncta suggests that the GAD65 antibody is labeling GABAergic terminals. The merged images in Figure 9D,E show that bouton-like varicosities along the axons colocalized with GAD65 labeling, suggesting that these varicosities were GABAergic terminals. To control for random overlap of GAD65-positive puncta and labeled axonal terminals, the GAD65 image was rotated 90°

clockwise before merging with the image of labeled SON axons (Fig. 9F). The GAD65-positive puncta rarely overlapped the labeled SON terminals in the rotated image.

3.4.5 Morphology of individual SON axonal arborizations in NL

The morphology of five isolated SON axonal branches was investigated in greater detail. It is unknown how much of the SON neuron's total axonal arbor was represented by the branches we describe below because we were not able to trace an axon back to its cell body in SON. However, we were able to follow each SON arbor to a single large-diameter axon outside NL. Figure 10 shows two representative SON axonal branches innervating high- and low-CF regions of NL. The SON axonal arborizations formed bouton-like axonal swellings across all laminae of NL regardless of whether they innervated the caudal, low-CF region of NL (Fig. 10A) or the rostral, high-CF region of NL (Fig. 10B).

We calculated the CF ranges of NL innervated by individual SON axonal branches. In contrast to excitatory inputs that innervate a narrow frequency band of NL, SON inhibitory inputs ramify broadly across the tonotopic axis (312 ± 74 μm, 0.86 ± 0.6 kHz, n = 5). This average distance (312 μm) represents about one-third of the total distance along the tonotopic axis (Seidl et al., 2010). The spread of SON arborizations across the mediolateral axis varies widely (448 ± 298 μm, n = 5), accounting for over half of this axis on average. Thus, it is likely that single axons ramify broadly within NL.

Burger et al. (2005) used retrograde tracing methods to show that single SON neurons innervate multiple auditory nuclei. We confirmed this finding by observing that individual SON axons formed branches and bouton-like structures within NL and NM (not shown) or NL and NA. Figure 11 shows an SON axon (white) that formed branches

and bouton-like swellings through the lateral edge of NL, exited NL, and innervated NA, where it formed an intricate arborization. The borders of nuclei are indicated with dotted lines. The axonal varicosities located in NL and NA are enlarged and presented in Figure 11B,C, respectively. One possibility is that labeled arborizations innervating multiple auditory brainstem nuclei did not necessarily originate from SON neurons but originated from neurons that were retrogradely labeled and sent axon collaterals into NL and NM or NA. On the other hand, no study has reported an axon projection from NA coursing through NL or NM, and NL axons do not send collaterals to NM or NA (Burger et al., 2005). Hence our working hypothesis is that SON axons often project to multiple ipsilateral nuclei in the dorsal brainstem.

3.5 Discussion

The aim of these experiments was to understand better the anatomical organization of inhibitory input to the low-frequency sound localization circuit in birds. The present study demonstrates that the GABAergic projection from superior olivary nucleus (SON) to nucleus laminaris (NL) is organized in a broad tonotopic pattern. Single SON axonal arborizations terminate on both dendritic laminae as well as the cell body layer and extend across large regions of NL. The SON-NL feedback loop is homotopic; NL neurons receive inhibitory input from the same region of the SON to which they project. In addition, our data demonstrated that single SON neurons project to multiple ipsilateral nuclei in the auditory brainstem, which is consistent with a previous study (Burger et al., 2005). Below we compare the topographic organization of the SON-NL connection to inhibitory projections in other auditory systems and to the excitatory inputs to NL and discuss functional implications of the SON axonal arbor organization in NL.

3.5.1 Methodological considerations

In this study, the structural patterning of the axonal projection from SON to NL was examined by using *in vivo* anterograde and retrograde tract tracing methods. In several cases, we were able to isolate and reconstruct axonal arbors that originated from single SON axons. Because the anterograde tracing methods used in this study did not allow the reconstruction of an SON axon from its origin at the soma, the total extent of axonal arbors of single SON neurons could not be determined.

Labeling of axonal terminals in NL following injections into SON was considered to be due to uptake of the tracers by SON neurons because no other known inputs to NL pass through or nearby SON in chickens. Recent studies reported a sparse projection from the ventral nucleus of the lateral lemniscus to NL in zebra finches (Wild et al., 2009, 2010). This projection is not GABAergic, whereas labeled terminals in the current study express GAD65.

Retrogradely labeled neurons in NL may either innervate SON or extend their axons through SON before innervating the lateral lemnisicus and nucleus mesencephalicus lateralis pars dorsalis (Boord, 1968; Conlee and Parks, 1986; Takahashi and Konishi, 1988). However, the possibility of two populations of retrogradely labeled NL neurons does not affect our conclusion that the SON-NL feedback loop is homotopic, because the vast majority of labeled neurons, regardless of their nature, were found within the anterogradely labeled terminal fields.

3.5.2 Broad topography of the projection from SON to NL

The topography of long-range inhibitory projections has received relatively little attention. Studying the topographic organization of these pathways has provided critical

insights into the function of the inhibitory input in these systems. For example, the inhibitory connection from the deep cerebellar nucleus (DCN) to the inferior olive (IO) follows a precise topographic arrangement so that a closed loop is formed among neurons of the IO, DCN, and cerebellar cortex (Hesslow, 1986; Nelson et al., 1989). This arrangement forms independent inhibitory feedback loops that each regulates the background activity of a microzone of Purkinje cells to control cerebellar learning. We found that, in contrast to the DCN-IO connection, the SON shows a broad pattern of innervation within NL.

Another example of a long-range inhibitory pathway is the commissural projection between the two superior colliculi (SC). This GABAergic projection follows a heterotopic organization. The medial SC contacts neurons in the lateral region of the contralateral SC and the lateral SC projects to the medial contralateral SC (Takahashi et al., 2007). This heterotopic arrangement allows regions of the SC representing upward saccades to inhibit contralateral regions representing downward saccades and visa versa. In contrast, our findings suggest that NL neurons receive inhibitory feedback from SON neurons that they contact. However, based on the methods used in the present study alone, we were unable to determine the total number of SON cells contacting a single NL neuron or to ascertain what fraction of these SON neurons receives input from this single NL cell.

The mammalian auditory brainstem possesses well-characterized inhibitory projection pathways. Two well-studied examples are the projection from the medial nucleus of the trapezoid body (MNTB) to the lateral superior olive (LSO; Boudreau and Tsuchitani, 1968; Sanes and Rubel, 1988) and the projection from the MNTB to the

medial superior olive (MSO), the mammalian analogue to NL (Grothe and Sanes, 1993, 1994). Both inhibitory pathways are involved in sound localization circuits and show topographic organizations with precision similar to that of the excitatory inputs from cochlear nuclei to LSO and MSO (Werthat et al., 2008). This organization allows neurons in the MSO and LSO to integrate timing information from multiple inputs at specific frequencies.

Likewise, in the avian auditory brainstem, the excitatory input from nucleus magnocellularis (NM) to NL shows a precise topography, with narrow terminal arborization orthogonal to the tonotopic dimension (Parks and Rubel, 1975; Young and Rubel, 1983). In stark contrast to the precision of the NM-NL connection, GABAergic neurons in small regions of SON innervate extensive territories of NL. In most cases, SON axonal terminations were distributed in a broadly topographic manner; i.e., the ventral SON innervates primarily the rostromedial region of NL, and the dorsal SON neurons innervate mainly the caudolateral NL, but injection sites that appeared to occupy less than one-eighth of SON typically labeled terminal arbors covering 30–60% of the frequency axis of NL. When we were able to trace single SON axons as they entered NL, we found that they traversed about one-third (0.9 ± 0.6 kHz, n = 5) of the tonotopic axis of NL. Our observations suggest that the topography of SON to NL connection is mapped mainly in the dorsoventral axis but not in the rostrocaudal and mediolateral axes. Occasionally, small injection sites labeled axonal terminals that occupied an even larger area of NL, and once even the whole nucleus. Although the cause of this variability remains to be determined, it raises the possibility that the projection from SON to NL contains both nontopographic and broadly topographic projections. The potential

functional significance of these projection patterns is discussed below (see under Functional implications of the projection from SON to NL).

3.5.3 Tonotopic relationship of SON and NL

A fundamental organizing principle of auditory regions of the brain is tonotopy, the orderly representation of the sound frequency to which neurons are most sensitive. Tonotopy arises from the coding of frequency along the receptor organ and the topographic organization throughout the ascending auditory pathways. Physiological methods are usually necessary to map the tonotopic organization and frequency tuning of auditory nuclei, but the tonotopy of projections can be studied anatomically when the tonotopic organization of the target structure is known and injections are made at positions where recordings are made.

The precise tonotopic organization of NL in hatchling chickens was quantitatively mapped by Rubel and Parks (1975), and several investigators have used this map to assess other physiological and anatomical properties of this nucleus (see Materials and Methods). Our results demonstrate that, overall, the SON projection to NL shows a tonotopic organization, but the arrangement is considerably less precise than the bilateral excitatory inputs from NM to NL. The complete tonotopic spread of single axon arborizations has not been determined but these small injections along with reconstructions of single axonal branches suggest that some SON axons extend across one to three octaves of the tonotopic dimension of NL.

A better understanding of the affect of coarsely organized inhibition in NL on ITD detection will require detailed tonotopic mapping of the SON. Although the tonotopic organization of the avian SON has not been examined in detail, Moiseff and

Konishi (1983) reported a dorsal (low frequency) to ventral (high frequency) tonotopic organization in the barn owl. Our study suggests the existence of a similar tonotopic organization in hatchling chickens. We saw no evidence of a tonotopic representation in the rostrocaudal or mediolateral dimensions; however, these interpretations should be viewed as preliminary until a thorough three-dimensional tonotopic map is published.

3.5.4 Organization of individual SON axonal terminals within NL

Occasionally, small injections confined to a subregion of SON produced little overlap of labeled axons and allowed us to reconstruct large terminal branches of individual axons. We observed that individual SON arbors terminate in both the dorsal and the ventral dendritic laminae, as well as the cell body layer of NL, which is consistent with previous tracing and immunohistochemical studies showing that inhibitory terminals are distributed across all laminae of NL (Code et al., 1989; Code and Churchill, 1991; Lachica et al., 1994; Nishino et al., 2008). In contrast, inhibitory synapses in the mammalian MSO appear to be mostly confined to the cell bodies (Clark, 1969; Perkins, 1973; Kapfer et al., 2002).

We also observed that branches from a single SON axon extended across roughly one-third of the distance along the tonotopic axis and half of the mediolateral dimension of NL. The large spread of individual SON axonal branches is thus consistent with the broad topography of the inhibitory projection to NL that we observed.

The SON receives excitatory input from NL and nucleus angularis (NA) and provides inhibition to NL, NA, and NM (Lachica et al., 1994; Yang et al., 1999; Monsivais et al., 2000; Burger et al., 2005). Our reconstructions further showed that

individual SON neurons project to both NA and NL or to both NM and NL, corroborating previous conclusions by Burger and colleagues (2005).

3.5.5 Functional implications of the projection from SON to NL

Our results provide insight into the functional role of this inhibitory feedback circuit on frequency mapping and ITD detection. In the majority of cases, we found a broad topographic organization along the tonotopic axis of NL. This organization of inhibition is desirable to enhance the recognition of a target signal among competing background signals having similar spectral properties, as described by Lewicki (2002). In addition, in a few cases, we found a nontopographic SON-NL projection. This projection pattern may further regulate the overall gain of the NL responses. This arrangement is highly beneficial under conditions of high background noise. The organization of SON input may allow NL to adapt to the overall sound level of the acoustic environment, by resetting the gain of the system to an optimal position on the input–output function. This interpretation is supported by physiological data suggesting that SON neurons integrate inputs over a long time scale and provide relatively long-lasting inhibition to NL neurons (Yang et al., 1999; Monsivais et al., 2000). Our data are consistent with the proposed integrative role of the SON in controlling the gain of the ITD processing system, especially at high sound levels (Burger et al., 2005; Nishino et al., 2008; Nishino and Ohmori, 2009).

We found two SON units that displayed frequency-specific suppression of their spontaneous spike rates. The responses of these two units may be shaped by a strong frequency-specific inhibition from the contralateral SON. This SON-SON projection has been shown previously (Burger et al., 2005).

3.6 Figures and Tables

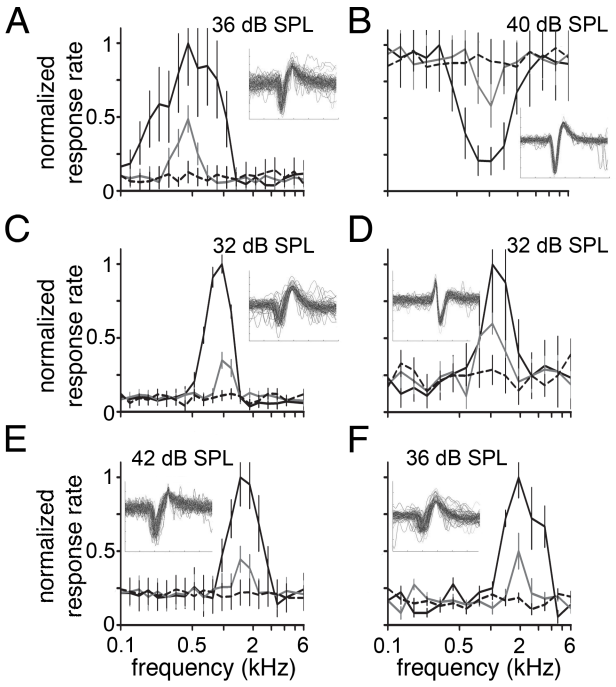

Figure 1. Normalized response to pure tones.
Firing rate as a function of tone frequency is plotted for six units recorded in the SON. Response rates to pure tones (0.1–6 kHz) presented at 70 dB SPL (black solid lines), threshold (gray lines), and 5 dB below threshold (black dotted lines) are shown. Each function (**A–F**) was normalized to the maximum firing rate obtained at 70 dB SPL; 85, 77, 98, 132, 88, and 90 spikes/sec, respectively. Error bars represent SEM and are shown for alternating data points for clarity. Threshold is noted at the top of each panel. **Insets** show 6-msec voltage traces of 100 overlaid waveforms. For five units (A,C–F), a single frequency evoked the maximum firing rate at both 70 dB SPL and threshold; BF = 0.49, 0.96, 1.04, 1.45, and 2.0 kHz, respectively. One unit (B) exhibited frequency-specific suppression. In this case, the BF (1.04 kHz) was defined as the frequency that induced the greatest suppression of spontaneous rate. Units were recorded from the SON immediately preceding tracer injection.

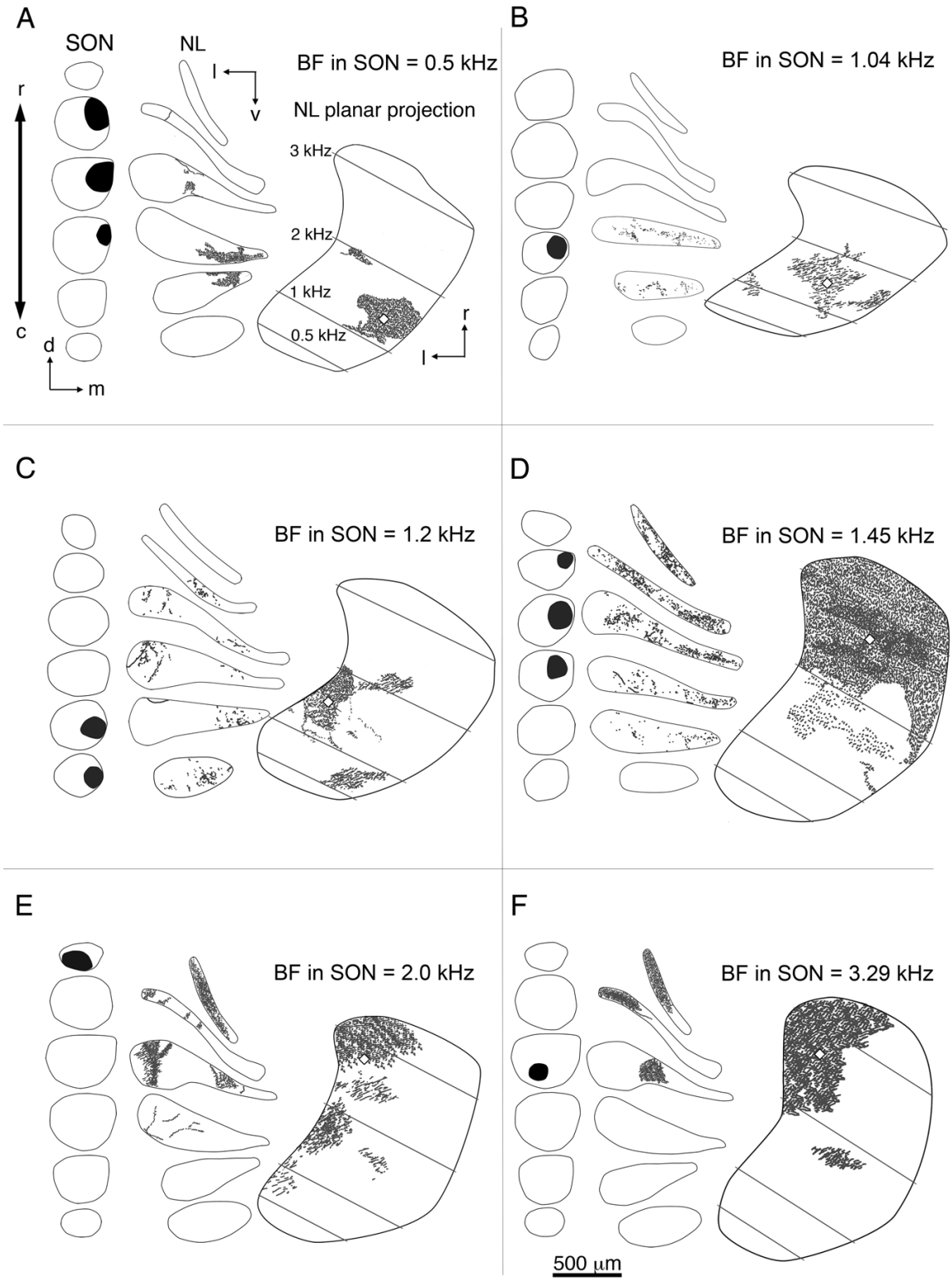
A
SON
NL
l
v
BF in SON = 0.5 kHz
NL planar projection
r
c
d
m
3 kHz
2 kHz
1 kHz
0.5 kHz
r
l
B
BF in SON = 1.04 kHz
C
BF in SON = 1.2 kHz
D
BF in SON = 1.45 kHz
E
BF in SON = 2.0 kHz
F
BF in SON = 3.29 kHz
500 μm

Figure 2. Line drawings depicting injection sites in SON of six representative cases that received a single injection and anterograde labeling in the ipsilateral NL.
Within each panel, the location of the injection (black areas) is shown in serial coronal sections through SON arranged from rostral to caudal (left). The distribution of anterograde labeling in NL (gray dashes) is shown in a series of coronal sections through NL (center) and on horizontal planar projection of NL (right). Black lines indicate the border of SON or NL. White lozenges represent the centers of mass of the terminal fields (see Materials and Methods). Gray lines indicate isofrequency bands across NL. Characteristic frequencies (CF) were calculated as described by Rubel and Parks (1975) and listed in A. BFs of the injection sites are listed at the top right of each panel. Examples show injections localized to the rostral (E,F), caudal (B,C), lateral (F), medial (A–D), dorsal (A,B,D), or ventral (F) SON. Anterograde labeling was found in rostral (D–F) or caudal regions of NL (A,B). E: This case shows anterograde labeling across the majority of the tonotopic axis in NL. For this case, the center of mass was determined using all anterograde labeling except for the small satellite of labeled terminals located in the 1.5-kHz CF region of NL. The frequency response curves of B,D,E are shown in Figure 1B,E,F, respectively. NL, nucleus laminaris; SON, superior olivary nucleus; BF, best frequency; c, caudal; d, dorsal; l, lateral; m, medial; r, rostral; v, ventral. Scale bar = 500 μm.

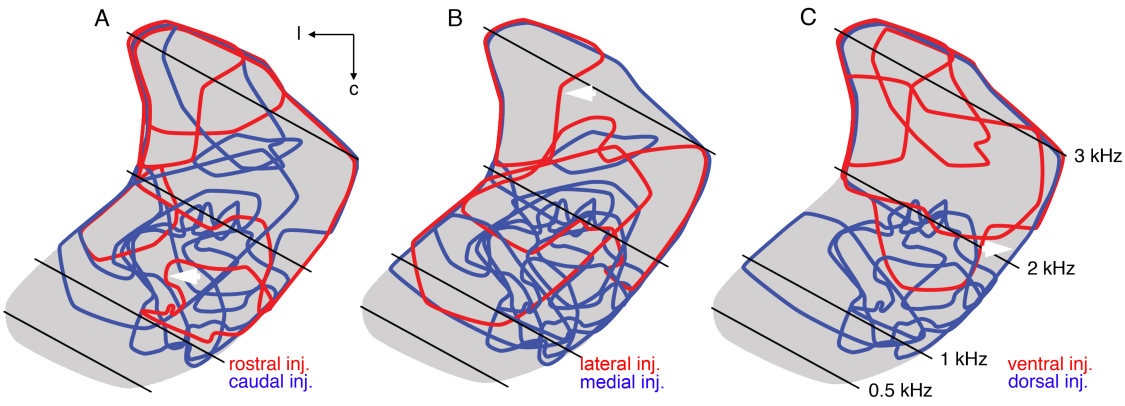

Figure 3. Comparative distribution of terminal fields in NL following injections into disparate halves of SON.
Contours of labeled terminal fields superimposed onto a single horizontal planar projection of NL (gray). Calculated CFs of the isofrequency bands (black lines) are listed in C. **A:** Distribution of terminal fields arising from injections restricted to either the rostral (red contours; n = 4) or the caudal (blue contours; n = 7) SON. No apparent separation of blue and red contours suggests no topography between the rostrocaudal axis of SON and anterograde labeling in NL. White arrow indicates red contour of terminal field illustrated in Figure 2A. **B:** Red and blue contours represent terminal fields following injections into lateral (n = 3) and medial (n = 8) SON, respectively. The red and blue contours overlap, suggesting no topography between the mediolateral axis of SON and anterograde terminal fields in NL. Arrow indicates red contour of terminal field illustrated in Figure 2F. **C:** Terminal fields from injections into dorsal (blue contours; n = 5) or ventral (red contours; n = 4) SON appear reasonably well segregated, suggesting a topographic projection from the dorsal SON to caudal NL and from the ventral SON to rostral NL. Arrow indicates blue contour of the terminal field illustrated in Figure 2D. NL, nucleus laminaris; SON, superior olivary nucleus; c, caudal; l, lateral.

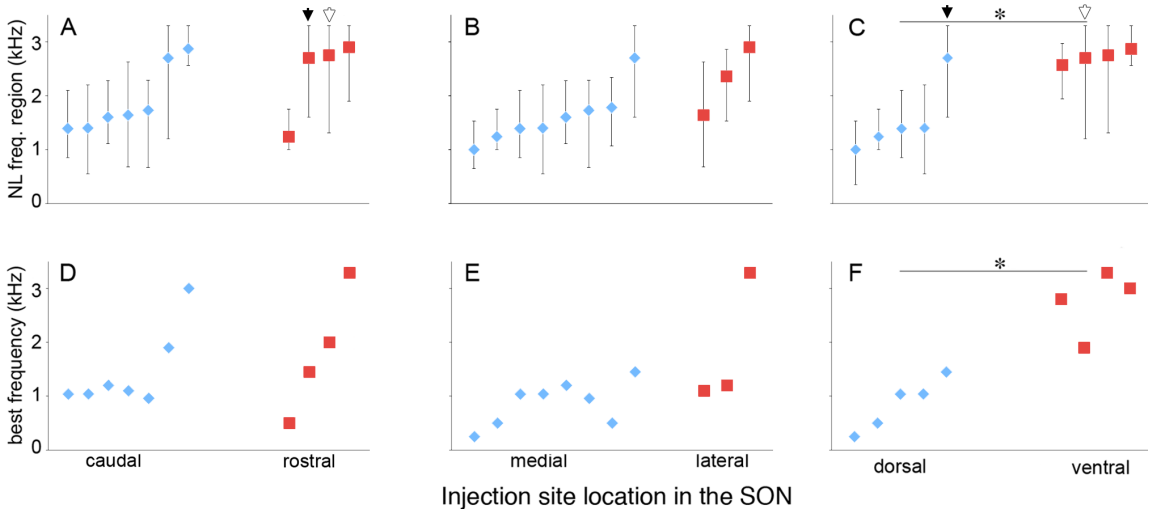

Figure 4. Topography of SON projections to NL. Cases are aligned along the abscissa by CF at the center of labeled terminal field in NL.
A–C: Extent of terminal fields across the frequency axis in NL. Lozenges and squares indicate tonotopic position of the centers of mass of the terminal fields (see Materials and Methods). Bars represent the frequency range of NL innervated by labeled SON axons. A: Cases with tracer injections localized to caudal (lozenges; n = 7) and rostral (squares; n = 4) SON. NL frequencies at the center of terminal fields were not different between rostral and caudal groups ($P = 0.53$). Black and white arrows indicate two cases with axonal labeling covering greater than half of the area of NL. B: Cases with medial (lozenges; n = 8) and lateral (squares; n = 3) injection sites. NL frequencies at the center of the terminal fields were not different between medial and lateral groups ($P = 0.50$). C: Cases with injections into dorsal (lozenges; n = 5) and ventral (squares, n = 4) SON. Projections from the dorsal SON innervated a lower frequency region of NL than projections from the ventral SON ($P = 0.032$). **D–F:** Lozenges and squares designate BFs at injection sites in SON. D: BFs of caudal injection sites (lozenges) and rostral injection sites (squares) were not significantly different ($P = 0.53$). E: BFs of medial (lozenges) and lateral (squares) injection sites were not significantly different ($P = 0.085$). F: BFs of dorsal (lozenges) injection sites were significantly lower than that of ventral (squares) injections ($P = 0.016$).

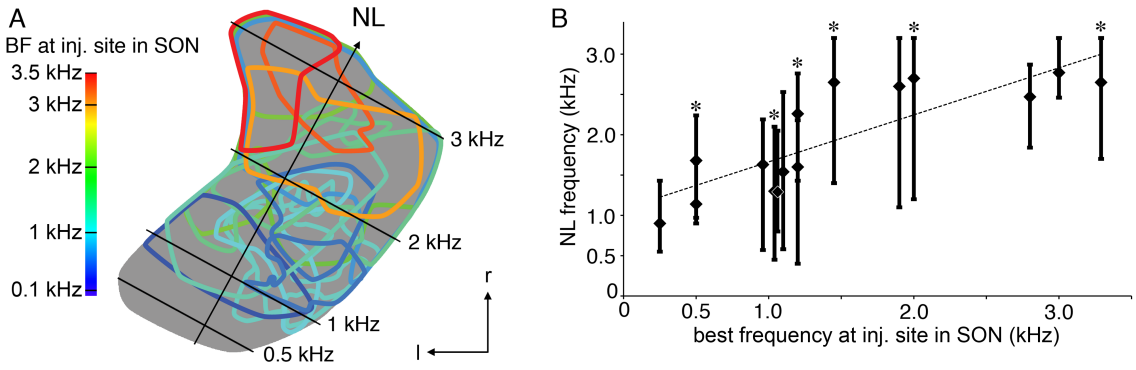

Figure 5. Tonotopic projections of the SON to NL.
A: Planar projection of NL illustrating tonotopic organization of the SON projection to NL. Calculated CFs of isofrequency bands (lines) and the tonotopic axis of NL (arrow) are shown. Distribution of SON terminal fields (n = 15 animals) mapped onto a single planar projection of NL (gray). The color of the contours represents the BF recorded at the injection site in SON using a color scale (left). **B:** Tonotopic position of labeled terminal fields in NL correlates with BF recorded at injection site in SON ($r^2 = 0.68$, $P < 0.001$, n = 15). For each case, the BF at the injection site is plotted against the CF of NL innervated by anterogradely labeled terminals. Lozenges indicate the CF of NL at the center of mass of the terminal field; bars indicate the CF range of NL innervated by the terminal field. For one of the two cases with BF = 1.04 kHz, the BF is slightly offset to 1.06 kHz and the center lozenge is outlined in white for visualization. Asterisks identify cases illustrated in Figure 2. NL, nucleus laminaris; SON, superior olivary nucleus; BF, best frequency; l, lateral; r, rostral.

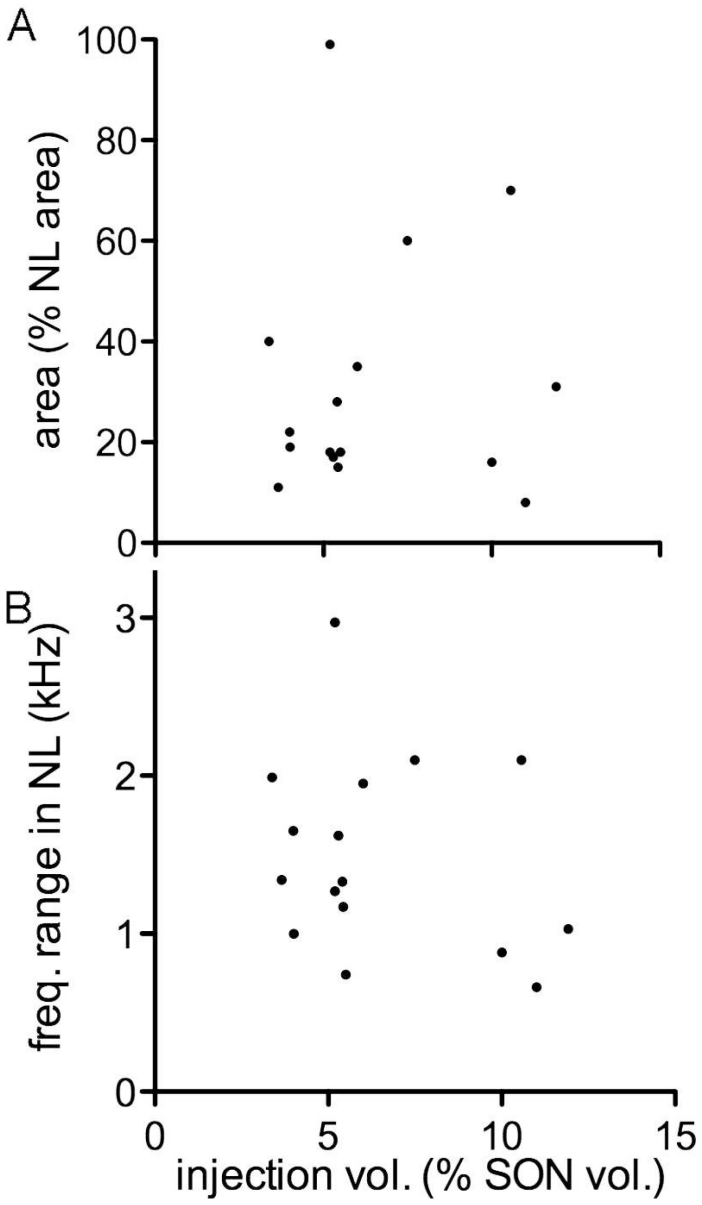

Figure 6. Size of the injection site in SON is not correlated with area and frequency range of labeled terminal fields in NL.
The injection size ranged from 4% to 12% (6.5% ± 2.8%) of the volume of the SON. **A:** The size of the injection site was not correlated with the percentage of NL innervated by the labeled terminal field ($r^2 = 0.006$, $P = 0.79$, n = 16). The innervated area of NL ranged from 8% to 99% (31% ± 24%). **B:** The size of the injection site in SON was not correlated with the frequency range of NL innervated by labeled axons ($r^2 = 0.059$, $P = 0.36$, n = 16).

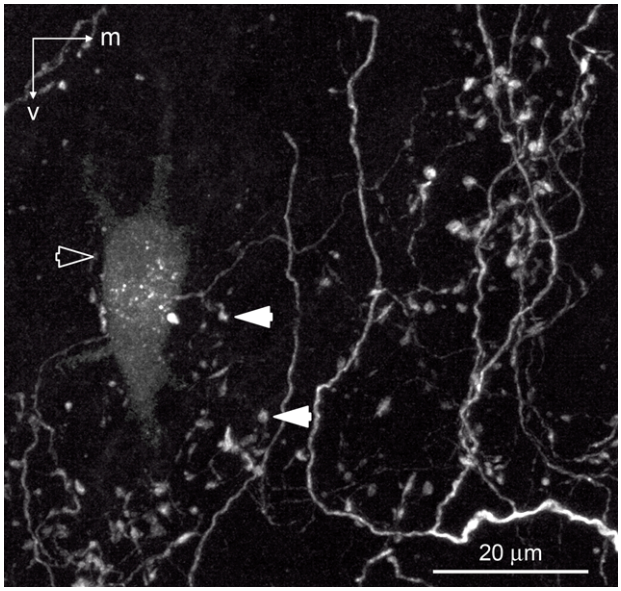

Figure 7. NL neuron surrounded by labeled SON axons.
Intermediate CF region of NL (between 1 and 2.5 kHz) showing a retrogradely labeled NL neuron (open arrowhead) surrounded by labeled SON axons (white; examples indicated with solid white arrowhead). m, Medial; v, ventral. Scale bar = 20 µm.

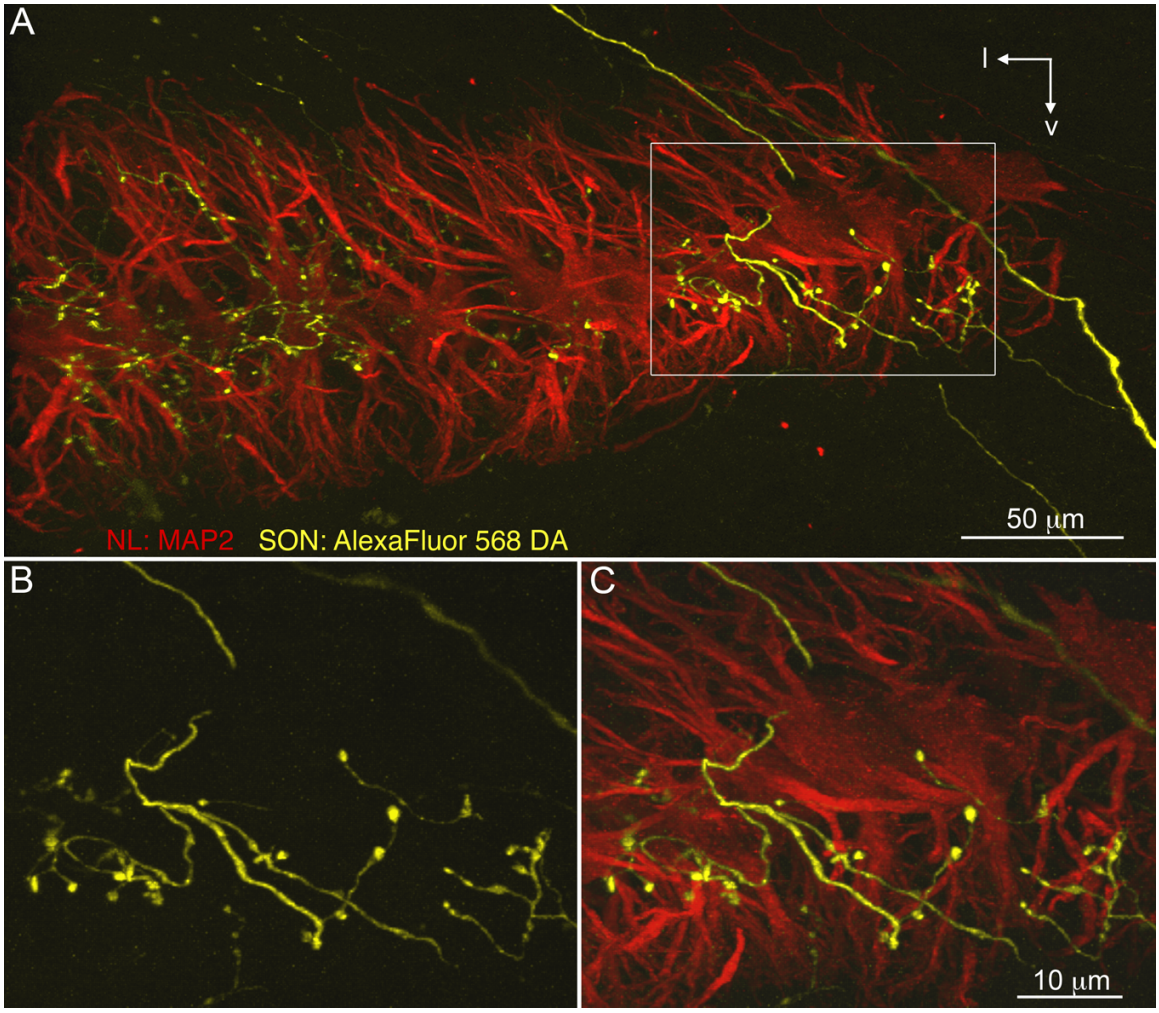

Figure 8. SON axonal arborizations in NL.
SON axons visualized with AlexaFluor 568 dextran amine (yellow) innervate NL. MAP2 immunoreactivity (red) reveals the dendrites and cell bodies of NL neurons. **A:** Fine SON axon branches with bouton-like swellings on all laminae. White rectangle shows location of the magnified images in B,C. **B:** Magnified image of the SON axon that entered NL dorsally, branched, and formed large varicosities. **C:** Immunostaining for MAP2 shows this SON axon branch formed varicosities on cell bodies and ventral dendrites of NL. l, Lateral; v, ventral. Scale bars = 50 µm in A; 10 µm in C (applies to B,C).

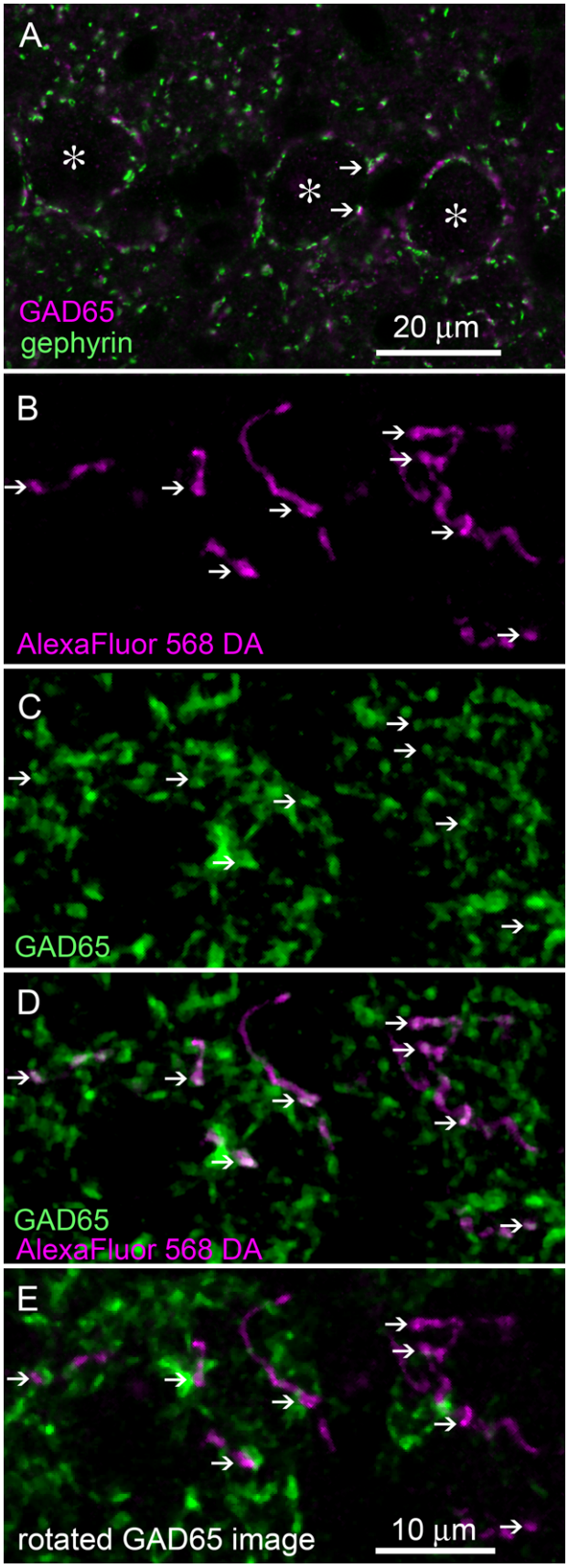
A
GAD65
gephyrin
20 µm
B
AlexaFluor 568 DA
C
GAD65
D
GAD65
AlexaFluor 568 DA
E
rotated GAD65 image
10 µm

Figure 9. SON axonal swellings in NL are GABAergic.
A: GAD65 immunolabeling (magenta) of GABAergic presynaptic site and gephyrin immunolabeling (green) of inhibitory postsynaptic sites are colocalized in NL (examples, arrows). Asterisks indicate NL cell bodies. **B:** Single plane confocal image of NL showing SON axons labeled with AlexaFluor 568 dextran amine (magenta). Arrows indicate locations of varicosities. **C:** GAD65 immunolabeling (green) in NL. **D:** Combined channel image shows labeled axonal varicosities colocalized with GAD65 puncta (white). **E:** High-magnification images. Combined channel image shows labeled axonal varicosities colocalized with GAD65 immunoreactivity (left; arrowheads). AlexaFluor 568 dextran amine (center; magenta) and GAD65 (right; green) labeling are shown separately. **F:** Combined channel image with the GAD65 image rotated 90° clockwise. The GAD65 puncta (green) show sparse colocalization with fluorescent tracer (magenta). Image taken from the cell body lamina in the intermediate region of NL. Scale bars = 20 μm in A; 3 μm in E; 10 μm in F (applies to B–D,F).

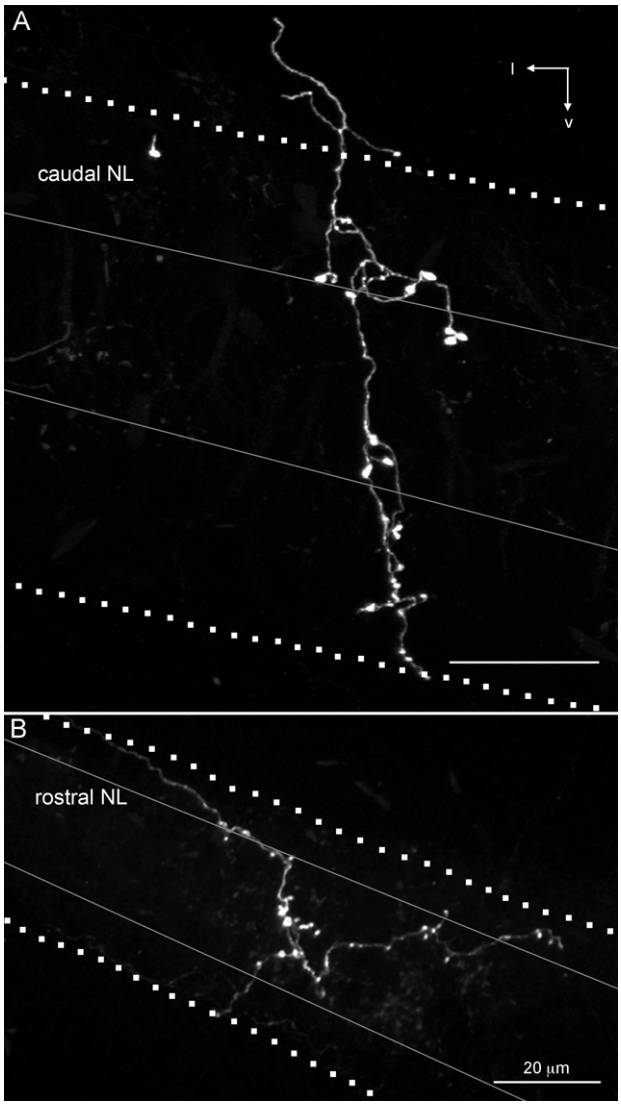

Figure 10. SON axonal branches ramifying in low-CF and high-CF regions in NL. AlexaFluor 568 dextran amine labeled SON axons (white) extending across all laminae of NL. In both examples, the axon branch enters NL from the dorsolateral brainstem; however, we observed axons entering NL from both the dorsal and ventral sides. Dotted lines indicate the boundaries of NL, gray lines indicate boundaries of cell body laminae within NL. **A:** Caudal, low-CF region of NL innervated by an SON axonal arbor. Image is a maximum intensity projection through a 200-μm-thick optical stack. **B:** Rostral, high-CF region of NL innervated by an SON axonal arbor. Image is a maximum intensity projection through a 300-μm-thick optical stack. l, lateral; v, ventral. Scale bars = 20 μm.

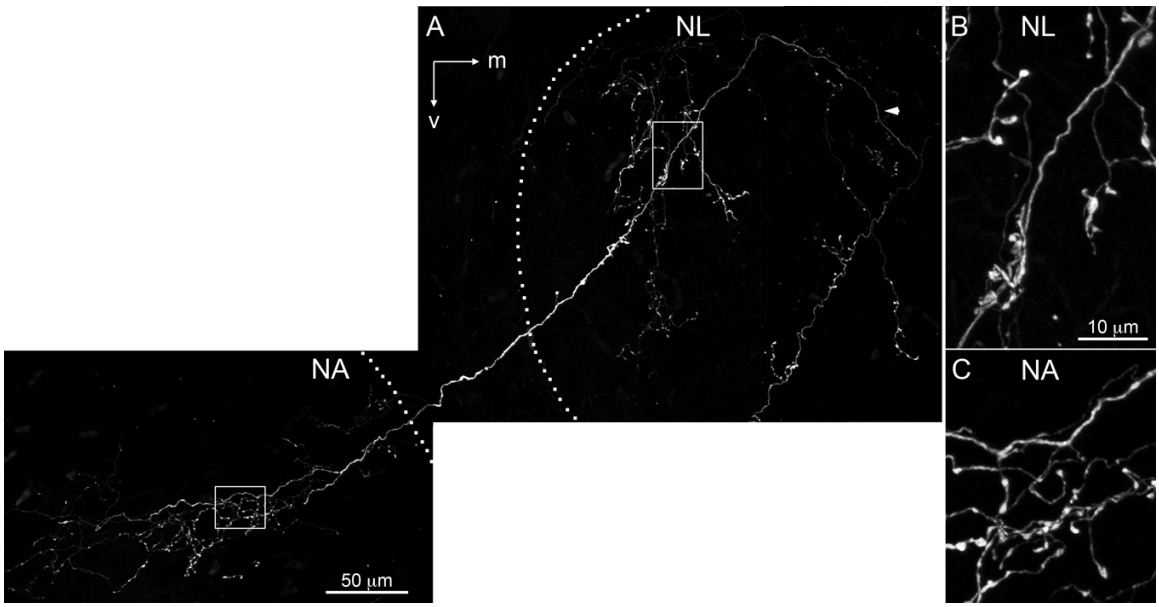

Figure 11. SON axonal arborization innervating multiple auditory nuclei.
A: Labeled SON axon (white) courses dorsolateral through NL (arrowhead) and turnes ventrolateral, forming branches and bouton-like swellings in the lateral NL, then innervates nucleus angularis (NA). Borders of the nucles are indicated with dotted lines. Rectangles show location of magnified images in B,C. **B:** Magnified image of the labeled SON axonal arbor within NL. **C:** Magnified image of the labeled SON axonal arbor within NA. NA, nucleus angularis; NL, nucleus laminaris; m, medial; v, ventral. Scale bars = 50 μm in A; 10 μm in B (applies to B,C).

Table 1. Primary antibodies used

Antigen	Immunogen	Manufacturer, species in the antibody was raised; mon- vs. polyclonal; catalog No.; lot No.	Dilution used
Microtubulin-associated protein 2 (MAP2)	Bovine brain MAP2 (aa 997-1332)	Chemicon; mouse; monoclonal; clone AP20; MAB3418; lot LV1486526	1:1000
Glutamate decarboxylase 65 (GAD65)	Human GAD65 from baculovirus-infected cells	Millipore; rabbit; polyclonal; AB5082: lot LV1580833	1:1000
Gephyrin	Purified rat gephyrin	Synaptic Systems; mouse; monoclonal; clone mAB7a; 147011; lot 147011/21	1:1000

Chapter 4
PATTERN OF GABAERGIC AXONAL ARBORIZATIONS IN A BRAINSTEM BINAURAL HEARING CIRCUIT

4.1 Abstract

The avian nucleus laminaris (NL) is involved in computation of interaural time differences (ITDs) that encode the location of a sound source along the horizontal plane. Neurons in NL are bipolar, with dorsal and ventral dendritic arbors receiving input from separate ears. NL neurons act as coincidence detectors that respond maximally when input from each ear arrives at the two dendritic arbors simultaneously. Computational and physiological studies demonstrated that the sensitivity of NL neurons to coincident inputs is modulated by an inhibitory feedback circuit via the superior olivary nucleus (SON). To understand the mechanism of this modulation, the pattern of single SON axonal arborizations in NL was examined in chickens. Initial experiments labeling individual SON neurons *in vitro* demonstrated widespread axonal arborizations in NL spanning both dorsal and ventral dendritic lamina. Further experiments will quantify the patterns of axon arborizations and provide information to better understand how inhibitory input controls the overall activity level of NL and enhances the specificity of frequency mapping and ITD detection.

4.2 Introduction

A fundamental question in neuroscience is how connections between neurons underlie information processing. Studies of the chicken auditory brainstem have demonstrated direct relationships between anatomical structures and sensory processing. The chicken brainstem contains a highly specialized circuit that detects interaural time differences (ITDs), the submillisecond differences in the arrival time of sound to the two ears, to

localize sounds along the horizontal plane. ITDs are detected by nucleus laminaris (NL) neurons responding maximally to coincident bilateral inputs from nucleus magnocellularis (NM) neurons (Carr and Konishi, 1990; Overholt et al., 1992). NL comprises a monolayer of bitufted neurons with segregated dorsal and ventral dendrites (Ramón y Cajal, 1908; Smith and Rubel, 1979). Input from the ipsilateral or contralateral ear is relayed through NM to the dorsal or ventral dendritic arbor, respectively. Furthermore, NM axons innervate narrow bands across NL to construct a precise tonotopic map (Parks and Rubel, 1975; Rubel and Parks, 1975; Young and Rubel, 1983). Orthogonal to its tonotopic map, NL is arranged by preferred ITD such that neighboring neurons have adjacent receptive fields along the horizontal plane (Parks and Rubel, 1975; Young and Rubel, 1983; Köppl and Carr, 2008).

In addition to understanding how the connectivity patterns of the excitatory pathway enable processing of binaural cues to localize sounds, we are beginning to understand how the organization of inhibitory connections underlies their modulation of circuit output. GABAergic signaling to NM and NL is provided by long-range projections from physiologically heterogeneous neurons of the superior olivary nucleus (SON) (Lachica et al., 1994, Yang et al., 1999; Monsivais et al., 2000; Burger et al., 2005). The broad tonotopic SON-NL projection provides sound-level-dependent inhibition to maintain ITD sensitivity in low frequency NL at very high sound levels (Nishino et al., 2008). But how SON inhibition modulates the precise activity patterns of NL is not fully understood. Our work addressed four open questions: Do multiple types of SON neurons provide information to NL? To what degree is SON providing lateral

inhibition in NL? Is the function of inhibition similar across the tonotopic map? Does inhibition differentially modulate ipsilateral and contralateral excitatory inputs?

In preliminary studies we used an *in vitro* intracellular labeling approach to examine the arborization patterns of single SON axons in NL. Moreover, we compared the innervation patterns of inhibitory SON axons to excitatory NM axons in NL to better understand how this specialized circuit processes ITDs to localize and segregate sounds along the horizontal plane. We are continuing this work and present the methods and preliminary findings in this chapter.

4.3 Materials and Methods

Experiments were conducted on white leghorn chicken embryos (*Gallus gallus domestic*), embryonic days (E) 15–21. All procedures were carried out in accordance with the National Institute of Health Guidelines of the Care and Use of Laboratory Animals and approved by the University of Washington Institutional Animal Care and Use Committee. All efforts were made to minimize animal number and pain of the animals.

4.3.1 Brainstem slice preparation

Embryos were quickly decapitated and the brainstem was removed into ice-cold oxygenated artificial CSF (ACSF) containing (in mM): 130 NaCl, 3 KCl, 1.25 NaH_2PO_4, 26 $NaHCO_3$, 1 $MgCl_2$, 2 $CaCl_2$ and 10 glucose; pH 7.4; 305 mOsm/L. All chemicals were obtained from Sigma-Aldrich. The brainstem was blocked anterior to the superior olivary nucleus (SON) and posterior to nucleus magnocellularis (NM) and glued into a vibratome slicing chamber (Technical Products International). The chamber was filled with ice-cold ACSF. The brainstem was sectioned coronally into one slice, 1700–1900 μm thick, containing nucleus laminaris (NL), NM and SON. These sections were placed in an

incubating chamber containing oxygenated ACSF at room temperature for 15 minutes to 1 hour.

After incubation, slices were transferred to a recording chamber mounted on the stage of a Zeis Axioskop FS. This chamber was constantly superfused with room temperature, oxygenated ACSF.

4.3.2 In vitro intracellular labeling

Glass pipettes were pulled to resistances of 80–150 MΩ. Pipettes were filled with 100 mM neurobiotin (Vector Labs) in 0.3 M potassium acetate (CH_3CO_2K), visually guided to SON using a 10x air objective and advanced through the tissue. Cell penetration was indicated by a sudden negative voltage drop to -30 – -70 mV. Neurobiotin was iontophoresed into the neuron with positive current (3 NA, 300 ms pulses, 2 Hz, 5 minutes). Current injections were controlled using an Axoclamp 2B amplifier (Molecular Devices). All experiments were controlled with a Macintosh G4. Protocols were written and run with Axograph, version 4.5, software (Molecular Devices).

Slices were placed in the incubating chamber containing oxygenated ACSF at room temperature for 1–2 hours. All slices were fixed by immersion in 4% paraformaldehyde in phosphate buffer for 1 hour to overnight. Slices were transferred to 30% sucrose in phosphate-buffered saline (PBS) until they sank. Each slice was frozen and resectioned at 100–200 μm using a freezing sliding microtome. Sections were washed in PBS, incubated in 2 μg/mL streptavidin-conjugated Alexa Fluor 488 (Invitrogen) in PBS for 4 hours and washed again in PBS.

4.3.3 Immunofluorescence

Primary antibodies against gephyrin (mouse, 1:1000, Synaptic Systems) and microtubulin-associated protein 2 (mouse, 1:1000, Chemicon) were diluted in 0.3% Triton X-100 and 5% normal donkey serum in PBS. Free-floating sections were incubated with primary antibody solutions for 2 days at 4°C. Following three washes with PBS, sections were incubated with secondary antibody (goat-anti mouse-conjugated Alexa Fluor 568, 1:1000, Invitrogen) diluted in 0.3% Triton X-100 in PBS for 4 hours at room temperature. Sections were washed with PBS, mounted on slides and coverslipped with Fluoromount (Sigma-Aldrich).

4.3.4 Multiphoton imaging

Multiphoton image stacks were acquired on a two-photon microscope (Olympus). The laser was tuned to 800 nm for imaging Alexa Fluor 488/Alexa Fluor 568. A 1.35 NA 60× oil-immersion objective was used (Olympus). All images are presented in the coronal view with dorsal up and lateral to the right.

4.3.4 Analysis

We used previously quantified tonotopic maps of NL (Rubel and Parks, 1975) and SON (Tabor et al., 2012) to predict characteristic frequencies (CFs) from the positions of cell bodies and arbors in the nuclei.

4.4 Results

Preliminary results of this study are presented below. First we describe the dendritic morphology of SON neurons and then we show two examples of individual SON axonal arborizations in NL.

4.4.1 SON contains morphologically heterogeneous neurons

Labeled SON neurons showed diverse dendritic arborization patterns. Most neurons had wide dendritic fields (Fig. 1A, B) extending across most of the tonotopic map in SON. Dendrites of neurons presented in Figure 1A and B covered the entire tonotopic map. In contrast, some SON neurons had dendritic arbors confined to a smaller region of SON (Fig. 1C, D). Using the quantitative tonotopic map of SON we calculated that the dendritic arbors pictured in Figure 1C and D span ~⅓ and ¼ of the tonotopic map, respectively. In addition, qualitatively, the density of branches within the dendritic field varied between different neuron types; for example, the dendritic arbor in Figure 1D was more dense than the arbor in Figure 1A. We predicted the CF of the cell bodies based on their location within SON (Fig. 1). The neurons shown in Figure 1A and B innervated NL.

4.4.2 SON axons innervate widely in NL

Two SON neurons visualized by intracellular labeling innervated NL. Figure 2 shows the morphology and spread of a single SON arbor corresponding to the cell body presented in Figure 1A. The axon spread across three coronal sections of NL (each 160 μm thick) and four image fields on the lateral side of NL. The arborization extended across ~⅓ of the tonotopic axis. The predicted CF of the cell body (2.2 kHz) was on the low end of the predicted CF region of NL innervated by the axon (~2–3.3 kHz). In each section the axon innervated the dorsal dendritic, ventral dendritic and cell body lamina of NL. NL was visualized with dense gephyrin immunolabeling.

Figure 3 shows images of another single axonal arborization in NL corresponding to the cell body in Figure 1B. The axon arbor innervated slightly more than ⅓ of the NL tonotopic map, covering the medial-lateral extent of NL. The predicted CF of the cell

body (2.5 kHz) in SON fell within the CF range of NL (1.7–3.3 kHz) innervated by its axon. The arbor spanned all lamina in NL; however, the relative coverage of axon branches in each lamina may be distributed unequally. For example, Figure 3A and B show regions of the arbor with more branches in the ventral lamina than the dorsal and cell body lamina.

4.5 Discussion

Preliminary data from two neurons indicated that single SON axonal arborizations innervated broadly in NL. Individual axons spanned all lamina, and extended across ~⅓ of the tonotopic map in NL. Initial experiments demonstrated that high frequency (HF) SON neurons innervated HF regions of NL, and further experiments will show the projection pattern to other regions of NL. These preliminary results are consistent with previous findings that small regions of SON had broad topographic projections to NL (Tabor et al., 2011). In addition, SON neurons contacting NL had dendritic arbors covering the entire SON tonotopic axis.

4.5.1 Possible functions of inhibition revealed by its anatomy

A widespread inhibitory axonal arbor is consistent with a high degree of divergence of SON inputs in NL. This broad arborization pattern contrasts dramatically with the precise and narrow pattern of excitatory arbors in NL, suggesting SON may provide lateral (*i.e.* surround) inhibition. Lateral inhibition is a physiological mechanism common in sensory systems to focus neuronal activity. In this system it may act to sharpen frequency tuning and acuity of sound localization.

4.5.2 Ongoing experiments

The work presented in this chapter is preliminary data of an ongoing study to quantify the axonal arborization patterns of single SON neurons in NL. In addition, we found a wide diversity in dendritic morphologies in SON. Both neurons innervating NL had wide dendritic fields, and whether other morphological types of SON neurons project to NL remains to be determined. In NL, we found single axons innervated wide regions, but quantitative analyses of reconstructed arbors are required to determine the arborization patterns underlying inhibitory input in NL. Finally, examining the distribution of gephyrin immunolabeled puncta along the axons will provide information to better understand how this inhibition modulates NL neuronal activity.

4.6 Figures

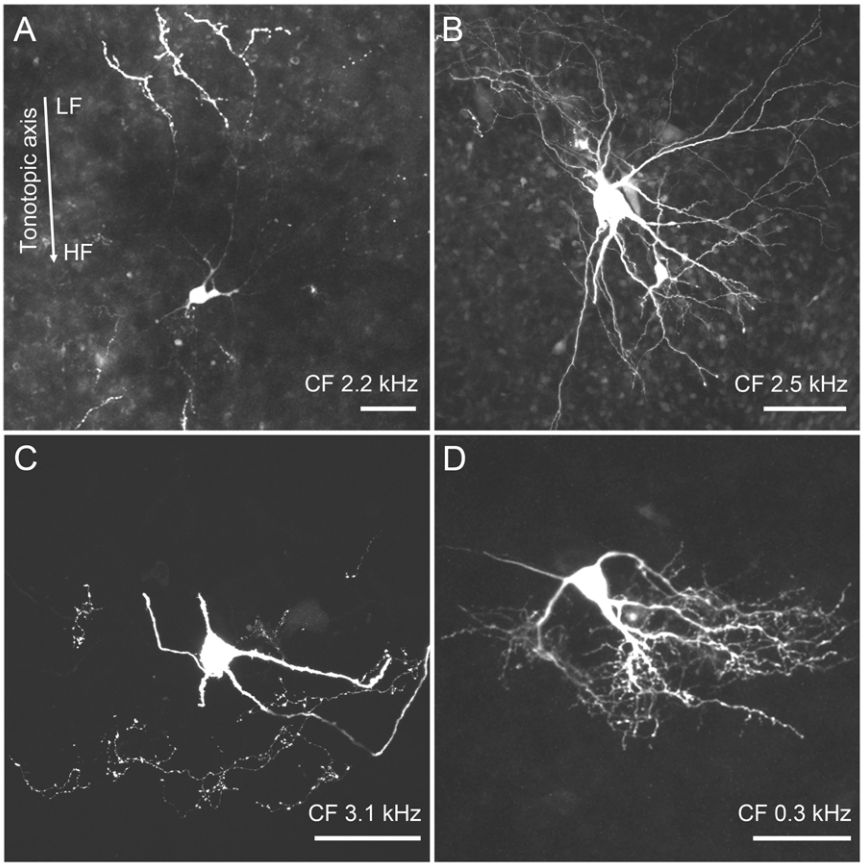

Figure 1. Heterogeneous dendritic arbor morphology in SON.
Tonotopic axis of SON indicated with white line in A. Characteristic frequencies predicted based on spatial location of cell body in SON are indicated. SON contains neurons with widespread dendritic fields (A, B), more confined fields (C, D), sparse branch arrangements (A), and more dense branch arrangements (D). A and B show SON neurons innervating NL and corresponding to axonal arborizations presented in Figures 2 and 3, respectively. Scale bars = 20 μm. Abbreviations: CF, characteristic frequencies; HF, high frequency; LF, low frequency.

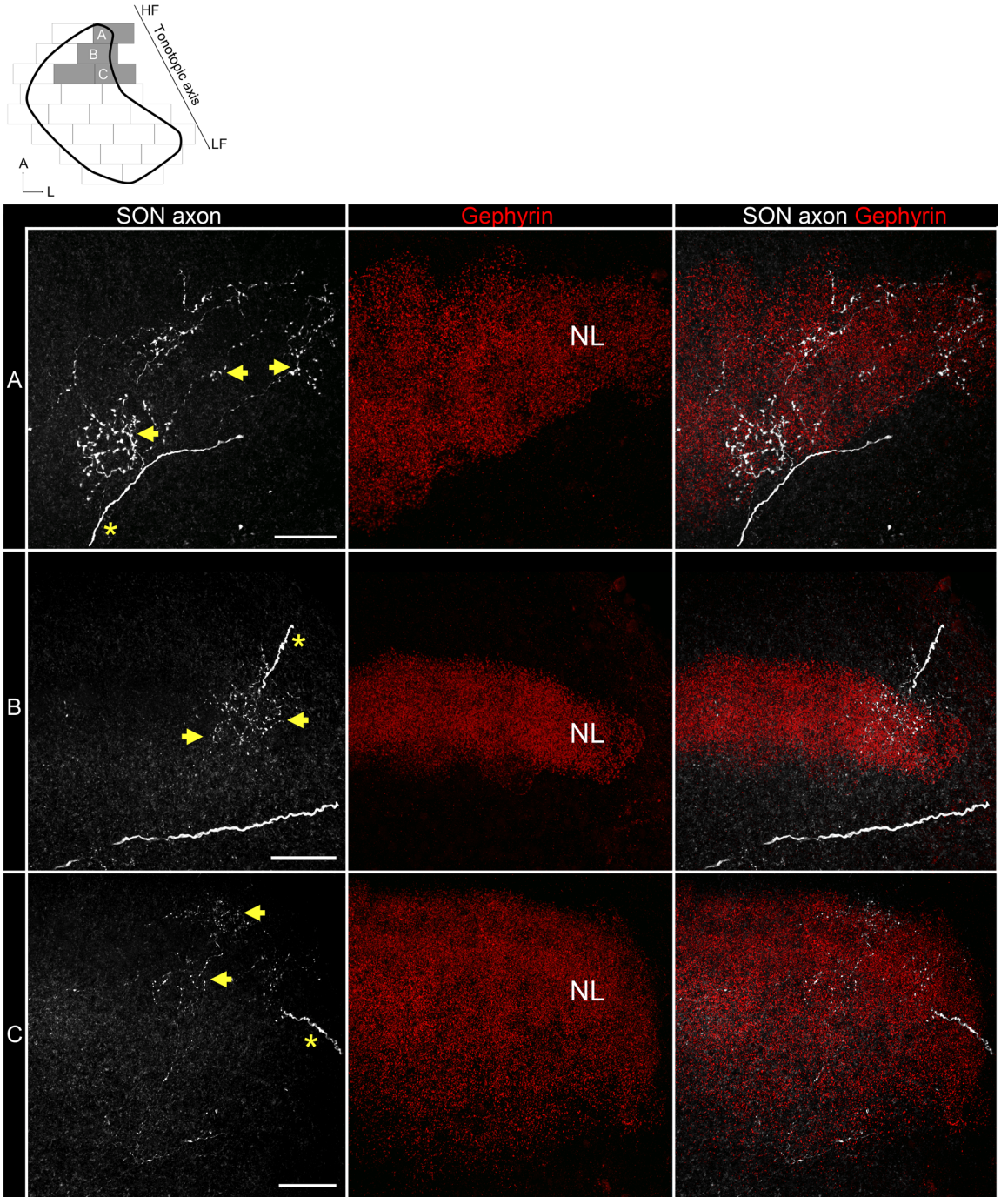
HF
Tonotopic axis
LF
A
B
C
A
L
SON axon
Gephyrin
SON axon Gephyrin
A
B
C
NL
NL
NL

Figure 2. Single SON axonal arbor in NL corresponding to cell body shown in Figure 1A. Image fields (squares) of eight coronal slices of NL are shown in horizontal schematic at top. Black line represents borders of NL, arrow indicates tonotopic axis. Image fields containing the labeled SON axon are shaded gray and lettered squares correspond to images. A-C, Labeled axon (left column), gephyrin immunolabeling (middle column) and combined images (right column) in NL. Axonal varicosities were numerous across the arborizations (yellow arrows). Asterisks indicate primary axon. NL was densely immunolabeled with gephyrin puncta, while surrounding tissue showed very low levels of labeling. Scale bars = 20 μm. Abbreviations: A, anterior; HF, high frequency; L, lateral; LF, low frequency.

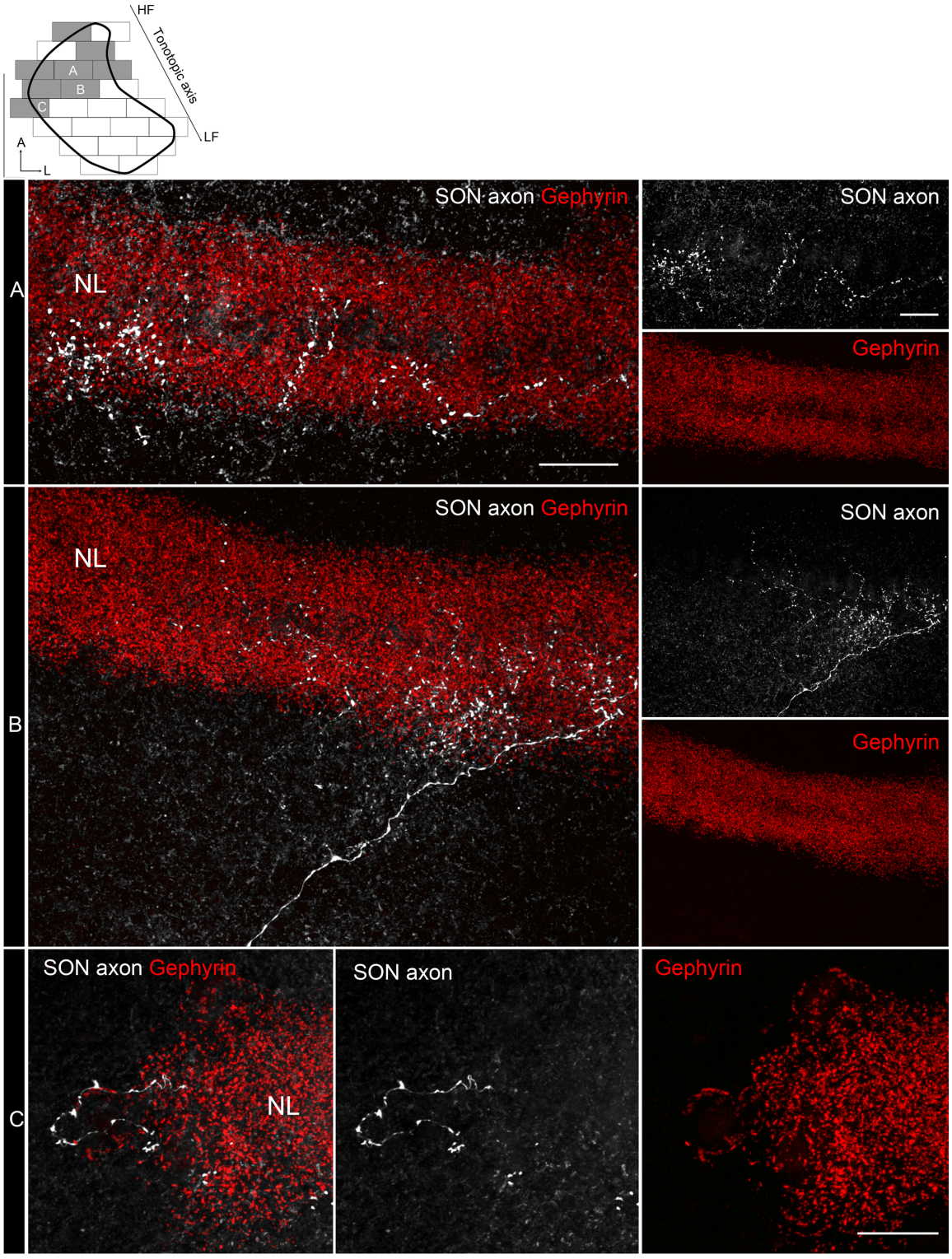
HF
Tonotopic axis
LF
A
B
C
A
L
A
SON axon Gephyrin
NL
SON axon
Gephyrin
B
SON axon Gephyrin
NL
SON axon
Gephyrin
C
SON axon Gephyrin
NL
SON axon
Gephyrin

Figure 3. Single SON axonal arbor in NL corresponding to cell body shown in Figure 1B. Image fields (squares) of eight coronal slices of NL are shown in horizontal schematic at top. Black line represents borders of NL, arrow indicates tonotopic axis. Image fields containing the labeled SON axon are shaded gray and lettered squares correspond to images. A and B, Labeled axon (white) and gephyrin immunolabeling (blue) in NL (left). Separated image channels shown on right. NL was densely immunolabeled with gephyrin puncta, while surrounding tissue showed very low levels of labeling. C, Axon along medial border of NL. Some immunolabeled gephyrin puncta appeared closely apposed to axon. Future work will analyze the distribution of gephyrin immunolabeled puncta along SON axons. Scale bars = 20 μm. Abbreviations: A, anterior; HF, high frequency; L, lateral; LF, low frequency.

Chapter 5
SUMMARY AND FUTURE DIRECTIONS

5.1 Summary

This dissertation examines the spatial organization of inhibitory long-range projections in binaural hearing. The coarse tonotopic organization of inhibition underlies its function to control the gain of a binaural processing circuit. In addition, the broad inhibitory innervation pattern, compared to the precisely organized excitatory connections, suggests that this circuit uses lateral inhibition to sharpen frequency tuning and acuity of sound localization.

5.2 Tonotopic map in SON

In Chapter 2 we examined the tonotopic organization and neural response properties in the superior olivary nucleus (SON), the predominate source of inhibitory inputs to a binaural processing circuit in the chicken brainstem (Fig. 1). Using predictive statistical methods we generated a quantitative 3D map of the relationship between characteristic frequency (CF) (*i.e.* sound frequency tuning of a neuron) and anatomical coordinates. This map revealed two major organizational features of SON. First, sound frequency is mapped coarsely across SON. Thus, in this inhibitory cell group there is a deterioration of the precise tonotopic organization that is present in its excitatory afferents. Second, neurons with sustained or onset response patterns are interspersed throughout all CF regions in SON. Thus, SON appears to process at least two types of auditory information in parallel.

5.3 Broad topography of the projection from SON to NL

Following our studies on spatial organization in SON, we examined the topographic arrangement of its projection to nucleus laminaris (NL). In Chapter 3 we demonstrated

that the GABAergic projection from SON to NL is organized in a coarse tonotopic pattern (Figure 1). Thus, gain control in NL – provided by SON – arises from broad topographic inhibition. Furthermore, observations from our tracing study raised the possibility that projections between NL and SON are reciprocal; a region of NL receives inhibition from the same region of SON that it innervates. In Chapter 3 we demonstrated also that single SON neurons project to multiple ipsilateral nuclei in the auditory brainstem, consistent with a previous study (Burger et al., 2005). Thus, SON provides crosstalk between multiple auditory pathways in the brainstem.

5.4 Axonal arborization patterns of single SON neurons in NL

In Chapter 4 we presented preliminary data from our project to examine the SON-NL projection at the single cell level. SON comprises morphologically diverse neurons. We observed two neurons with widespread dendritic arbors projecting to NL, innervating large regions of its tonotopic map and all lamina (Figure 1). Comparing axonal arborization patterns of inhibitory (broad) to excitatory (narrow) inputs in NL raises the possibility that SON provides lateral inhibition to sharpen frequency tuning and acuity of sound localization. Below we synthesize some of our and other's findings on SON input in NL. We also compare SON in the chicken brainstem to inhibition in the mammalian auditory brainstem. Finally, we leave the reader with some future directions and remaining questions.

5.5 Possible functions of SON

Firing patterns of SON neurons to ipsilateral tones appear to be shaped primarily by the inputs from nucleus angularis (NA), one of two main excitatory inputs to SON. Although SON physiology closely resembles NA, we cannot exclude contributions from NL. It is

possible that sustained responders in SON derive their responses from NL inputs. Also, we did not assess the binaural response properties of SON neurons, that could reveal a currently unexplored contribution from NL's projection to SON response properties.

5.5.1 Sound-level-dependent inhibition – gain control

A physiological study demonstrated *in vivo* that sound-level-dependent inhibition from SON controls the gain of NL neurons (Nishino et al., 2008). We examined the physiological response properties of SON neurons to better understand how they regulate neuronal activity in NL. The majority of SON neurons encode sound level in their sustained firing rates. This response pattern is well-suited to regulate the gain of the circuit. Other SON response patterns, such as phase-locking and onset responses, may provide temporally patterned inhibition to the network (Coleman et al., 2011); however, the relatively slow kinetics of inhibitory postsynaptic currents (~20 ms time course) (cf. Yang et al., 1999; Kuo et al., 2009) compared to the rapid excitatory postsynaptic currents (~1 ms time course) (Raman et al., 1994) in NL argues against this role. Although timed inhibition is important for binaural processing in gerbil medial superior olive (MSO) (Brand et al., 2002; for review, see Grothe, 2003), its role in the avian auditory brainstem remains to be tested.

We also examined the neuronal substrate underlying SON's function in binaural processing. In NL, gain control is provided by a broad tonotopic inhibition. This arrangement is beneficial under conditions of high background noise. The organization of SON input may allow NL to adapt to the overall sound level of the acoustic environment, by setting the gain of the system to an optimal position on the input–output function.

5.5.2 Lateral inhibition

A recent *in vivo* physiological study revealed that inhibitory input to nucleus magnocellularis (NM) is more broadly tuned to sound frequency than excitatory input to NM (Fukui et al., 2010). In many sensory neurons this relation between the tuning of (broad) inhibition and (narrow) excitation sharpens selectivity. In NL, the tuning of inhibitory and excitatory inputs to single neurons remains unknown. But, the contrast between the broad topographic organization of the SON-NL projections and the precise NM-NL projections, which innervate highly restricted regions of the tonotopic axis (Young and Rubel, 1983), suggests an anatomical substrate for lateral sharpening of frequency tuning in NL neurons. Lateral inhibition may also sharpen acuity of sound localization (*i.e.* ITD detection), as indicated by an *in vitro* physiological study of GABAergic signaling in NL neurons (Funabiki et al., 1998).

5.6 Comparison with mammals

The mammalian auditory system does not appear to have an exact homolog or analog to SON. Instead, mammals have multiple nuclei that provide inhibition to the auditory brainstem and the inner ear. These nuclei, including the medial nucleus of the trapezoid body (MNTB) and a number of periolivary nuclei, provide a range of functions similar to SON in birds. Network functions of SON are categorized into three general groups: (1) balancing binaural activity levels (Burger et al., 2005; Dasika et al., 2005; Fukui et al., 2010; for review, see Burger et al., 2011), (2) providing feedback inhibition to the cochlear nuclei and NL in the caudal brainstem (Lachica et al., 1994; Yang et al., 1999; Monsivais et al., 2000; Burger et al., 2005), and (3) providing feed-forward inhibition to the lateral lemniscus (LL) and midbrain (Conlee and Parks, 1986; Westerberg and Schwarz, 1995; Wild et al., 2009).

These three categories of network inhibition are present in the mammalian auditory system. First, binaural balancing is performed by the lateral olivocochlear efferents in rodents (Groff and Liberman, 2003; Darrow et al., 2006). Second, feedback inhibition to all subdivisions of the mammalian cochlear nucleus is provided by glycinergic and GABAergic input from periolivary regions, in particular, the contralateral ventral nucleus of the trapezoid body, and the ipsilateral MNTB and lateral nucleus of the trapezoid body (LNTB) (Adams, 1983; Spangler et al., 1985; Schofield, 1994; Warr and Beck, 1996; Ostapoff et al., 1997). Inhibition to MSO (analogous to NL) is provided by MNTB and LNTB (Cant and Hyson, 1992; Grothe and Sanes, 1993). Third, feed-forward inhibition to the LL and auditory midbrain is provided by a combination of various nuclei, including the MNTB, LNTB (Yavuzoglu et al., 2010), and superior periolivary nucleus (also named the dorsomedial periolivary nucleus) in mammals (Kadner and Berrebi, 2008; Saldana et al., 2009; Kopp-Scheinpflug et al., 2011). The comparatively simple organization of inhibition in the avian auditory brainstem (i.e. one nucleus is the predominate source of all three categories of inhibition) makes this an appealing model for studying the functions of network inhibition in auditory processing in vertebrates.

5.7 Future directions

Work presented here raises several interesting avenues for future exploration. Below we discuss some of these open questions and propose future directions for researching inhibition in the chicken auditory brainstem.

5.7.1 Examine physiological properties of SON neurons

SON comprises a heterogeneous population of neurons, both in their physiological responses and their cellular morphology. *How do physiological types relate to*

morphological types of neurons? In NA, *in vitro* electrophysiological experiments matched the five electrophysiological types to the four morphological types of neurons (Soares et al., 2002; Fukui and Ohmori, 2003; for review, see Macleod and Carr, 2007). Although five cell types have been identified in both *in vitro* and *in vivo* physiological studies in NA, which *in vivo* type corresponds to which *in vitro* type remains to be determined. But, in the mammalian cochlear nucleus, studies using *in vivo* intracellular labeling correlated *in vivo* physiological response with cell morphology of the five cell types (Rhode et al., 1983; Rouiller and Ryugo, 1984). Similar experimental approaches could be used to relate cell morphology to *in vitro* physiology and to *in vivo* response patterns in SON neurons. One hypothesis is that SON neurons with dendrites spanning the entire tonotopic axis are more broadly tuned than neurons with dendrites confined to a small tonotopic region of SON. Relating morphology to physiology is critical to understand how different features of auditory stimuli are processed by inhibitory neurons and what auditory information is transmitted to NL neurons by SON projections.

Recent studies demonstrated that SON influences binaural processing (Nishino et al., 2008; Fukui et al., 2010). In Chapter 1 we introduced multiple functions of SON (proposed or demonstrated) important for regulating auditory computations in a wide range of sound environments (Peña et al., 1996; Burger et al., 2005; Dasika et al., 2005; Nishino et al., 2008; Fukui et al., 2010; for reviews, see Nishino and Ohmori, 2009; Burger et al., 2011). SON neuronal responses to pure tones presented to the ipsilateral ear are described in detail (Coleman et al., 2011), providing a basis to understand how SON processes auditory information. *What are the response patterns of SON neurons to bilateral and complex auditory stimuli?* To advance our understanding of SON function,

especially in binaural processing, examining neuronal responses to bilateral stimuli and other more complex stimuli (e.g. sounds containing multiple frequencies) is required. One hypothesis is that SON neuronal activity is suppressed by contralateral sounds and excited by ipsilateral sounds, similar to the main response pattern found in the owl SON (Moiseff and Konishi, 1983). Another possible finding is that chicken SON neurons are sensitive to binaural cues; however, only 3% of owl SON neurons showed ITD sensitivity and no neurons showed sensitivity to interaural level differences (Moiseff and Konishi, 1983). These studies will demonstrate the activity patterns SON transmits to auditory centers during binaural hearing.

5.7.2 Explore how SON inhibitory input influences NL physiology

In NM, pharmacological manipulations paired with physiological recordings of single neurons demonstrated that inhibition was tuned to a broader sound frequency range than excitation and that GABAergic signaling sharpens sound frequency tuning (Fukui et al., 2010). Although the anatomical organization of inputs suggests SON provides lateral inhibition to NL, this function remains to be tested *in vivo*. Previous studies examined the effect of SON on ITD tuning *in vivo*, but did not test its effect on sound frequency tuning (Nishino et al., 2008). *Does SON provide lateral inhibition to sharpen sound frequency tuning in NL neurons? In vivo* pharmacological and electrophysiological methods can examine the sound frequency tuning of inhibitory and excitatory inputs to single NL neurons to determine whether SON provides lateral inhibition to sharpen sound frequency tuning. In addition, these methods can be used to address another question. Although we hypothesize that NL localizes sounds using binaural cues to segregate sound sources in the auditory environment (*i.e*. the cocktail party effect), its function has only

been explored with simple auditory stimuli. How NL responds to a more complex sound environment remains to be explored. In fact, the surprising finding that silencing SON did not affect response patterns of middle and high CF NL neurons may be because only pure tones were presented (Nishino et al., 2008) while inhibition's function is probably more critical in processing auditory signals in complex sound environments. *How do NL neurons respond to complex sound stimuli and how does SON inhibitory input shape their response?* In addition to addressing this question using *in vivo* physiological methods, computer simulations of the chicken brainstem circuit can be used to test the influence of SON on an NL neuron's firing patterns in various sound environments. Previous simulations of this circuit have been extremely beneficial in shaping hypotheses and guiding physiological studies in this system (Peña et al., 1996; Burger et al., 2005; Dasika et al., 2005; Nishino et al., 2008). Adding anatomical data from our work to these models (e.g. broad tonotopic inhibitory input) and simulating complex sound stimuli may provide information to shape future physiological studies of inhibition in this system. One hypothesis is that in sound environments with multiple competing sound sources and many sound frequencies, SON input is critical for maintaining precise NL activity patterns needed to segregate and localize sound sources.

5.7.3 Development of SON long-range inhibitory projections

Studies in the mammalian auditory brainstem have determined developmental strategies of precise long-range inhibitory projections. In the inhibitory MNTB-LSO projection, tonotopic precision is present at very early stages in development (Sanes and Rubel, 1988; Sanes and Siverls, 1991), but some developmental reorganization occurs using experience-independent (Kim and Kandler, 2003) and experience-dependent mechanisms

(Sanes et al., 1992; Sanes and Takács, 1993). During development of MNTB-MSO projections, some experience-dependent reorganization narrows MNTB axonal arborizations (Werthat et al., 2008) and shifts the distribution of inhibitory synapses onto MSO cell bodies (Kapfer et al., 2002). In contrast to these precisely organized inhibitory projections, the SON projection innervates broadly across the tonotopic map in NL. *What is the developmental strategy of the broad tonotopic projection from GABAergic SON neurons to NL?* One hypothesis is that this projection establishes its mature pattern at early stages in development, similar to the excitatory projections to NL (Parks and Rubel, 1975; Young and Rubel, 1986). Applying the methods described in Chapter 4 to embryonic stages when GABAergic signaling is developing in NL (Code et al., 1989; Code and Churchill, 1991; Tang and Lu, 2012) can reveal the developmental plan of the SON-NL projection. In addition, this system provides a unique opportunity to compare the development of broad inhibitory and precise excitatory projections to a laminar nucleus. How these projections interact during development is an intriguing question for future research.

5.8 Figures

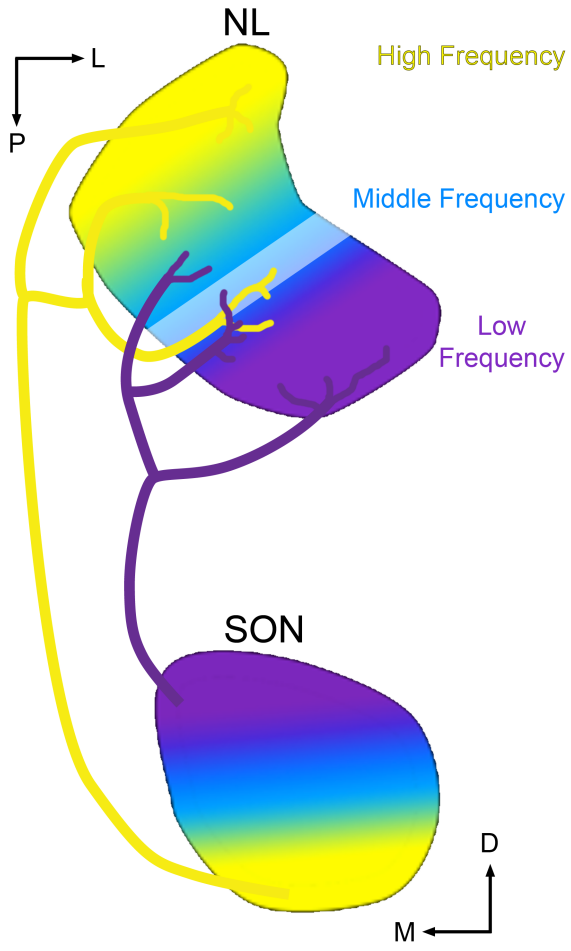

Figure 1. Tonotopic organization of SON and its broad topographic projection to NL. For comparison, the white band indicates the extent of a single excitatory axonal arborization in NL. In Chapter 2 we mapped the tonotopic organization of SON. In Chapter 3 we demonstrated the broad topographic SON-NL projection. In Chapter 4 we began to examine the widespread axonal arborizations of single SON neurons in NL. Abbreviations: D, dorsal; L, lateral; M, medial; P, posterior.

BIBLIOGRAPHY

Adams JC. 1983. Multipolar cells in the ventral cochlear nucleus project to the dorsal cochlear nucleus and the inferior colliculus. Neurosci Lett 37:205-208.

Agmon-Snir H, Carr CE, Rinzel J. 1998. The role of dendrites in auditory coincidence detection. Nature 393:268–272.

Alonso A, Köhler C. 1982. Evidence for separate projections of hippocampal pyramidal and non-pyramidal neurons to different parts of the septum in the rat brain. Neurosci Lett 31:209–214.

Appell PP, Behan M. 1990. Sources of subcortical GABAergic projections to the superior colliculus in the cat. J Comp Neurol 302:143-158.

Bajo VM, Merchan MA, Malmierca MS, Nodal FR, Bjaalie JG. 1999. Topographic organization of the dorsal nucleus of the lateral lemniscus in the cat. J Comp Neurol 407:349-366.

Brand A, Behrend O, Marquardt T, McAlpine D, Grothe B. 2002. Precise inhibition is essential for microsecond interaural time difference coding. Nature 417:543-547.

Boord RL. 1968. Ascending projections of the primary cochlear nuclei and nucleus laminaris in the pigeon. J Comp Neurol 133:523-541.

Boord RL, Rasmussen GL. 1963. Projection of the cochlear and lagenar nerves on the cochlear nuclei of the pigeon. J Comp Neurol 120:463-75.

Boudreau JC, Tsuchitani C. 1968. Binaural interaction in the cat superior olive S segment. J Neurophysiol 31:442-454.

Burger RM, Cramer KS, Pfeiffer JD, Rubel EW. 2005. Avian superior olivary nucleus provides divergent inhibitory input to parallel auditory pathways. J Comp Neurol 481:6-18.

Burger RM, Fukui I, Ohmori H, Rubel EW. 2011. Inhibition in the balance: binaurally coupled inhibitory feedback in sound localization circuitry. J Neurophysiol 106:4-14.

Caceres A, Binder LI, Payne MR, Bender P, Rebhun L, Steward O. 1984. Differential subcellular localization of tubulin and the microtubule-associated protein MAP2

in brain tissue as revealed by immunocytochemistry with monoclonal hybridoma antibodies. J Neurosci 4:394-410.

Cant NB, Hyson RL. 1992. Projections from the lateral nucleus of the trapezoid body to the medial superior olivary nucleus in the gerbil. Hear Res 58:26-34.

Carr CE, Boudreau RE. 1991. Central projections of auditory nerve fibers in the barn owl. J Comp Neurol 314:306–318.

Carr CE, Fujita I, Konishi M. 1989. Distribution of GABAergic neurons and terminals in the auditory system of the barn owl. J Comp Neurol 286:190-207.

Carr CE, Konishi M. 1988. Axonal delay lines for time measurement in the owl's brainstem. Proc Natl Acad Sci USA 85:8311–8315.

Carr CE, Konishi M. 1990. A circuit for detection of interaural time differences in the brain stem of the barn owl. J Neurosci 10:3227-3246.

Carr CE, Soares D. 2002. Evolutionary convergence and shared computational principles in the auditory system. Brain Behav Evol 59:294-311.

Clark GM. 1969. The ultrastructure of nerve endings in the medial superior olive of the cat. Brain Res 14:293-305.

Clopton BM, Winfield JA, Flammino FJ. 1974. Tonotopic organization: review and analysis. Brain Res 76:1-20.

Code RA, Burd GD, Rubel EW. 1989. Development of GABA immunoreactivity in brainstem auditory nuclei of the chick: ontogeny of gradients in terminal staining. J Comp Neurol 284:504-518.

Code RA, Churchill L. 1991. GABAA receptors in auditory brainstem nuclei of the chick during development and after cochlea removal. Hear Res 54:281-295.

Cohen YE, Knudsen EI. 1999. Maps versus clusters: different representations of auditory space in the midbrain and forebrain. Trends Neurosci 22:128-135.

Coleman WL, Fischl MJ, Weimann SR, Burger RM. 2011. GABAergic and glycinergic inhibition modulate monaural auditory response properties in the avian superior olivary nucleus. J Neurophysiol 105:2405-2420.

Conlee JW, Parks TN. 1986. Origin of ascending auditory projections to the nucleus mesencephalicus lateralis pars dorsalis in the chicken. Brain Res 367:96-113.

Cook DL, Schwindt PC, Grande LA, Spain WJ. 2003. Synaptic depression in the localization of sound. Nature 421:66–70.

Darrow KN, Simons EJ, Dodds L, Liberman MC. 2006. Dopaminergic innervation of the mouse inner ear: evidence for a separate cytochemical group of cochlear efferent fibers. J Comp Neurol 498:403-414.

Dasika VK, White JA, Carney LH, Colburn HS. 2005. Effects of inhibitory feedback in a network model of avian brain stem. J Neurophysiol 94:400-414.

Flanagan JG. 2006. Neural map specification by gradients. Curr Opin Neurobiol 16:59-66.

Fukui I, Burger RM, Ohmori H, Rubel EW. 2010. GABAergic inhibition sharpens the frequency tuning and enhances phase locking in chicken nucleus magnocellularis neurons. J Neurosci 30:12075-12083.

Fukui I, Ohmori H. 2003. Developmental changes in membrane excitability and morphology of neurons in the nucleus angularis of the chicken. J Physiol 548:219–232.

Funabiki K, Koyano K, Ohmori H. 1998. The role of GABAergic inputs for coincidence detection in the neurones of nucleus laminaris of the chick. J Physiol 508 (Pt 3):851-869.

Goldberg JM, Brown PB. 1969. Response of binaural neurons of dog superior olivary complex to dichotic tonal stimuli: some physiological mechanisms of sound localization. J Neurophysiol 32:613–636.

Gray L, Rubel EW. 1985. Development of absolute thresholds in chickens. J Acoust Soc Am 77:1162-1172.

Groff JA, Liberman MC. 2003. Modulation of cochlear afferent response by the lateral olivocochlear system: activation via electrical stimulation of the inferior colliculus. J Neurophysiol 90:3178-3200.

Grothe B. 2003. New roles for synaptic inhibition in sound localization. Nat Rev Neurosci 4:540-550.

Grothe B, Sanes DH. 1993. Bilateral inhibition by glycinergic afferents in the medial superior olive. J Neurophysiol 69:1192-1196.

Grothe B, Sanes DH. 1994. Synaptic inhibition influences the temporal coding properties of medial superior olivary neurons: an in vitro study. J Neurosci 14:1701-1709.

Haas HL, Jeffreys JGR. 1984. Low calcium field burst discharge of CA1 pyramidal neurons in rat hippocampal slices. J Physiol. 354:185-201.

Heil P, Scheich H. 1985. Quantitative analysis and two-dimensional reconstruction of the tonotopic organization of the auditory field L in the chick from 2-deoxyglucose data. Exp Brain Res 58:532-543.

Henkel CK, Fuentes-Santamaria V, Alvarado JC, Brunso-Bechtold JK. Quantitative measurement of afferent layers in the ferret inferior colliculus: DNLL projections to sublayers. Hear Res 177:32-42.

Hesslow G. 1986. Inhibition of inferior olivary transmission by mesencephalic stimulation in the cat. Neurosci Lett 63:76-80.

Huang ZJ, Di Cristo G, Ango F. 2007. Development of GABA innervation in the cerebral and cerebellar cortices. Nat Rev Neurosci 8:673-686.

Howard MA, Rubel EW. 2010. Dynamic spike thresholds during synaptic integration preserve and enhance temporal response properties in the avian cochlear nucleus. J Neurosci 30:12063–12074.

Hyson RL. 2005. The analysis of interaural time differences in the chick brain stem. Physiol Behav 86:297-305.

Hyson RL, Overholt EM, Lippe WR. 1994. Cochlear microphonic measurements of interaural time differences in the chick. Hear Res 81:109–118.

Hyson RL, Reyes AD, Rubel EW. 1995. A depolarizing inhibitory response to GABA in brainstem auditory neurons of the chick. Brain Res 677:117-126.

Jhaveri S, Morest DK. 1982. Sequential alterations of neuronal architecture in nucleus magnocellularis of the developing chicken: a Golgi study. Neuroscience 7:837–853.

Jinno S. 2009. Sructural organization of long-range GABAergic projection system of the hippocampus. Front Neuroanat 3:1-9.

Jinno S, Klausberger , Marton LF, Dalezios Y, Roberts JD, Fuentealba P, Bushong EA, Henze D, Buzsáki G, Somogyi P. 2007. Neuronal diversity in GABAergic long-range projections from the hippocampus. J Neurosci 27:8790–8804.

Joseph AW, Hyson RL. 1993. Coincidence detection by binaural neurons in the chick brain stem. J Neurophysiol 69:1197–1211.

Kadner A, Berrebi AS. 2008. Encoding of temporal features of auditory stimuli in the medial nucleus of the trapezoid body and superior paraolivary nucleus of the rat. Neuroscience 151:868-887.

Kapfer C, Seidl AH, Schweizer H, Grothe B. 2002. Experience-dependent refinement of inhibitory inputs to auditory coincidence-detector neurons. Nat Neurosci 5:247-253.

Kim G, Kandler K. 2003. Elimination and strengthening of glycinergic/GABAergic connections during tonotopic map formation. Nat Neurosci 6:282-290.

Klausberger T, Somogyi P. 2008. Neuronal diversity and temporal dynamics: the unity of hippocampal circuit operations. Science 321:53–57.

Klump G. 2000. Sound localization in birds. In: Dooling RJ, Fay RR, Popper AN (eds) Comparative hearing: birds and reptiles. Springer, New York, pp 249–307.

Knudsen EI, du Lac S, Esterly SD. 1987. Computational maps in the brain. Ann Rev Neurosci 10:41-65.

Knudsen EI, Konishi M. 1978. A neural map of auditory space in the owl. Science 200:795–797.

Knudsen EI, Konishi M. 1979. Mechanisms of sound localization in the barn owl (Tyto alba). J Comp Physiol [A] 133:13–21.

Kopp-Scheinpflug C, Tozer AJ, Robinson SW, Tempel BL, Hennig MH, Forsythe ID. 2011. The sound of silence: ionic mechanisms encoding sound termination. Neuron 71:911-925.

Köppl C. 2001. Tonotopic projections of the auditory nerve to the cochlear nucleus angularis in the barn owl. J Assoc Res Otolaryngol 2:41-53.

Köppl C, Carr CE. 2003. Computational diversity in the cochlear nucleus angularis of the barn owl. J Neurophysiol 89:2313-2329.

Köppl C, Carr CE. 2008. Maps of interaural time difference in the chicken's brainstem nucleus laminaris. Biol Cybern 98:541-559.

Kuba H, Koyano K, Ohmori H. 2002. Synaptic depression improves coincidence detection in the nucleus laminaris in brainstem slices of the chick embryo. Eur J Neurosci 15:984–990.

Kuba H, Yamada R, Fukui I, Ohmori H. 2005. Tonotopic specialization of auditory coincidence detection in nucleus laminaris of the chick. J Neurosci 25:1924-1934.

Kuo SP, Bradley LA, Trussell LO. 2009. Heterogeneous kinetics and pharmacology of synaptic inhibition in the chick auditory brainstem. J Neurosci 29:9625-9634.

Lachica EA, Rubsamen R, Rubel EW. 1994. GABAergic terminals in nucleus magnocellularis and laminaris originate from the superior olivary nucleus. J Comp Neurol 348:403-418.

Lewicki MS. 2002. Efficient coding of natural sounds. Nat Neurosci 5:356-363.

Lippe W, Rubel EW. 1985. Ontogeny of tonotopic organization of brain stem auditory nuclei in the chicken: implications for development of the place principle. J Comp Neurol 237:273-289.

Losonczy A, Zhang L, Shigemoto R, Somogyi P, Nusser Z. 2002. Cell type dependence and variability in the short-term plasticity of EPSCs in identified mouse hippocampal interneurones. J Physiol (Lond) 542:193–210.

Lu T, Trussell LO. 2001. Mixed excitatory and inhibitory GABA-mediated transmission in chick cochlear nucleus. J Physiol 535:125-131.

MacDonald GH, Rubel EW. 2008. Three-dimensional imaging of the intact mouse cochlea by fluorescent laser scanning confocal microscopy. Hear Res 243:1-10.

MacLeod KM, Carr CE. 2007. Beyond timing in the auditory brainstem: intensity coding in the avian cochlear nucleus angularis. Prog Brain Res 165:123-33.

Manley GA, Brix J, Kaiser A. 1987. Developmental stability of the tonotopic organization of the chick's basilar papilla. Science 237:655-656.

Masterton B, Heffner H, Ravizza R. 1969. The evolution of human hearing. J Acoust Soc Am 45:966-985.

Matsunaga W, Miyata S, Hashimoto Y, Lin SH, Nakashima T, Kiyohara T, Matsumoto T. 1999. Microtubule-associated protein-2 in the hypothalamo-neurohypophysial system: low-molecular-weight microtubule-associated protein-2 in pituitary astrocytes. Neuroscience 88:1289-1297.

Miyashita T, Rockland KS. 2007. GABAergic projections from the hippocampus to the retrosplenial cortex in the rat. Eur J Neurosci 26:1193–1204.

Moiseff A, Konishi M. 1981. Neuronal and behavioral sensitivity to binaural time differences in the owl. J Neurosci 1:40-48.

Moiseff A, Konishi M. 1983. Binaural characteristics of units in the owl's brainstem auditory pathway: precursors of restricted spatial receptive fields. J Neurosci 3:2553-2562.

Monsivais P, Rubel EW. 2001. Accommodation enhances depolarizing inhibition in central neurons. J Neurosci 21:7823-7830.

Monsivais P, Yang L, Rubel EW. 2000. GABAergic inhibition in nucleus magnocellularis: implications for phase locking in the avian auditory brainstem. J Neurosci 20:2954-2963.

Nelson BJ, Adams JC, Barmack NH, Mugnaini E. 1989. Comparative study of glutamate decarboxylase immunoreactive boutons in the mammalian inferior olive. J Comp Neurol 286:514-539.

Nishino E, Ohmori H. 2009. The modulation by intensity of the processing of interaural timing cues for localizing sounds. Mol Neurobiol 40:157-165.

Nishino E, Yamada R, Kuba H, Hioki H, Furuta T, Kaneko T, Ohmori H. 2008. Sound-intensity-dependent compensation for the small interaural time difference cue for sound source localization. J Neurosci 28:7153-7164.

Ostapoff EM, Benson CG, Saint Marie RL. 1997. GABA- and glycine-immunoreactive projections from the superior olivary complex to the cochlear nucleus in guinea pig. J Comp Neurol 381:500-512.

Overholt EM, Rubel EW, Hyson RL. 1992. A circuit for coding interaural time differences in the chick brainstem. J Neurosci 12:1698-1708.

Parks TN, Gill SS, Jackson H. 1987. Experience-independent development of dendritic organization in the avian nucleus laminaris. J Comp Neurol 260:312-319.

Parks TN, Rubel EW. 1975. Organization and development of brain stem auditory nuclei of the chicken: organization of projections from n. magnocellularis to n. laminaris. J Comp Neurol 164:435-448.

Parks TN, Rubel EW. 1978. Organization and development of the brain stem auditory nuclei of the chicken: primary afferent projections. J Comp Neurol 180:439–448.

Pearson KG. 1979. Local neurons and local interactions in the nervous system of invertebrates. In: Schmitt FO, Worden FG. (eds) The Neurosciences Fourth Study Program. MIT Press, Cambridge.

Peña JL, Viete S, Albeck Y, Konishi M. 1996. Tolerance to sound intensity of binaural coincidence detection in the nucleus laminaris of the owl. J Neurosci 16:7046-7054.

Perkins RE. 1973. An electron microscopic study of synaptic organization in the medial superior olive of normal and experimental chinchillas. J Comp Neurol 148:387-415.

Person AL, Cerretti DP, Pasquale EB, Rubel EW, Cramer KS. 2004. Tonotopic gradients of Eph family proteins in the chick nucleus laminaris during synaptogenesis. J Neurobiol 60:28-39.

Raman IM, Zhang S, Trussell LO. 1994. Pathway-specific variants of AMPA receptors and their contribution to neuronal signaling. J Neurosci 14:4998-5010.

Ramón y Cajal S. 1908. *Les ganglions terminaux du nerf acoustique des oiseaux. Trab Inst Cajal Invest Biol* 6:195–225.

Reyes AD, Rubel EW, Spain WJ. 1996. In vitro analysis of optimal stimuli for phase-locking and time-delayed modulation of firing in avian nucleus laminaris neurons. J Neurosci 16:993-1007.

Rhode WS, Oertel D, Smith PH. 1983. Physiological response properties of cells labeled intracellularly with horseradish peroxidase in cat ventral cochlear nucleus. J Comp Neurol 213:448–63.

Rouiller EM, Ryugo DK. 1984. Intracellular marking of physiologically characterized cells in the ventral cochlear nucleus of the cat. J Comp Neurol 225:167-86.

Rubel EW, Parks TN. 1975. Organization and development of brain stem auditory nuclei of the chicken: tonotopic organization of n. magnocellularis and n. laminaris. J Comp Neurol 164:411-433.

Ryals BM, Rubel EW. 1982. Patterns of hair cell loss in chick basilar papilla after intense auditory stimulation. Frequency organization. Acta Otolaryngol 93:205-210.

Sachs MB, Sinnott JM, Hienz RD. 1978. Behavioral and physiological studies of hearing in birds. Fed Proc 37:2329-2335.

Saldana E, Aparicio MA, Fuentes-Santamaria V, Berrebi AS. 2009. Connections of the superior paraolivary nucleus of the rat: projections to the inferior colliculus. Neuroscience 163:372-387.

Sanes DH, Friauf E. 2000. Development and influence of inhibition in the lateral superior olivary nucleus. Hear Res 147:46-58.

Sanes DH, Merickel M, Rubel EW. 1989. Evidence for an alteration of the tonotopic map in the gerbil cochlea during development. J Comp Neurol 279:436-444.

Sanes DH, Rubel EW. 1988. The ontogeny of inhibition and excitation in the gerbil lateral superior olive. J Neurosci 8:682-700.

Sanes DH, Siverls V. 1991. Development and specificity of inhibitory terminal arborizations in the central nervous system. J Neurobiol 22:837-54.

Sanes DH, Song J, Tyson J. 1992. Refinement of dendritic arbors along the tonotopic axis of the gerbil lateral superior olive. Brain Res Dev Brain Res 67:47-55.

Sanes DH, Takács C. 1993. Activity-dependent refinement of inhibitory connections. Eur J Neurosci 5:570-4.

Saunders SS, Salvi RJ. 1993. Psychoacoustics of normal adult chickens: thresholds and temporal integration. J Acoust Soc Am 94:83-90.

Schofield BR. 1994. Projections to the cochlear nuclei from principal cells in the medial nucleus of the trapezoid body in guinea pigs. J Comp Neurol 344:83-100.

Seidl AH, Rubel EW, Harris DM. 2010. Mechanisms for adjusting interaural time differences to achieve binaural coincidence detection. J Neurosci 30:70-80.

Shneiderman A, Oliver DL, Henkel CK. 1988. Connections of the dorsal nucleus of the lateral lemniscus: an inhibitory parallel pathway in the ascending auditory system? J Comp Neurol 276:188-208.

Smith DJ, Rubel EW. 1979. Organization and development of brain stem auditory nuclei of the chicken: dendritic gradients in nucleus laminaris. J Comp Neurol 186:213-239.

Smith ZD, Gray L, Rubel EW. 1983. Afferent influences on brainstem auditory nuclei of the chicken: n. laminaris dendritic length following monaural conductive hearing loss. J Comp Neurol 220:199-205.

Soares D, Chitwood RA, Hyson RL, Carr CE. 2002. Intrinsic neuronal properties of the chick nucleus angularis. J Neurophysiol 88:152-162.

Spangler KM, Warr WB, Henkel CK. 1985. The projections of principal cells of the medial nucleus of the trapezoid body in the cat. J Comp Neurol 238:249-262.

Tabor KM, Wong RO, Rubel EW. 2011. Topography and morphology of the inhibitory projection from superior olivary nucleus to nucleus laminaris in chickens (Gallus gallus). J Comp Neurol 519:358-375.

Takahashi T, Moiseff A, Konishi M. 1984. Time and intensity cues are processed independently in the auditory system of the owl. J Neurosci 4:1781-1786.

Takahashi M, Sugiuchi Y, Shinoda Y. 2007. Commissural mirror-symmetric excitation and reciprocal inhibition between the two superior colliculi and their roles in vertical and horizontal eye movements. Journal of Neurophysiology 98:2664-2682.

Takahashi TT, Konishi M. 1988. Projections of nucleus angularis and nucleus laminaris to the lateral lemniscal nuclear complex of the barn owl. J Comp Neurol 274:212-238.

Tang ZQ, Lu Y. 2012. Development of GPCR Modulation of GABAergic Transmission in Chicken Nucleus Laminaris Neurons. PLoS One 7:1-10.

Terleph TA, Mello CV, Vicario DS. 2006. Auditory topography and temporal response dynamics of canary caudal telencephalon. J Neurobiol 66:281-292.

Thevenaz P, Ruttimann UE, Unser M. 1998. A pyramid approach to subpixel registration based on intensity. IEEE Trans Image Process 7:27-41.

Tsuchitani C, Boudreau JC. 1966. Single unit analysis of cat superior olive S segment with tonal stimuli. J Neurophysiol 29:684-697.

van Groen T, Wyss JM. 2003. Connections of the retrosplenial granular b cortex in the rat. J Comp Neurol 463:249–263.

von Bartheld CS, Code RA, Rubel EW. 1989. GABAergic neurons in brainstem auditory nuclei of the chick: distribution, morphology, and connectivity. J Comp Neurol 287:470-483.

Wang Y, Rubel EW. 2008. Rapid regulation of microtubule-associated protein 2 in dendrites of nucleus laminaris of the chick following deprivation of afferent activity. Neuroscience 154:381-389.

Warchol ME, Dallos P. 1990. Neural coding in the chick cochlear nucleus. J Comp Physiol A 166:721-734.

Warr WB, Beck JE. 1996. Multiple projections from the ventral nucleus of the trapezoid body in the rat. Hear Res 93:83-101.

Watanabe A, Bullock TH. 1960. Modulation of activity of one neuron by subthreshold slow potential in another in lobster cardiac ganglion. J Gen Physiol 43:1031-45.

Werthat F, Alexandrova O, Grothe B, Koch U. 2008. Experience-dependent refinement of the inhibitory axons projecting to the medial superior olive. Dev Neurobiol 68:1454-1462.

Westerberg BD, Schwarz DW. 1995. Connections of the superior olive in the chicken. J Otolaryngol 24:20-30.

Wild JM, Krutzfeldt NO, Kubke MF. 2009. Connections of the auditory brainstem in a songbird, Taeniopygia guttata. III. Projections of the superior olive and lateral lemniscal nuclei. J Comp Neurol 518:2149-2167.

Wild JM, Krutzfeldt NO, Kubke MF. 2010. Connections of the auditory brainstem in a songbird, Taeniopygia guttata. III. Projections of the superior olive and lateral lemniscal nuclei. J Comp Neurol 518:2149-67.

Yamada R, Kuba H, Ishii TM, Ohmori H. 2005. Hyperpolarization-activated cyclic nucleotide-gated cation channels regulate auditory coincidence detection in nucleus laminaris of the chick. J Neurosci 25:8867-8877.

Yang L, Monsivais P, Rubel EW. 1999. The superior olivary nucleus and its influence on nucleus laminaris: a source of inhibitory feedback for coincidence detection in the avian auditory brainstem. J Neurosci 19:2313-2325.

Yavuzoglu A, Schofield BR, Wenstrup JJ. 2010. Substrates of auditory frequency integration in a nucleus of the lateral lemniscus. Neuroscience 169:906-919.

Yin TC, Chan JC. 1990. Interaural time sensitivity in the medial superior olive of cat. J Neurophysiol 64:465–488.

Young SR, Rubel EW. 1983. Frequency-specific projections of individual neurons in chick brainstem auditory nuclei. J Neurosci 3:1373-1378.

Young SR, Rubel EW. 1986. Embryogenesis of arborization pattern and topography of individual axons in N. laminaris of the chicken brain stem. J Comp Neurol 254:425-459.

CURRICULUM VITAE

EDUCATION

University of Washington, Seattle, WA, USA
Ph.D. Program in Neurobiology & Behaviour, 2012
Advisors: Edwin Rubel, Ph.D. and Rachel Wong, Ph.D.

University of Iowa, Iowa City, IA, USA
B.S. Biological Sciences with Honors, 2001

RESEARCH EXPERIENCE

Lab of Edwin Rubel, Ph.D. and Rachel Wong, **Ph.D.**, U of Washington
Graduate student October 2006 – May 2012

- Used *in vivo* physiology combined with quantitative mapping methods to determine the tonotopic organization of inhibitory neurons in the avian auditory brainstem.
- Examined topography and synaptic connectivity patterns of inhibitory input in the low-frequency sound localization circuit.
- Ph.D. thesis title: *Spatial organization of long-range inhibition in binaural hearing*

Lab of Andres Barria, Ph.D., University of Washington
Graduate rotation student Spring 2006

- Studied the affect of AMPA receptor subunit NR2A at synapses by analyzing the frequency and kinetics of spontaneous postsynaptic currents in rat hippocampus.

Lab of Adrienne Fairhall, Ph.D., University of Washington
Graduate rotation student Winter 2006

- Investigated adaptation of Hodgkin Huxley cell model to changes in stimulus variance by comparing the linear filter and nonlinear threshold function for cell models at different G_{Na}/G_K ratios.

Lab of Marc Binder, Ph.D., University of Washington
Graduate rotation student Fall 2005

- Determined the firing properties of cortical pyramidal neurons in rat using whole-cell patch-clamp and reverse correlation techniques with white noise inputs.

Lab of Ned Kalin, M.D., University of Wisconsin
Research Technologist July 2004 – September 2005

- Examined the regulation of corticotrophin-releasing factor (CRF) family members and the expression of various protein kinases and transcription factors like CREB in relation to adaptive and maladaptive stress responses in rats.

Lab of Jonathon Poulton, Ph.D., University of Iowa
Undergraduate student October 1999 – June 2001

- Determine size and expression patterns of coumarinyl glucoside β-glucosidase gene family, responsible for regulating levels of the anti-coagulate coumarin, in white sweetclover (*Melilotus alba* Desr.).
- Honors thesis title: *The role of the coumarinyl glucoside β-glucosidase gene family in coumarin biosynthesis in white sweetclover (Melilotus alba Desr.)*

OTHER TRAINING

Accepted to: **Marine Biological Laboratory Course** August 2012
Zebrafish Development & Genetics

Accepted to: **Cold Spring Harbor Laboratory Course** July 2012
Advanced Techniques in Molecular Neuroscience

Stowers Institute for Medical Research September 2008
Advanced Microscopy Workshop

TEACHING EXPERIENCE

Introduction to Systems & Behavioral Neurobiology Spring 2010
Teaching assistant for Michael Kennedy, Ph.D., Max Sizemore, Ph.D.

Gene Action Winter 2009
Teaching assistant for Richard Gray, Ph.D., Elizabeth Traxler, Ph.D.

Sensory and Perceptual Processes Fall 2009
Teaching assistant for Ellen Covey, Ph.D.

Introduction to Neurobiology Fall 2008
Teaching assistant for S. Carlson, Ph.D., D. Perkel, Ph.D., J. Sullivan, Ph.D.

Signaling Mechanisms in Excitable Cells Fall 2007
Teaching assistant for Peter Detwiler, Ph.D., Bertil Hille, Ph.D.

PUBLICATIONS

Provisionally accepted

Seidl AH*, Sanchez JT*, Schecterson LC*, **Tabor KM***, Wang Y*, Kashima DT*, Poynter G, Huss D, Fraser SE, Rubel EW, Lansford R (provisionally accepted) Validation of the transgenic quail as a model for research in the avian nervous system – a comparative study of the auditory brainstem.

Peer reviewed

Tabor KM, Coleman WL, Rubel EW, Burger RM. 2012. Tonotopic organization of the superior olivary nucleus in chickens. J Comp Neurol. 520:1493-508.

Tabor KM, Wong RO, Rubel EW. 2011. Topography and morphology of inhibitory projection from superior olivary nucleus to nucleus laminaris in chickens (*Gallus gallus*). J Comp Neurol. 519:358-75.

ABSTRACTS

Tabor KM, Coleman WL, Rubel EW, Burger RM. 2011. Tonotopic mapping of superior olivary nucleus in chickens. Abstr. Association for Research in Otolaryngology 34st midwinter research meeting.

Tabor KM, Wong RO, Rubel EW. 2010. Topography and morphology of superior olivary nucleus projection to nucleus laminaris in chickens. Abstr. Gordon Research Conference: Auditory Systems.

Tabor KM, Rubel EW. 2008. Topography and morphology of superior olivary nucleus projections upon nucleus laminaris in chickens. Abstr. Association for Research in Otolaryngology 31st midwinter research meeting.

AWARDS AND HONORS

Neuroscience training grant, University of Washington. 2011-2012.
Auditory Neuroscience training grant, U of Washington. 2006-9; 2010-1.
University of Iowa: honors thesis in Biological Sciences, 2001
Academic excellence award and scholarship, University of Iowa, 1999
Academic tuition scholarship, University of Iowa, 1997
Advanced Placement Scholar designation, College Board, 1997